

Supplementary Information

Potent strategy towards strongly emissive nitroaromatics through a weakly electron-deficient core

Bartłomiej Sadowski,^[a] Marzena Kaliszewska,^[b] Yevgen M. Poronik,^[a] Małgorzata Czichy,^[c] Patryk Janasik,^[c] Marzena Banasiewicz,^[d] Dominik Mierzwa,^[a] Wojciech Gadomski,^[b] Trevor D. Lohrey,^{[e][f]} John A. Clark,^[g] Mieczysław Łapkowski,*^[c] Bolesław Kozankiewicz,*^[d] Valentine I. Vullev,*^{[g][h][i][j]} Andrzej L. Sobolewski,*^[d] Piotr Piątkowski,*^[b] Daniel T. Gryko*^[a]

^[a] Institute of Organic Chemistry, Polish Academy of Sciences, Kasprzaka 44/52, 01-224 Warsaw, Poland

^[b] Department of Chemistry, University of Warsaw, Zwirki i Wigury 101, 02-089 Warsaw, Poland

^[c] Faculty of Chemistry, Silesian University of Technology, Strzody 9, 44-100 Gliwice, Poland

^[d] Institute of Physics, Polish Academy of Sciences, Aleja Lotników 32/46, 02-668 Warsaw, Poland

^[e] Department of Chemistry, University of California, Berkeley, 420 Latimer Hall, Berkeley, CA, USA

^[f] Chemical Sciences Division, Lawrence Berkeley National Laboratory, 1 Cyclotron Road, Berkeley, CA, USA

^[g] Department of Bioengineering, University of California, Riverside, 900 University Ave., Riverside, CA 92521, USA

^[h] Department of Chemistry, University of California, Riverside, 900 University Ave., Riverside, CA 92521, USA

^[i] Department of Biochemistry, University of California, Riverside, 900 University Ave., Riverside, CA 92521, USA

^[j] Materials Science and Engineering Program, University of California, Riverside, 900 University Ave., Riverside, CA 92521, USA

Table of contents

1.	Experimental part	S2
2.	X-ray crystal structures of selected compounds.....	S11
3.	Spectroscopic measurements.....	S14
4.	Computational details.....	S73
5.	Electrochemical and spectroelectrochemical studies	S114
6.	Phosphorescence studies.	S127
7.	^1H and ^{13}C NMR spectra of new compounds.	S129

1. Experimental part

General Remarks. All reagents and solvents were purchased from commercial sources and were used as received unless otherwise noted. Reagent grade solvents (CH_2Cl_2 , hexanes) were distilled prior to use. Toluene was dried by distillation over sodium and stored under argon. Transformations with moisture- and oxygen-sensitive compounds were performed under a stream of argon. The reaction progress was monitored by means of thin-layer chromatography (TLC), which was performed on aluminum foil plates, covered with silica gel 60 F254. Product purifications were done by means of column chromatography with Kieselgel 60. The identity and purity of prepared compounds were proved by ^1H NMR and ^{13}C NMR spectroscopies as well as by mass spectrometry (via EI-MS or ESI-MS). HRMS (ESI-TOF) and HRMS (EI): double-focusing magnetic sector instruments with EBE geometry were utilized. NMR spectra were measured on 400, 500 or 600 MHz instruments. Chemical shifts (δ , ppm) were determined with CDCl_3 as the internal reference; J values are given in Hz. All melting points for crystalline products were measured with an automated melting point apparatus and are given without correction. Compounds **1**¹, **2**², **8**³ and **10**³ were synthesized as described earlier.

Synthesis of commercially unavailable bromoarenes.

¹ M. Grzybowski, I. Deperasińska, M. Chotkowski, M. Banasiewicz, A. Makarewicz, B. Kozankiewicz, D. T. Gryko, *Chem. Commun.* **2016**, 52, 5108-5111.

² B. Sadowski, S.-H. Su, T.-C. Lin, T. D. Lohrey, I. Deperasińska, P.-T. Chou, Daniel T. Gryko, *J. Mater. Chem. C* **2018**, 6, 12306-12313.

³ B. Sadowski, M. F. Rode, D. T. Gryko, *Chem. Eur. J.* **2018**, 24, 855-864.

2-Bromo-4-methoxy-1-nitrobenzene. To a solution of 2-bromo-4-fluoro-1-nitrobenzene (1.0 g, 4.5 mmol, 1.0 eq) in DMSO (7 mL) was added sodium methoxide (364.5 mg, 6.75 mmol). The reaction mixture was stirred at room temperature for 24 h and then an additional portion of sodium methoxide was added (~200 mg). After three days of stirring at room temperature, 20 mL of water was added and the aqueous layer was extracted with dichloromethane (3 x 30 mL). The combined organic layers were dried over MgSO₄, filtered and concentrated under reduced pressure. The crude product was purified by column chromatography (SiO₂, hexanes : dichloromethane, 1:1) to give 522.0 mg (50% yield) of product. R_f = 0.68 (SiO₂, hexanes : dichloromethane, 1:1). Mp. 44 - 45 °C (Lit.⁴ 43 - 45 °C). ¹H NMR (500 MHz, CDCl₃, 25 °C) δ 7.98 (d, 1H, J = 9.0 Hz), 7.22 (d, 1H, J = 3.0 Hz), 6.91 (dd, 1H, J₁ = 9.0 Hz, J₂ = 2.5 Hz), 3.89 (s, 3H). ¹³C NMR (126 MHz, CDCl₃, 25 °C) δ 162.9, 128.1, 120.2, 117.0, 113.7, 56.3.

1-Bromo-8-nitronaphthalene. The title compound was prepared according to the literature procedure for the bromination of nitrobenzene,⁵ when a stoichiometric amount of FeCl₃ was used. However, in our case we obtained a mixture of at least five major isomers (according to TLC analysis), inseparable through column chromatography. Using 20%_{mol} of FeCl₃ relative to 1-nitronaphthalene resulted in a mixture where two major and few minor products can be identified. The major ones were separated using column chromatography, however these fractions contained minor impurities as other mono-brominated isomers (elemental analyses – see below – agree well with the calculated element composition). Those minor impurities could not be removed through either crystallization (EtOH) or the next column chromatography. The exact substitution pattern of both major isomers was confirmed by NMR spectroscopy (see the chapter entitled *¹H and ¹³C NMR spectra of new compounds*) and the structure of 1-bromo-8-nitronaphthalene was also confirmed indirectly by growing a single crystal of compound 7.

⁴ Y. J. Zhang, H. Wei, W. Zhang, *Tetrahedron* **2009**, *65*, 1281-1286.

⁵ K. Tanemura, T. Suzuki, Y. Nishida, K. Satsumabayashi, T. Horaguchi, *Chem. Lett.* **2003**, *32*, 932-933.

Procedure: A mixture of 1-nitronaphthalene (1.73 g, 10 mmol, 1.0 eq), NBS (1.958 g, 11 mmol, 1.1 eq), and anhydrous FeCl₃ (324.4 mg, 2 mmol, 20%_{mol}) was heated at 150 °C for 2 h. The flask was cooled down to room temperature, 30 mL of water was added and the mixture was extracted with dichloromethane (3 x 30 mL). The extracts were dried over MgSO₄ and evaporated under vacuum. The residue was chromatographed (SiO₂, hexanes : dichloromethane = 3:1) to give 104.0 mg (20% yield) of 1-bromo-8-nitronaphthalene and 122.0 mg (24% yield) of 1-bromo-5-nitronaphthalene. 1-Bromo-8-nitronaphthalene was subjected to the direct arylation reaction without further purification.

Analytical data for 1-bromo-8-nitronaphthalene. R_f = 0.33 (SiO₂, hexanes : dichloromethane, 3:1). Mp. 95 - 96 °C. ¹H NMR (600 MHz, CDCl₃, 25 °C) δ 8.03 (dd, 1H, J₁ = 7.8 Hz, J₂ = 1.2 Hz), 7.96 (dd, 1H, J₁ = 7.2 Hz, J₂ = 1.2 Hz), 7.92 (dd, 1H, J₁ = 8.4 Hz, J₂ = 1.2 Hz), 7.75 (dd, 1H, J₁ = 7.2 Hz, J₂ = 1.2 Hz), 7.54 (dd, 1H, J₁ = 7.8 Hz, J₂ = 1.2 Hz), 7.44 (dd, 1H, J₁ = 7.8 Hz, J₂ = 0.6 Hz). ¹³C NMR (151 MHz, CDCl₃, 25 °C) δ 148.6, 136.2, 135.4, 132.8, 128.7, 128.0, 125.2, 123.7, 122.8, 116.7. HRMS (EI) calcd for C₁₀H₆NO₂Br 250.9582 [M⁺], found 250.9577. Anal. calcd for C₁₀H₆NO₂Br: C, 47.65; H, 2.40; N, 5.56; Br, 31.70; found: C, 47.63; H, 2.39; N, 5.41; Br, 31.77.

Analytical data for 1-bromo-5-nitronaphthalene. R_f = 0.55 (SiO₂, hexanes : dichloromethane, 3:1). Mp. 119 - 120 °C. ¹H NMR (600 MHz, CDCl₃, 25 °C) δ 8.61 (d, 1H, J = 8.4 Hz), 8.47 (d, 1H, J = 8.4 Hz), 8.23 (dd, 1H, J₁ = 7.8 Hz, J₂ = 1.2 Hz), 7.94 (dd, 1H, J₁ = 7.2 Hz, J₂ = 0.6 Hz), 7.65 (dd, 1H, J₁ = 8.1 Hz, J₂ = 1.2 Hz), 7.54 (dd, 1H, J₁ = 8.1 Hz, J₂ = 1.2 Hz). ¹³C NMR (151 MHz, CDCl₃, 25 °C) δ 147.3, 133.6, 132.8, 131.8, 129.5, 126.5, 125.6, 124.5, 123.6, 123.0. HRMS (EI) calcd for C₁₀H₆NO₂Br 250.9582 [M⁺], found 250.9584. Anal. calcd for C₁₀H₆NO₂Br: C, 47.65; H, 2.40; N, 5.56; Br, 31.70; found: C, 47.93; H, 2.47; N, 5.38; Br, 31.65.

General procedure for a single direct arylation reaction and analytical data for all new compounds.

In a 50 mL Schlenk flask containing a magnetic stirring bar were placed: **1** (0.4 mmol, 173.2 mg, 2.0 eq), aryl bromide (0.2 mmol, 1.0 eq), tris(dibenzylideneacetone)dipalladium(0) (9.4 mg, 0.01 mmol, 5%_{mol}), PCy₃·HBF₄ (7.4 mg, 0.02 mmol, 10%_{mol}), pivalic acid (6.2 mg, 0.06 mmol, 30%_{mol}), K₂CO₃

(55.5 mg, 0.4 mmol, 2.0 eq) and anhydrous, degassed toluene (10 mL). The content of the flask was stirred at 120 °C. After indicated time, all solvents were evaporated off and the residue was purified by column chromatography. All further manipulations are described below.



6,12-Diheptyl-3-(4-nitrophenyl)-5H,11H-dipyrrolo[1,2-b:1',2'-

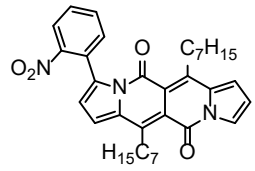
g][2,6]naphthyridine-5,11-dione (3). Prepared using 1-bromo-4-nitrobenzene (40.4 mg, 0.2 mmol). Time of heating: 24 h. Product was purified using column chromatography (SiO₂, hexanes : dichloromethane, 1:1). The residue after chromatography was reprecipitated from dichloromethane/methanol mixture to give 70.0 mg (63% yield) of product. R_f = 0.51 (SiO₂, hexanes : dichloromethane, 1:1). Mp. 117 - 118 °C. ¹H NMR (600 MHz, CDCl₃, 25 °C) δ 8.25 (dd, 2H, J₁ = 7.2 Hz, J₂ = 1.8 Hz), 7.85 (dd, 1H, J₁ = 3.0 Hz, J₂ = 2.5 Hz), 7.61 (dd, 2H, J₁ = 7.2 Hz, J₂ = 1.8 Hz), 6.94 (d, 1H, J = 3.6 Hz), 6.87 (dd, 1H, J₁ = 3.6 Hz, J₂ = 1.2 Hz), 6.64 (d, 1H, J = 3.6 Hz), 6.55 (t, 1H, J = 3.6 Hz), 3.32 (t, 2H, J = 7.8 Hz), 3.16 (t, 2H, J = 7.8 Hz), 1.71 (quintet, 2H, J = 7.2 Hz), 1.62 (quintet, 2H, J = 7.2 Hz), 1.58-1.53 (m, 2H), 1.47-1.38 (m, 4H), 1.36-1.25 (m, 10H), 0.90 (t, 3H, J = 7.2 Hz), 0.86 (t, 3H, J = 6.6 Hz). ¹³C NMR (151 MHz, CDCl₃, 25 °C) δ 159.7, 158.3, 147.1, 145.4, 144.8, 139.5, 137.5, 136.5, 133.3, 129.5, 123.1, 122.7, 119.9, 117.0, 116.0, 115.7, 115.4, 115.4, 32.1, 31.9, 31.0, 31.0, 30.6, 30.5, 30.3, 29.4, 29.3, 22.8, 22.8, 14.3, 14.2. HRMS (ESI, negative mode) calcd for C₃₄H₃₈N₃O₄ 552.2862 [M-H⁺], found 552.2853.



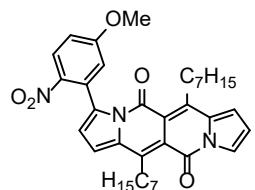
6,12-Diheptyl-3-(3-nitrophenyl)-5H,11H-dipyrrolo[1,2-b:1',2'-

g][2,6]naphthyridine-5,11-dione (4). Prepared using 1-bromo-3-nitrobenzene (40.4 mg, 0.2 mmol). Time of heating: 24 h. Product was purified using column chromatography (SiO₂, hexanes : dichloromethane 1:1). The residue after chromatography was reprecipitated from dichloromethane/methanol mixture to give 82.0 mg (74% yield) of product. R_f = 0.57 (SiO₂, hexanes : dichloromethane 1:1). Mp. 128 - 129 °C. ¹H NMR (500 MHz, CDCl₃, 25 °C) δ 8.34 (t, 1H, J = 2.0 Hz), 8.23-8.21 (m, 1H), 7.85 (dd, 1H, J₁ = 3.0 Hz, J₂ = 1.0 Hz), 7.79 (dd, 1H, J₁ = 8.0 Hz, J₂ = 1.0 Hz), 7.56 (t, 1H, J = 8.0 Hz), 6.94 (d, 1H, J = 4.0 Hz), 6.86 (dd, 1H, J₁ = 3.5 Hz, J₂ = 1.0 Hz), 6.62 (d, 1H, J = 4.0 Hz), 6.54 (t, 1H, J = 3.0 Hz), 3.32 (t, 2H, J = 8.0 Hz), 3.16 (t, 2H, J = 8.0

Hz), 1.72 (quintet, 2H, J = 7.5 Hz), 1.66-1.53 (m, 4H), 1.45-1.38 (m, 4H), 1.36-1.23 (m, 10H), 0.91 (t, 3H, J = 7.0 Hz), 0.85 (t, 3H, J = 7.0 Hz). ^{13}C NMR (126 MHz, CDCl_3 , 25 °C) δ 159.9, 158.4, 147.8, 145.3, 144.9, 137.3, 136.0, 134.7, 134.6, 133.4, 128.5, 123.9, 122.6, 119.3, 116.9, 115.9, 115.7, 115.4, 115.1, 32.1, 31.9, 31.0, 31.0, 30.6, 30.6, 30.4, 30.3, 29.4, 29.2, 22.8, 22.8, 14.3, 14.2. HRMS (EI) calcd for $\text{C}_{34}\text{H}_{39}\text{N}_3\text{O}_4$ 553.2941 [M^+], found 553.2941.

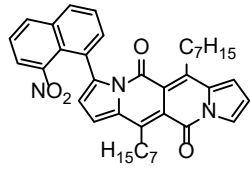


6,12-Diheptyl-3-(2-nitrophenyl)-5H,11H-dipyrrolo[1,2-b:1',2'-g][2,6]naphthyridine-5,11-dione (5). Prepared using 1-bromo-2-nitrobenzene (40.4 mg, 0.2 mmol). Time of heating: 48 h. Product was purified using column chromatography (SiO_2 , hexanes : dichloromethane, 2:1). The residue after chromatography was reprecipitated from dichloromethane/methanol mixture to give 31.0 mg (28% yield) of product. R_f = 0.26 (SiO_2 , hexanes : dichloromethane, 2:1). Mp. 165 - 166 °C. ^1H NMR (500 MHz, CDCl_3 , 25 °C) δ 8.21 (d, 1H, J = 8.5 Hz), 7.82 (d, 1H, J = 2.0 Hz), 7.67 (t, 1H, J = 7.5 Hz), 7.58-7.52 (m, 2H), 6.95 (d, 1H, J = 3.5 Hz), 6.82 (d, 1H, J = 3.0 Hz), 6.54-6.51 (m, 2H), 3.39-2.95 (br m, 4H), 1.73 (br s, 2H), 1.59-1.49 (m, 4H), 1.44-1.24 (m, 14H), 0.92-0.86 (m, 6H). ^{13}C NMR (126 MHz, CDCl_3 , 25 °C) δ 159.7, 158.4, 148.3, 145.7, 144.9, 135.1, 133.5, 133.1, 132.0, 129.5, 129.1, 124.6, 122.5, 118.0, 116.7, 115.7, 115.6, 115.1, 115.0, 32.1, 32.0, 31.0, 30.9, 30.6, 30.6, 30.3, 29.4, 29.0, 22.9, 22.8, 14.3, 14.2. HRMS (EI) calcd for $\text{C}_{34}\text{H}_{39}\text{N}_3\text{O}_4$ 553.2941 [M^+], found 553.2953.



6,12-Diheptyl-3-(5-methoxy-2-nitrophenyl)-5H,11H-dipyrrolo[1,2-b:1',2'-g][2,6]naphthyridine-5,11-dione (6). Prepared using ethyl 2-bromo-4-methoxy-1-nitrobenzene (46.4 mg, 0.2 mmol). Time of heating: 24 h. Product was purified using column chromatography (SiO_2 , hexanes : dichloromethane, 2:1). The residue after column was reprecipitated from dichloromethane/methanol mixture to give 38.5 mg (33% yield) of product. R_f = 0.17 (SiO_2 , hexanes : dichloromethane, 2:1). Mp. 160 - 161 °C. ^1H NMR (500 MHz, CDCl_3 , 25 °C) δ 8.25 (d, 1H, J = 9.0 Hz), 7.82 (dd, 1H, J_1 = 3.0 Hz, J_2 = 1.0 Hz), 7.00-6.94 (m, 3H), 6.82 (d, 1H, J = 2.5 Hz), 6.52-6.51 (m, 2H), 3.93 (s, 3H), 3.40-2.94 (br m, 4H), 1.77-1.68 (m, 2H), 1.59-1.50 (m, 4H), 1.44-1.27 (m, 14H), 0.92-0.86 (m, 6H). ^{13}C NMR (126 MHz, CDCl_3 , 25 °C) δ 163.0, 159.6, 158.4, 145.6,

144.9, 141.6, 135.2, 135.0, 133.5, 131.9, 127.2, 122.5, 117.7, 117.4, 116.7, 115.6, 115.5, 115.2, 115.0, 113.1, 56.1, 32.1, 32.0, 31.0, 30.9, 30.6, 30.6, 30.3, 30.3, 29.4, 29.0, 22.9, 22.8, 14.3, 14.3. HRMS (EI) calcd for C₃₅H₄₁N₃O₅ 583.3046 [M⁺], found 583.3043.

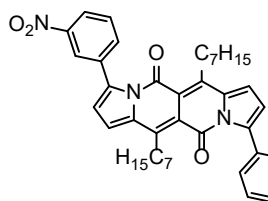


6,12-Diheptyl-3-(8-nitronaphthalen-1-yl)-5H,11H-dipyrrolo[1,2-b:1',2'-g][2,6]naphthyridine-5,11-dione (7). Prepared using 1-bromo-8-nitronaphthalene (50.4 mg, 0.2 mmol). Time of heating: 72 h. Product was purified using column chromatography (SiO₂, hexanes : dichloromethane, 2:1). The residue after column was reprecipitated from dichloromethane/methanol mixture to give 8.5 mg (7% yield, average yield for two runs) of product. R_f = 0.11 (SiO₂, hexanes : dichloromethane, 2:1). Mp. 150 - 151 °C. ¹H NMR (500 MHz, CDCl₃, 25 °C) δ 8.11 (d, 1H, J = 8.5 Hz), 8.00 (dd, 1H, J₁ = 7.5 Hz, J₂ = 1.0 Hz), 7.83 (d, 2H, J = 2.0 Hz), 7.74 (d, 1H, J = 7.5 Hz), 7.70-7.65 (m, 2H), 7.51 (t, 1H, J = 8.0 Hz), 6.95 (d, 1H, J = 4.0 Hz), 6.78 (d, 1H, J = 3.0 Hz), 6.51 (t, 1H, J = 3.5 Hz), 6.47 (d, 1H, J = 4.0 Hz), 3.46 (m, 1H), 3.20 (m, 1H), 3.08 (m, 1H), 2.91 (m, 1H), 1.84-1.65 (m, 2H), 1.60-1.54 (m, 2H), 1.51-1.46 (m, 2H), 1.45-1.39 (m, 2H), 1.36-1.32 (m, 4H), 1.26-1.15 (m, 8H), 0.91 (t, 3H, J = 6.5 Hz), 0.84 (t, 3H, J = 7.0 Hz). ¹³C NMR (126 MHz, CDCl₃, 25 °C) δ 159.4, 158.5, 149.2, 145.3, 144.3, 137.4, 134.9, 134.5, 133.5, 133.4, 131.9, 129.2, 128.9, 126.7, 124.3, 123.9, 123.7, 122.1, 118.0, 116.1, 116.0, 115.4, 115.4, 114.8, 32.1, 31.9, 31.1, 30.7, 30.6, 30.6, 30.2, 30.0, 29.4, 29.0, 22.9, 22.8, 14.3, 14.3. HRMS (EI) calcd for C₃₈H₄₁N₃O₄ 603.3097 [M⁺], found 603.3109.

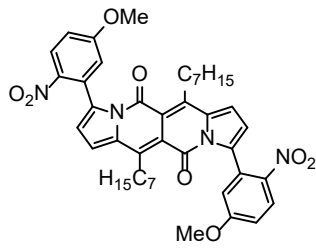
General procedure for a double direct arylation reaction and analytical data for all new compounds.

In a 25 mL Schlenk flask containing a magnetic stirring bar were placed: **1** (0.1 mmol, 43.3 mg, 1.0 eq), tris(dibenzylideneacetone)dipalladium(0) (9.2 mg, 0.01 mmol, 10 %_{mol}), PCy₃·HBF₄ (7.4 mg, 0.02 mmol, 20 %_{mol}), pivalic acid (6.2 mg, 0.06 mmol, 60 %_{mol}), K₂CO₃ (55.5 mg, 0.4 mmol, 4.0 eq) and the haloarene (0.3 mmol, 3.0 eq). The vessel was evacuated and backfilled with argon (3 times). Next, anhydrous, degassed toluene (2 mL) was added using a syringe. The vessel was tightly closed and again

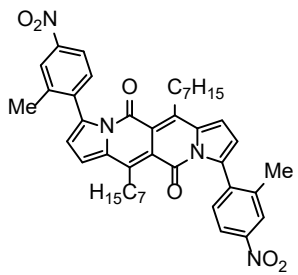
carefully evacuated and backfilled with argon (3 times). The content of the flask was stirred at 120 °C. After indicated time, all solvents were evaporated off and the residue was purified by column chromatography. All further manipulations are described below.



6,12-Diheptyl-3,9-bis(3-nitrophenyl)-5H,11H-dipyrrolo[1,2-b:1',2'-g][2,6]naphthyridine-5,11-dione (9). Prepared using 1-bromo-3-nitrobenzene (60.6 mg, 0.3 mmol). Time of heating: 24 h. Product was purified using column chromatography (SiO₂, hexanes : dichloromethane, 1:2) and recrystallized from acetonitrile to give 34.0 mg (50% yield) of product. R_f = 0.69 (SiO₂, hexanes : dichloromethane, 1:2). Mp. 208 - 209 °C. ¹H NMR (500 MHz, CDCl₃, 25 °C) δ 8.35 (t, 2H, J = 2.0 Hz), 8.23 (dd, 2H, J₁ = 8.0 Hz, J₂ = 1.0 Hz), 7.80 (d, 2H, J = 8.0 Hz), 7.57 (t, 2H, J = 8.0 Hz), 6.93 (d, 2H, J = 4.0 Hz), 6.62 (d, 2H, J = 3.5 Hz), 3.21-3.18 (m, 4H), 1.69-1.63 (m, 4H), 1.49-1.43 (m, 4H), 1.36-1.26 (m, 12H), 0.86 (t, 6H, J = 7.0 Hz). ¹³C NMR (126 MHz, CDCl₃, 25 °C) δ 159.6, 147.8, 144.6, 137.3, 136.0, 134.6, 128.6, 123.9, 122.7, 119.3, 116.0, 116.0, 31.9, 30.7, 30.5, 30.3, 29.2, 22.8, 14.2. HRMS (EI) calcd for C₄₀H₄₂N₄O₆ 674.3104 [M⁺], found 674.3086.



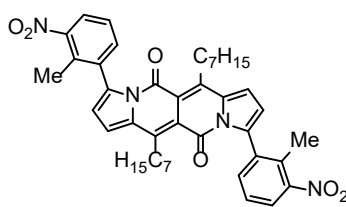
6,12-Diheptyl-3,9-bis(5-methoxy-2-nitrophenyl)-5H,11H-dipyrrolo[1,2-b:1',2'-g][2,6]naphthyridine-5,11-dione (11). Prepared using 2-bromo-4-methoxy-1-nitrobenzene (69.6 mg, 0.3 mmol). Time of heating: 72 h. Product was purified using column chromatography (SiO₂, hexanes : dichloromethane 1:1) followed by a SEC column (toluene). The residue after columns was dissolved on hot in *n*-hexane and the flask was stored overnight in the fridge. The crystals were filtered off to give 11.0 mg (15% yield) of product. R_f = 0.28 (SiO₂, hexanes : dichloromethane, 1:1). Mp. 171 - 172 °C. ¹H NMR (600 MHz, CDCl₃, 25 °C) δ 8.25 (d, 2H, J = 7.5 Hz), 6.99 (d, 1H, J = 2.4 Hz), 6.98 (d, 1H, J = 2.4 Hz), 6.95 (d, 2H, J = 2.4 Hz), 6.88 (d, 2H, J = 3.6 Hz), 6.48 (d, 2H, J = 2.4 Hz), 3.93 (s, 6H), 3.28-2.92 (br m, 4H), 1.62-1.53 (br s, 4H), 1.43-1.40 (m, 4H), 1.35-1.25 (m, 12H), 0.89 (t, 6H, J = 6.6 Hz). ¹³C NMR (151 MHz, CDCl₃, 25 °C) δ 162.9, 141.6, 135.1, 127.2, 127.2, 117.6, 117.4, 115.6, 113.3, 56.1, 32.0, 30.7, 30.7, 30.4, 29.0, 22.8, 14.3. HRMS (EI) calcd for C₄₂H₄₆N₄O₈ 734.3316 [M⁺], found 734.3293.



6,12-Diheptyl-3,9-bis(2-methyl-4-nitrophenyl)-5*H*,11*H*-dipyrrolo[1,2-

b:1',2'-g][2,6]naphthyridine-5,11-dione (12). Prepared using 1-bromo-2-methyl-4-nitrobenzene (64.8 mg, 0.3 mmol). Product was purified using column chromatography (SiO₂, hexanes : dichloromethane, 1:1). The residue

after column was reprecipitated from dichloromethane/methanol mixture to give 33.7 mg (48% yield) of product. *R_f* = 0.25 (SiO₂, hexanes : dichloromethane, 1:1). Mp. 244 - 245 °C. ¹H NMR (500 MHz, CDCl₃, 25 °C) δ 8.13 (d, 2H, *J* = 2.0 Hz), 8.11 (d, 1H, *J* = 2.0 Hz), 8.09 (d, 1H, *J* = 2.5 Hz), 7.42 (d, 2H, *J* = 8.0 Hz), 6.92 (d, 2H, *J* = 4.0 Hz), 6.44 (d, 2H, *J* = 4.0 Hz), 3.14 (br s, 4H), 2.28 (s, 6H), 1.63-1.57 (m, 4H), 1.45-1.39 (m, 4H), 1.33-1.23 (m, 12H), 0.86 (t, 6H, *J* = 7.0 Hz). ¹³C NMR (126 MHz, CDCl₃, 25 °C) δ 159.1, 147.6, 144.8, 140.7, 139.3, 136.3, 134.9, 130.2, 124.5, 120.7, 118.3, 115.8, 115.6, 31.8, 30.6, 30.2, 29.2, 22.8, 20.5, 14.2. HRMS (EI) calcd for C₄₂H₄₆N₄O₆ 702.3417 [M⁺], found 702.3441.



6,12-Diheptyl-3,9-bis(2-methyl-3-nitrophenyl)-5*H*,11*H*-dipyrrolo[1,2-

b:1',2'-g][2,6]naphthyridine-5,11-dione (13). Prepared using ethyl 1-bromo-2-methyl-3-nitrobenzene (64.8 mg, 0.3 mmol). Product was purified

using column chromatography (SiO₂, hexanes : dichloromethane, 1:1). The residue after column was reprecipitated from dichloromethane/methanol mixture to give 41.7 mg (59% yield) of product. *R_f* = 0.31 (SiO₂, hexanes : dichloromethane, 1:1). Mp. 232 - 234 °C. ¹H NMR (500 MHz, CDCl₃, 25 °C) δ 7.92 (d, 2H, *J* = 8.0 Hz), 7.51 (d, 2H, *J* = 6.5 Hz), 7.37 (t, 2H, *J* = 7.5 Hz), 6.90 (d, 2H, *J* = 3.5 Hz), 6.43 (d, 2H, *J* = 4.0 Hz), 3.24-3.06 (br m, 4H), 2.33 (s, 6H), 1.64-1.57 (m, 4H), 1.46-1.40 (m, 4H), 1.34-1.24 (m, 12H), 0.87 (t, 6H, *J* = 6.5 Hz). ¹³C NMR (126 MHz, CDCl₃, 25 °C) δ 159.1, 150.4, 144.7, 137.2, 136.4, 134.6, 133.6, 132.8, 126.0, 124.3, 118.3, 115.5, 31.9, 30.7, 30.6, 30.3, 29.2, 22.8, 17.2, 14.2. HRMS (EI) calcd for C₄₂H₄₆N₄O₆ 702.3417 [M⁺], found 702.3426.

2. X-ray crystal structures of selected compounds

X-ray crystallography for the exemplary DPNDs, **7**, **9** and **12**, unambiguously confirms the twisted conformations of the constructed dyes (Figures S1-S2, see below). In these derivatives, the DPND core adopts a nearly planar geometry. Deviations from the planarity are greater for **7** (0.075 Å), **9** (0.108 Å) and **12** (0.115 Å) than those noted for an analog of **1** bearing ethyl alkyl chains¹ (0.018 Å). In addition to the interactions between the carbonyl oxygens and the alkyl chains, the introduction of aryl rings at positions 3 and 9 of the DPND core introduces steric repulsion between these aryl substituents and the carbonyl moieties within the central core. This same set of interactions is responsible for the significant deviation of the bond angles around the carbonyl carbons from their ideal trigonal planar value of 120°.

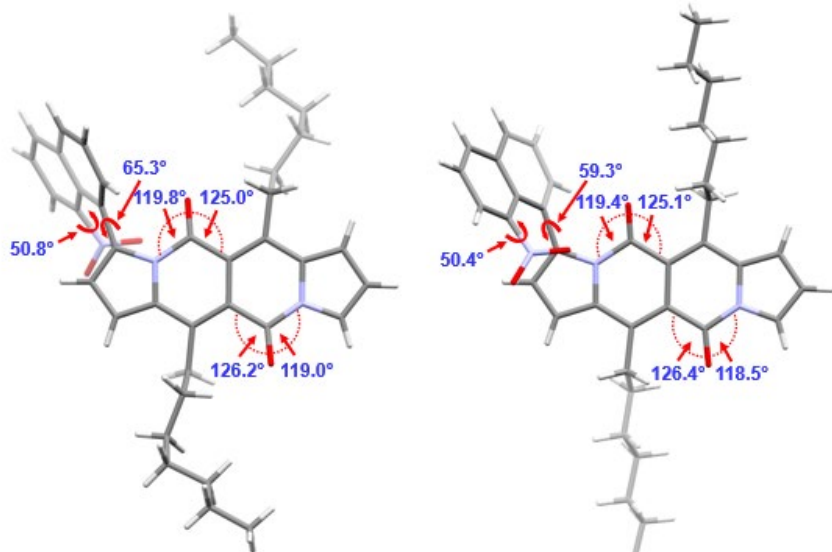
The average dihedral angles between adjacent aryl moieties in **9** and **12** are calculated to be 51.6° and 56.1°, respectively. These values are smaller than that determined previously for molecule **2** (58.9°),² suggestive of planarity-inducing weak electronic communication between the nitro-enriched aryls and the DPNd core. Intuitively, *peri* interactions in **7** considerably enhance steric repulsion, which results in a large dihedral angle (59.3-65.3°) as well as a significant distortion of the nitro group (Figure S1a). As the rotation of the naphthyl unit around the C_{naphthyl}-CDPNd bond is blocked, compound **7** crystallizes as a racemic mixture of (*P*)-and (*M*)-isomers (Figure S1a). The analysis of these crystal structures demonstrates that the introduction of nitrophenyl moieties at the peripheries of DPNd leads to molecules with slightly decreased dihedral angles, on average, as revealed by comparing the values of **9** and **12** with that of **2**.² Nevertheless, the nitroaromatics that we synthesized for this investigation still adopt twisted conformations in spite of the weak electronic coupling through biaryl linkages.

Table S1. Summary of crystal data for derivatives **7** and **9** and **12**.

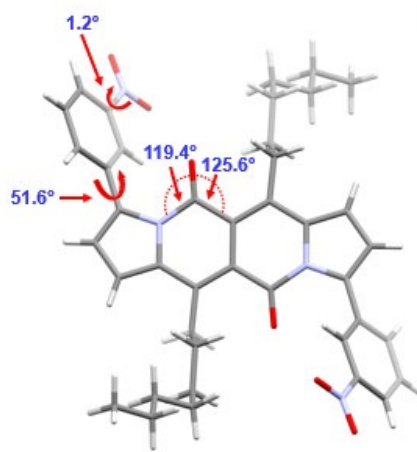
Compound	7	9	12
Chemical formula	C ₃₈ H ₄₁ N ₃ O ₄	C ₄₀ H ₄₂ N ₄ O ₆	C ₄₂ H ₄₆ N ₄ O ₆
Weight (g·mol⁻¹)	603.74	674.77	702.83
Crystal system	Monoclinic	Monoclinic	Monoclinic
Space group	P2 ₁ /n	P2 ₁ /n	P2 ₁ /c
a (Å)	28.1693(2)	4.2829(4)	4.8094(2)
b (Å)	7.8436(4)	27.290(2)	12.3555(4)
c (Å)	28.7267(2)	14.9334(13)	31.0929(10)
α (°)	90	90	90
β (°)	99.930(1)	91.466(4)	93.544(2)
γ (°)	90	90	90
Volume (Å³)	6252.0(3)	1744.9(3)	1844.09(11)
Z	8	2	2
Density (Mg m⁻³)	1.283	1.284	1.266
Temperature (K)	100	100	296
F(000)	2576.0	716.0	748.0

Indep. Refl.	11425	4022	3383
Final R indices [I > 2σ(I)]	R = 0.0537 R _w = 0.1326	R = 0.0580 R _w = 0.1615	R = 0.0821 R _w = 0.2792
S	1.147	1.068	1.037

(a)



(b)



(c)

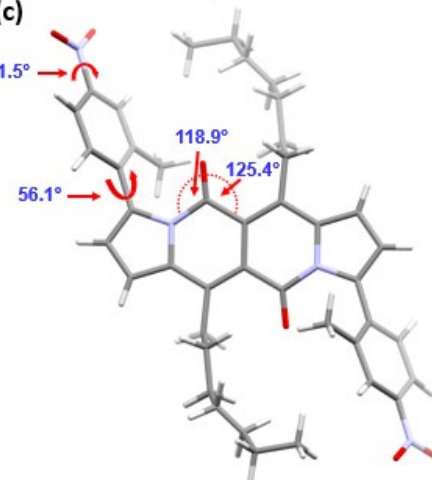


Figure S1. The crystallographic structures of DPNDs **7** (a, isomer (*P*) – left, isomer (*M*) – right), **9** (b) and **12** (c) and selected structural parameters.

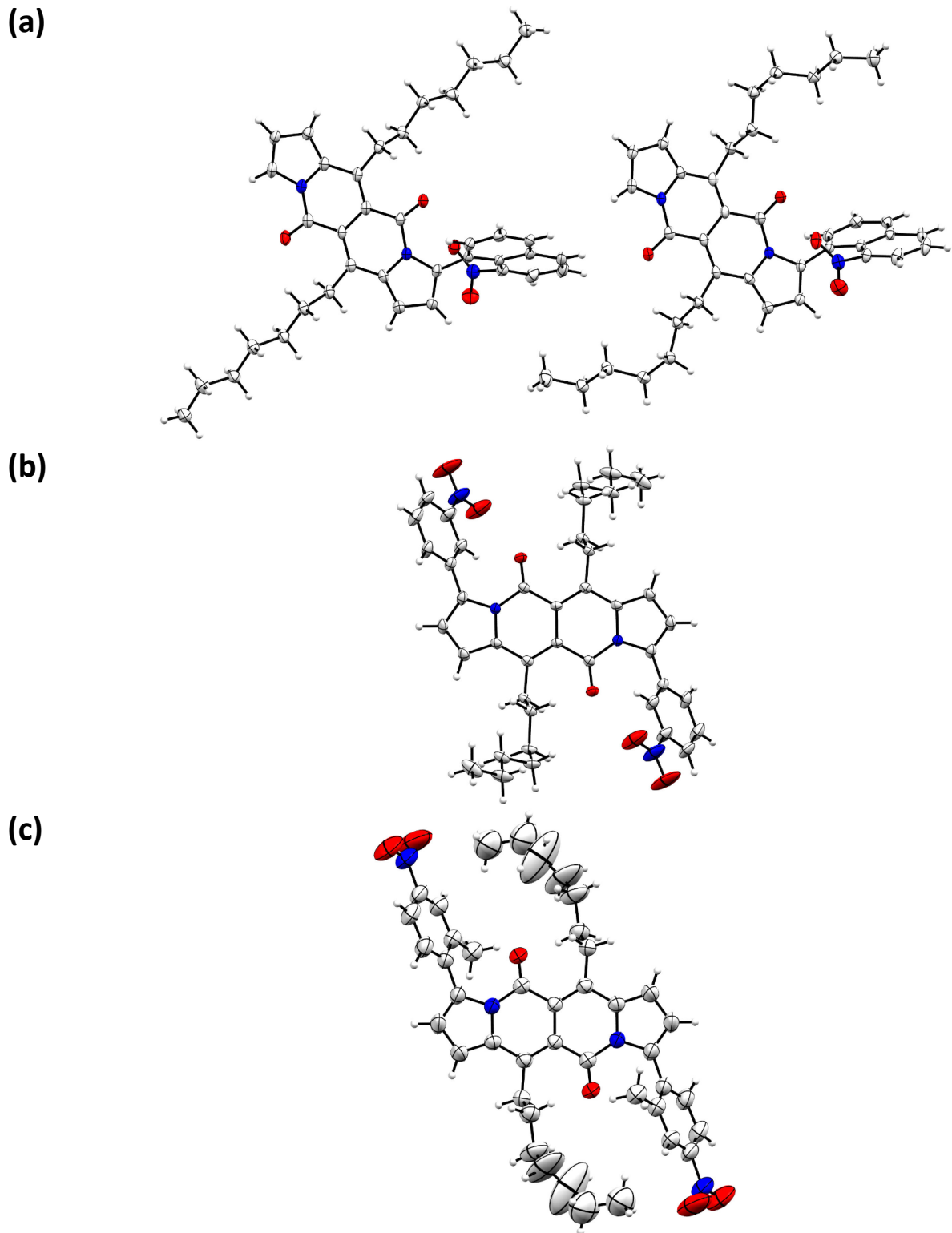


Figure S2. Solid-state structures of **7** (a), **9** (b) and **12** (c) as determined by X-ray crystallography. All non-hydrogen atoms are depicted as thermal ellipsoids at the 50% probability level. Legend: C, gray; N, blue; O, red; H, white.

3. Spectroscopic measurements

General Remarks. The femtosecond transient absorption setup used in this research has been described elsewhere.⁶ The device is composed of a Ti:sapphire oscillator (Micra 10, Coherent) amplified by a 1 kHz regenerative amplifier (Legend Elite, Coherent). The amplified output pulse centered at 800 nm with energy of 2.9 mJ and time duration of 45 fs after being split generates the pump pulse in an optical parametric amplifier (OPERA SOLO, Coherent). Another part of 800 nm beam is directed to the sapphire crystal generating white light continuum that covers the spectral range between 400 and 1100 nm. The detection system is composed of a monochromator (Acton SP2300, Princeton Instruments) and a pair of diode array detectors working in spectral range between 400 and 1000 nm. The samples were excited at 480 nm with pump intensity of 400 μ W and measured in the range of 500–760 nm. The beam radius was 0.4 mm. To detect the isotropic response of the medium, the magic angle configuration of pump and probe beams was applied. The instrument response function (I_{IRF}) was measured in ACN and the fit of gaussian function to temporal profile of transient absorption signal gave τ_{IRF} of 150 fs.

Time-integrate UV–VIS absorption spectra were recorded on Shimadzu UV-3101PC spectrometer.

Emission spectra were recorded on FluoroLog HORIBA Jobin Yvon spectrometer. The measurements of **time-resolved fluorescence** were carried out using time-correlated single photon counting system FluoroLog HORIBAJobin Yvon with FluoroHub. The IRF of the experiments was 1.5 ns.

Global analysis of transient absorption signals. The multiexponential function convolved with the instrument response function represented by gaussian function was used to globally fit the transient absorption decays in whole spectral range as follows:

$$\Delta A(\lambda, t) = \Delta A_\infty(\lambda) + \int dt' \sum_{i=1}^n A_i(\lambda) e^{-\frac{t'}{\tau_i}} I_{IRF}(t - t')$$

$$I_{IRF} = \frac{1}{\sqrt{2\pi}\tau_{IRF}} e^{-\left(\frac{t}{\tau_{IRF}}\right)^2} \quad (S1)$$

⁶ N. Subba, K. Polok, P. Piatkowski, B. Ratajska-Gadomska, R. Biswas, W. Gadomski, P. Sen, *J. Phys. Chem. B* **2019**, *123*, 9212–9221.

where $\Delta A(\lambda,t)$ is wavelength- and time-dependent transient absorption (TA) signal, $\Delta A_\infty(\lambda)$ is non-zero offset of TA decays. $A_i(\lambda)$ is pre-exponential factor (amplitude) related to time constants τ_i of multiexponential fits to the experimental data.

Steady-state (time-integrated) and time-resolved absorption and emission studies.

Comparison of the absorption spectra of dyes in different solvents indicates small red shift of their maxima in DCB, DCM and ACN as compared to those in HEX (Figure S3-S15 and Table S2). Moreover the shift in chlorinated solvents is larger than that in the most polar ACN. Usually, bathochromic shift in the absorption band with increasing surroundings polarity is ascribed to a stronger stabilization of the excited state as compared to S_0 one.^{7,8} Such situation happens when dipole moment (μ) of S_1 is larger than that in S_0 . If this mechanism is responsible for the observed changes, however, we would expect the largest absorption shift in ACN as compared to those in DCB and DCM, which is not the case. The interactions of DPND and its derivatives with solvents cannot be simply explained by effect of surroundings polarity, but some specific local interactions might influences the observed photophysical properties. Due to a presence of an electron acceptor (carbonyl) and donor (pyrrole) groups local interactions with solvent molecule are possible. It was reported that strong localization of electronic charge on C=O and N-C bonds in S_0 and S_1 states of DPND may significantly influence solvents molecules, especially the cavity of polar solvent.¹ The largest red shift is observed for dyes in DCB which has the highest viscosity (1.32 cP) among all utilized solvents. The viscous surroundings may impede the intramolecular movements (*e.g.* rotation or twisted motion) of side groups and/or changes in the planarity of chromophore leading to stabilization of S_1 , which result in decrease of its energy.⁹ The change of nonpolar surroundings form HEX to more polar solvents leads to a red shift in the emission spectra of all dyes. However, in most dyes almost no difference between main maximum band of all dyes is observed in DCB, DCM and ACN, thus supporting the statement that the change in

⁷ B. Maity, A. Chatterjee, D. Seth, *Photochemistry and Photobiology* **2014**, *90*, 734-746.

⁸ C. Reichardt, Solvents and Solvent Effects in Organic Chemistry, Wiley-VCH, Weinheim **2003**.

⁹ P. Piatkowski, M. Moreno, M. Liras, F. Sanchez, A. Douhal, *J. Mater. Chem. C* **2019**, *7*, 7872-7884.

polarity cannot fully explain the observed shift in these dyes (Figures S3-S15 and Table S2). The change in $\lambda_{\text{em}}^{\text{max}}$ shows that slightly larger bathochromic shift occurs in the most viscous DCB solvent which suggests the stabilization of S_1 state by hindering of intramolecular movements, in agreement with the results for the absorption.

A close examination of the solvent dependence on absorption reveals that the chlorinated solvents tend to decrease \mathcal{E}_{abs} (Figure 4A,B). One may ascribe this effect to halogen bonding¹⁰ of the solvent with the dyes, stabilizing their S_1 state relative to their S_0 states (or indistinguishably, destabilizing their S_0 state relative to their S_1 state), leading to a decrease in the S_0 - S_1 energy gap.¹¹ Such effects of halogenated solvents on the electronic states of solvated dyes are especially pronounced when the chromophores contain both electron acceptor and donor moieties.¹²

Except for **3**, the two ester solvents, PB and SOA, induce pronounced bathochromic shifts in the fluorescence maxima that do not follow the polarity trends observed with hydrocarbon and halogenated solvents (Figure 4A,B). A close examination of the emission spectra reveals two vibronic peaks, separated by about 0.2 eV, which dominate the band maxima (Figures S3-S28). For most solvents the high-energy vibronic peak dominates the fluorescence bands. For SOA and PB, however, the low-energy peak defines the emission maxima (Figure S15). While these ester-induced changes in the vibronic amplitudes are in the order of about 10% or less, they induce 0.2 eV bathochromic shifts in the fluorescence maxima. Hydrogen bonding cannot account for this behavior: the dyes and the ester solvents have hydrogen-bond acceptors but no hydrogen-bond donors. Considering the high polarity of ester and amide groups,¹³ electrostatic interactions can account for the observed effects on the amplitudes of the vibronic features in the $S_1 \rightarrow S_0$ radiative transitions. Charge localization on the C=O

¹⁰ A. R. Vota, P. Khuu, K. Oishi, P. S. Ho, *Nat. Chem.* **2009**, *1*, 74-79.

¹¹ R. M. El-Shishtawy, F. A. M. Al-Zahrani, S. M. Afzal, M. A. N. Razvi, Z. M. Al-amshany, A. H. Bakry, A. M. Asiri, *RSC Adv.*, **2016**, *6*, 91546-91556.

¹² Y. Ooyama, R. Asada, S. Inoue, K. Komaguchi, I. Imae, Y. Harima, *New J. Chem.*, **2009**, *33*, 2311-2316.

¹³ S. Upadhyayula, D. Bao, B. Millare, S. S. Sylvia, K. M. Masum Habib, K. Ashraf, A. Ferreira, S. Bishop, R. Bonderer, S. Baqai, X. Jing, M. Penchev, M. Ozkan, C. S. Ozkan, R. K. Lake, V. I. Vullev, *J. Phys. Chem. B* **2011**, *115*, 9473-9490.

and N-C bonds, reported for the S_0 and S_1 states of DPND,¹ make these dyes prone to interactions with small polar groups in their solvent media, perturbing their optical transitions.

Our spectroscopic studies suggest that a transition through a dark state, $S_1^{(\text{dark})}$, is principally responsible for the quenching of the fluorescence of the nitroaryl DPNDs under study. The polarity of this state leads to the observed solvent effects on the fluorescence quantum yields of these compounds. We observed two patterns of behavior: (1) Compounds **3**, **4**, **8**, **9**, **12** and **13**, containing *meta*-nitrophenyl and *para*-nitrophenyl substituents (Figure 2), fluoresce strongly in non-polar media. An increase in solvent polarity weakens their fluorescence (Figure 4D). This behavior is consistent with the formation of a dark excited state that is more polar than the fluorescent S_1 state. (2) Compounds **5**, **6**, **7**, **10** and **11**, with *ortho* or *peri* nitro groups on their aryl substituents (Figure 2), are weakly fluorescent even in non-polar media (Figure 4D). An increase in media polarity completely quenches their emission (Table S2). This behavior is consistent with a transition to a highly polarized dark state that most likely has pronounced CT character and a high propensity for non-radiative deactivation to the ground state.

The amplitudes of the terms with the nanosecond lifetimes dominate the TA dynamics of the fluorescent DPNDs (Figures S40–S52). The negative values of the amplitudes at $\lambda \lesssim 650$ nm and the positive values at $\lambda \gtrsim 650$ nm are consistent with a decay of the 700 nm EA band that is simultaneous with the bleach recovery and the decrease in the SE signal. That is, the deactivation of the fluorescent S_1 state leads to the ground state without accumulation of any intermediate transients. For non-radiative deactivation that proceeds through a dark state ($S_1^{(\text{fl})} \rightarrow X_1^{(\text{dark})} \rightarrow S_0$), this finding indicates that the first transition from $S_1^{(\text{fl})}$ to $X_1^{(\text{dark})}$ is the rate-limiting step. The relatively large rate of the second step, $X_1^{(\text{dark})} \rightarrow S_0$, suggests that most likely the dark state has a singlet character, i.e., $X_1^{(\text{dark})} = S_1^{(\text{dark})}$ and the transition to S_0 does not involve intersystem crossing.

An increase in solvent polarity shortens the nanosecond lifetimes obtained from TCSPC. For **3**, **4**, **9** and **12** such an increase in polarity shortens their emission-decay lifetimes sufficiently to place them in the dynamic range of the pump-probe TA. As a consequence, tri-exponential global fits for two of the dyes produce sub-nanosecond lifetimes, τ_3 , that follow the polarity trend (Table S3). For **4** in

DCM, TA global fits produce $\tau_3 = 0.4$ ns, which is (1) an order of magnitude smaller than the excited-state lifetime of **4** in DCM, obtained from emission decays, and (2) more than three times larger than τ_2 that the TA global fits produced for **4** in ACN. The tri-exponential global fit of the TA for **11** in DCB gives a similar 0.4 ns lifetime that is six times larger than τ_2 in DCM. The di-*ortho*-nitrophenyl derivative, **9**, gives the longest picosecond lifetimes, and its τ_2 of 0.3 ns in ACN follows the polarity trend of the lifetimes obtained from emission decays for less polar solvents (Tables S2 and S3).

Table S2. Photophysical properties of DPNDs **1-13**.

cmpd	solvent ^a	$\mathcal{E}_{\text{abs}}/\text{eV}^b$	$\varepsilon \cdot 10^{-3}/\text{M}^{-1}\cdot\text{cm}^{-1}$ ^c	$\mathcal{E}_{\text{fl}}/\text{eV}^b$	$\Delta \mathcal{E}/\text{eV}^d$	Φ_{fl}	τ / ns ^e	$k_r \cdot 10^{-8}/\text{s}^{-1}f$	$k_{\text{nr}} \cdot 10^{-8}/\text{s}^{-1}f$	$\mathcal{E}_{\text{abs}}^{\text{theory}}/\text{eV}^g$	$\mathcal{E}_{\text{fl}}^{\text{theory}}/\text{eV}^g$
1	HEX	2.49	24	2.43	0.06	0.63	3.9	1.62	0.95	—	—
	DCB	2.44	28	2.35	0.09	0.81	5.1	1.59	0.37		
	DCM	2.46	25	2.37	0.09	0.73	5.7	1.28	0.47		
	ACN	2.49	26	2.36	0.13	0.65	5.7	1.14	0.61		
	PB	2.48	—	2.23	0.25	0.60	—	—	—		
	SOA	2.46	—	2.22	0.24	0.76	—	—	—		
2	HEX	2.32	26	2.15	0.17	0.27	2.5	1.08	2.92	—	—
	DCB	2.26	29	2.08	0.18	0.52	4.0	1.3	1.2		
	DCM	2.30	23	2.08	0.22	0.42	3.6	1.17	1.61		
	ACN	2.32	25	2.08	0.24	0.38	3.7	1.03	1.68		
	PB	2.31	—	1.97	0.34	0.46	—	—	—		
	SOA	2.30	—	1.98	0.32	0.67	—	—	—		
3	HEX	2.39	21	2.10	0.29	0.42	2.0	2.1	2.9	2.66 (0.82)	2.21 (0.84)
	DCB	2.32	22	2.02	0.30	0.76	3.8	2	0.63		
	DCM	2.34	20	2.02	0.32	0.36	2.6	1.38	2.46		
	ACN	2.39	22	2.01	0.38	0.006	0.075	1.34	66		
	PB	2.37	—	2.04	0.33	0.42	—	—	—		
	SOA	2.35	—	2.04	0.31	0.59	—	—	—		
4	HEX	2.42	25	2.28	0.14	0.48	2.3	2.09	2.26	2.68 (0.80)	2.23 (0.83)
	DCB	2.35	26	2.22	0.13	0.62	4.0	1.55	0.95		
	DCM	2.38	27	2.22	0.16	0.09	0.442	2.04	21		
	ACN	2.40	23	2.22	0.18	0.02	0.149	1.34	66		
	PB	2.40	—	2.09	0.31	0.42	—	—	—		

	SOA	2.38	—	2.10	0.28	0.75	—	—	—		
5	HEX	2.41	27	2.21	0.20	0.025	—	—	—	2.61 (0.71)	2.06 (0.65)
	DCB	2.35	22	2.10	0.25	— ^h	0.031	—	> 320		
	DCM	2.39	22	2.09	0.30	— ^h	0.007	—	> 1400		
	ACN	2.40	23	2.17	0.23	— ^h	0.004	—	> 2500		
	PB	2.40	—	2.01	0.39	0.004	—	—	—		
	SOA	2.38	—	2.01	0.37	0.026	—	—	—		
6	HEX	2.41	24	2.26	0.15	0.16	2.0	0.8	4.2	—	—
	DCB	2.33	24	2.10	0.23	0.02	0.117	1.71	84		
	DCM	2.35	23	2.19	0.16	— ^h	—	—	—		
	ACN	2.39	27	2.13	0.26	— ^h	—	—	—		
	PB	2.40	—	2.06	0.34	0.032	—	—	—		
	SOA	2.38	—	2.06	0.32	0.11	—	—	—		
7	HEX	2.41	24	2.21	0.20	0.008	—	—	—	2.58 (0.68)	1.91 (0.56)
	DCB	2.36	23	2.09	0.27	— ^h	0.026	—	> 380		
	DCM	2.38	19	2.10	0.28	— ^h	0.014	—	> 710		
	ACN	2.39	23	2.18	0.21	— ^h	0.013	—	> 770		
	PB	2.40	—	2.07	0.33	0.006	—	—	—		
	SOA	2.38	—	2.09	0.29	0.017	—	—	—		
8	HEX	2.30	21	2.11	0.19	0.28	2.2	1.27	3.27	2.50 (0.99)	2.05 (1.06)
	DCB	2.22	24	2.02	0.20	0.45	3.6	1.25	1.52		
	DCM	2.25	22	2.03	0.22	0.41	3.4	1.21	1.73		
	ACN	2.26	25	2.01	0.25	0.07	—	—	—		
	PB	2.27	—	1.92	0.35	0.48	—	—	—		
	SOA	2.25	—	1.94	0.31	0.77	—	—	—		
9	HEX	2.34	27	2.17	0.17	0.36	2.3	1.57	2.78	—	—
	DCB	2.27	31	2.11	0.26	0.49	3.6	1.36	1.42		
	DCM	2.31	33	2.11	0.20	0.28	2.2	1.27	3.27		
	ACN	2.33	30	2.12	0.21	0.04	0.309	1.29	31		
	PB	2.32	—	1.98	0.34	0.43	—	—	—		
	SOA	2.31	—	2.01	0.30	0.78	—	—	—		
10	HEX	2.33	21	2.09	0.24	0.08	—	—	—	2.41 (0.83)	1.90 (0.83)
	DCB	2.22	22	2.03	0.19	0.02	0.076	2.63	129		
	DCM	2.30	21	2.03	0.27	— ^h	0.012	—	> 830		
	ACN	2.30	18	2.02	0.28	— ^h	0.007	—	> 1400		
11	HEX	2.33	28	2.15	0.18	0.35	2.4	1.46	2.71	—	—

	DCB	2.27	26	2.05	0.22	0.37	0.37	1.63	25		
	DCM	2.30	29	2.06	0.24	— ^h	0.061	—	> 160		
	ACN	2.30	25	2.06	0.24	— ^h	0.034	—	> 290		
	PB	2.31	—	1.97	0.34	0.11	—	—	—		
	SOA	2.30	—	1.96	0.34	0.25	—	—	—		
12	HEX	2.39	20	2.20	0.19	0.83	4.0	2.07	0.43	—	—
	DCB	2.34	23	2.10	0.24	0.61	4.3	1.42	0.91		
	DCM	2.35	21	2.09	0.26	0.49	3.3	1.48	1.54		
	ACN	2.37	19	2.09	0.28	0.013	0.049	2.65	201		
	PB	2.37	—	2.01	0.36	0.72	—	—	—		
	SOA	2.36	—	2.04	0.32	0.90	—	—	—		
13	HEX	2.39	24	2.21	0.18	0.87	4.4	1.98	0.29	2.59 (0.84)	2.11 (0.86)
	DCB	2.36	28	2.19	0.17	0.94	4.7	2.0	0.13		
	DCM	2.38	25	2.19	0.19	0.92	4.8	1.92	0.17		
	ACN	2.39	28	2.19	0.20	0.43	2.7	1.59	2.11		
	PB	2.39	—	2.09	0.30	0.74	—	—	—		
	SOA	2.38	—	2.07	0.31	0.95	—	—	—		

^a HEX = *n*-hexane ($\varepsilon = 1.89$, $n = 1.375$, $fo(\varepsilon, n^2) = -1.8 \times 10^{-4}$, $\eta = 0.31$ cP); DCB = 1,2-dichlorobenzene ($\varepsilon = 9.93$, $n = 1.5514$, $fo(\varepsilon, n^2) = 0.37$, $\eta = 1.32$ cP)¹⁴; DCM = dichloromethane ($\varepsilon = 9.08$, $n = 1.424$, $fo(\varepsilon, n^2) = 0.44$, $\eta = 0.45$ cP); ACN = acetonitrile ($\varepsilon = 37.5$, $n = 1.3393$, $fo(\varepsilon, n^2) = 0.61$, $\eta = 0.37$ cP); PB = propyl butyrate ($\varepsilon = 4.3$, $n = 1.40$, $fo(\varepsilon, n^2) = 0.30$, $\eta = 0.781$ cP)¹⁵; SOA = sucrose octaacetate ($\varepsilon = 4.5$, $n = 1.466$, $fo(\varepsilon, n^2) = 0.27$, $\eta \rightarrow \infty$).¹⁶ Onsager polarity, $fo(x) = 2(x - 1)/(2x + 1)$, $fo(\varepsilon, n^2) = fo(\varepsilon) - fo(n^2)$. ^b Absorption and fluorescence maxima. ^c Molar extinction coefficients at the absorption maxima of the spectra plotted against wavelength abscissas. ^d Stokes' shifts. ^e Lifetimes of the emissive excited states obtained from time-correlated single photon counting (for $\tau \gtrsim 1.5$ ns) and from transient-absorption spectroscopy (for $\tau \lesssim 1.5$ ns). ^f Radiative and non-radiative decay rate constants: $k_r = \Phi_{fl} \tau^{-1}$ and $k_{nr} = (1 - \Phi_{fl})\tau^{-1}$. ^g S₀→S₁ absorption and S₁→S₀ fluorescence energies and oscillator strengths (*f*) (given in brackets for the respective transition) computed with the ADC(2)/cc-pVDZ method at the MP2/ADC(2) equilibrium geometry of the S₀/S₁ state, respectively (see Computational Studies for more details). ^h $\Phi_{fl} < 10^{-3}$.

¹⁴ a) M. Terazima, *J. Chem. Phys.* **1996**, *104*, 4988. b) A. I. Abramovich, L. V. Lanshina, I. D. Kargin, *Russ. Chem. Bull.* **2017**, *66*, 828–832. c) A. Rostamkolahi, A. Rostami, F. Koohyar, F. Kiani, *Chem. Pap.* **2013**, *67*, 1433–1441.

¹⁵ G. J. Cox, J. H. Ferguson, M. L. Dodds, *Ind. Eng. Chem.* **1933**, *25*, 968–970.

¹⁶ A. H. Gill, F. P. Dexter, *Ind. Eng. Chem.* **1934**, *26*, 881.

Table S3. Values of TA time components (τ_1 , τ_2 and τ_3) and emission lifetimes (τ_{emis}). The TA time constants are from global double multiexponential fits of the TA decays of dyes in various solvents upon excitation at 480 nm. For the chromophores in which the decays were longer than the time window of the TA experiment (1.5 ns), the value of the longest time component was taken from the results of time-resolved emission studies and it was kept constant during the fit. The emission lifetimes are from monoexponential fit to emission decays.

Dye	Solvent	τ_1/ps	τ_2/ps	τ_3/ps	$\tau_{\text{emis}}/\text{ps}$
1	DCB	0.9	106	-	5100
	DCM	0.6	56	-	5700
	ACN	0.2	26	-	5700
2	DCB	1.6	132	-	4000
	DCM	1	123	-	3600
	ACN	0.7	101	-	3700
3	DCB	3	29	-	3800
	DCM	2.2	11	-	2600
	ACN	2.4	75	-	-
4	DCB	1.8	28	-	4000
	DCM	1.4	19	442	-
	ACN	1	149	-	-
5	DCB	2.2	31	-	-
	DCM	1.1	7.2	-	-
	ACN	1.1	4.4	-	-
6	DCB	4.8	117	-	-
	DCM	1.5	21	-	-
	ACN	1.1	8.9	-	-
7	DCB	5	26	-	-
	DCM	2.3	14	-	-
	ACN	2.4	13	-	-
8	DCB	2.9	40	-	3600
	DCM	1.3	31	-	3400
9	DCB	5.9	119	-	3600
	DCM	2.3	106	-	2200
	ACN	1.9	309	-	-
10	DCB	4.1	76	-	-
	DCM	1.3	12	-	-
	ACN	0.8	7	-	-
11	DCB	2	18	368	-
	DCM	2.2	61	-	-
	ACN	1.7	34	-	-
12	DCB	5.3	81	-	4300
	DCM	1.5	52	-	3300
	ACN	2.1	49	-	-
13	DCB	5.6	89	-	4700
	DCM	2.6	44	-	4800

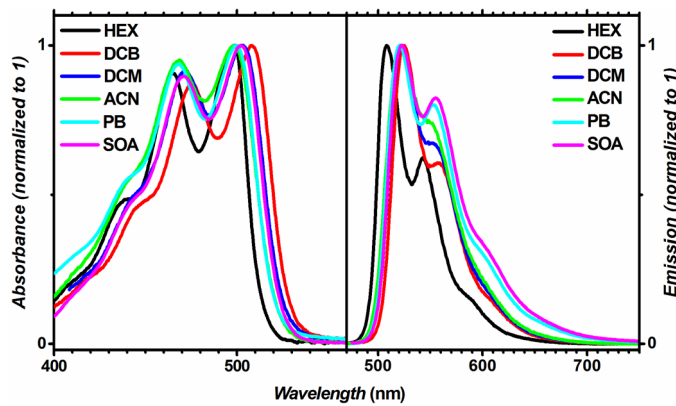


Figure S3. Absorption and emission spectra of **1** in HEX, DCB, DCM, ACN, PB and SOA. The emission spectra were recorded upon excitation at 450 nm.

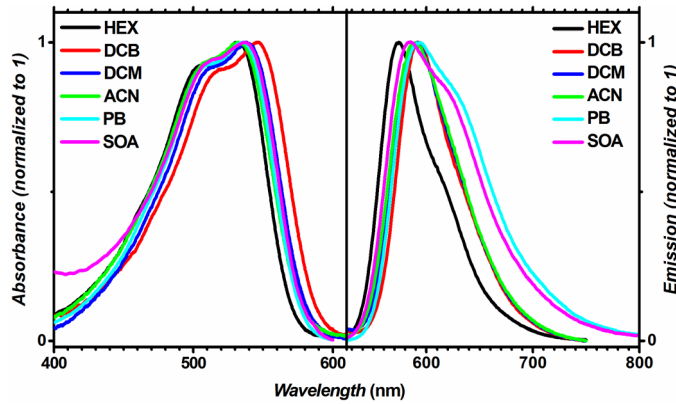


Figure S4. Absorption and emission spectra of **2** in HEX, DCB, DCM, ACN, PB and SOA. The emission spectra were recorded upon excitation at 450 nm.

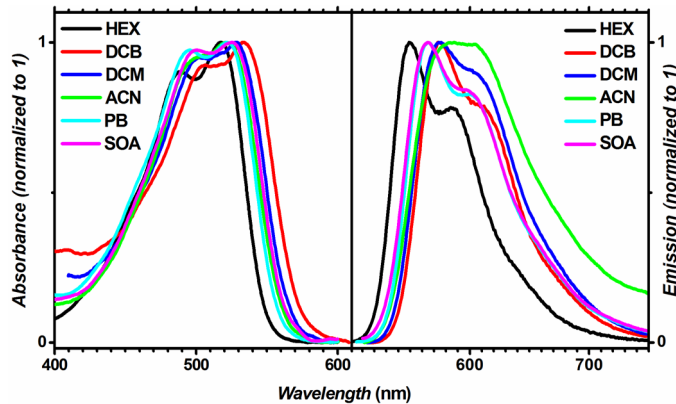


Figure S5. Absorption and emission spectra of **3** in HEX, DCB, DCM, ACN, PB and SOA. The emission spectra were recorded upon excitation at 450 nm.

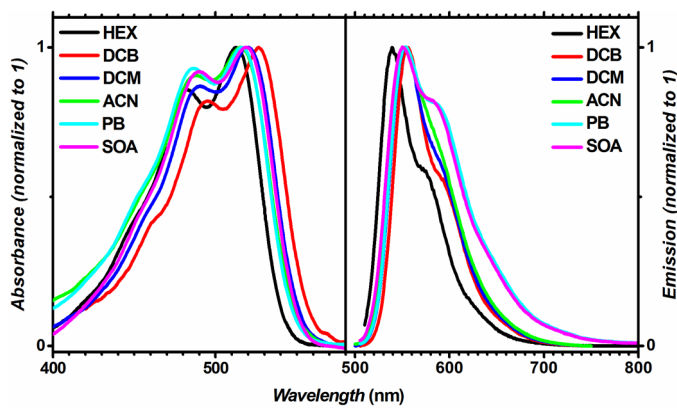


Figure S6. Absorption and emission spectra of **4** in HEX, DCB, DCM, ACN, PB and SOA. The emission spectra were recorded upon excitation at 500 nm.

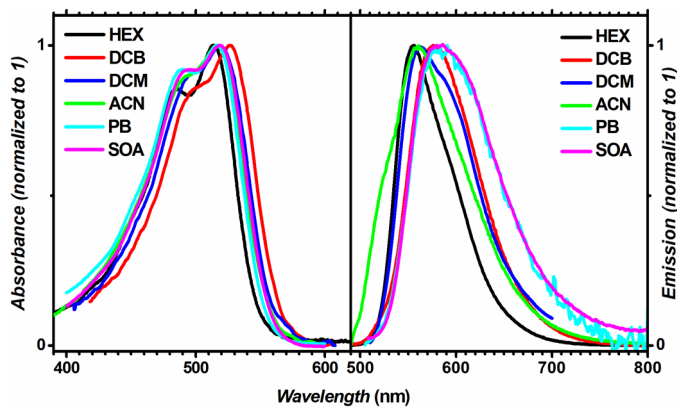


Figure S7. Absorption and emission spectra of **5** in HEX, DCB, DCM, ACN, PB and SOA. The emission spectra were recorded upon excitation at 480 nm.

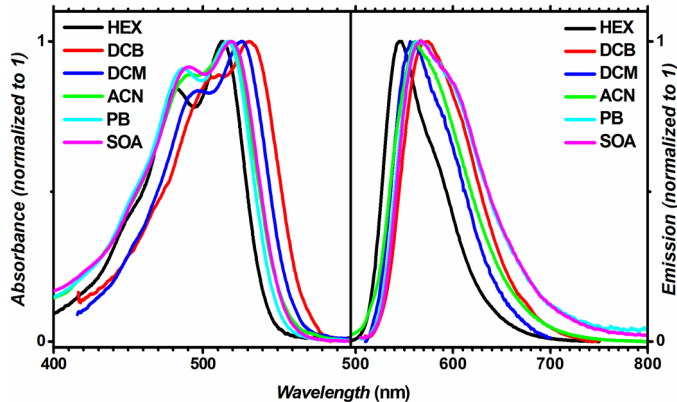


Figure S8. Absorption and emission spectra of **6** in HEX, DCB, DCM, ACN, PB and SOA. The emission spectra in HEX/ACN and DCB/DCM were recorded upon excitation at 480 and 500 nm.

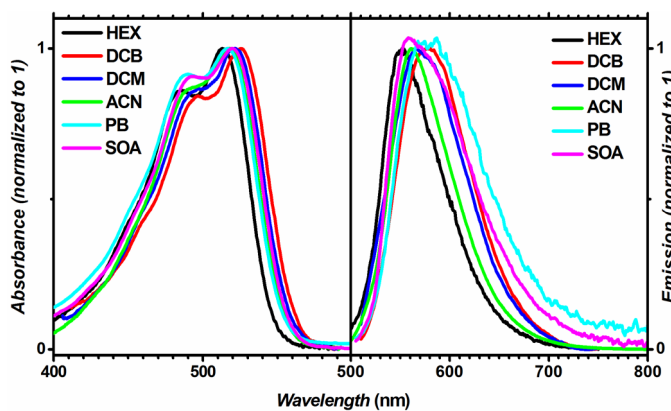


Figure S9. Absorption and emission spectra of **7** in HEX, DCB, DCM, ACN, PB and SOA. The emission spectra in HEX/ACN and DCB/DCM were recorded upon excitation at 490 and 500 nm.

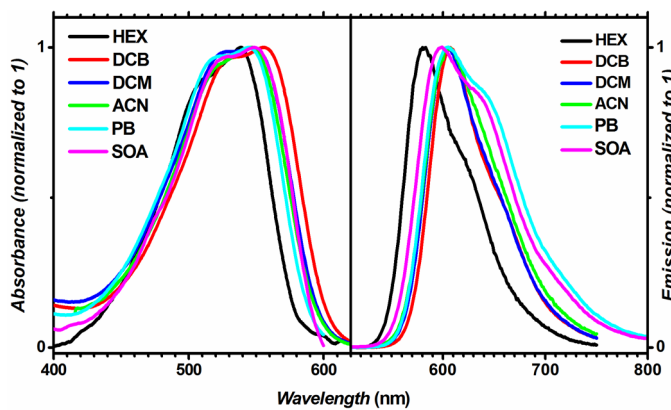


Figure S10. Absorption and emission spectra of **8** in HEX, DCB, DCM, ACN, PB and SOA. The emission spectra were recorded upon excitation at 505 nm.

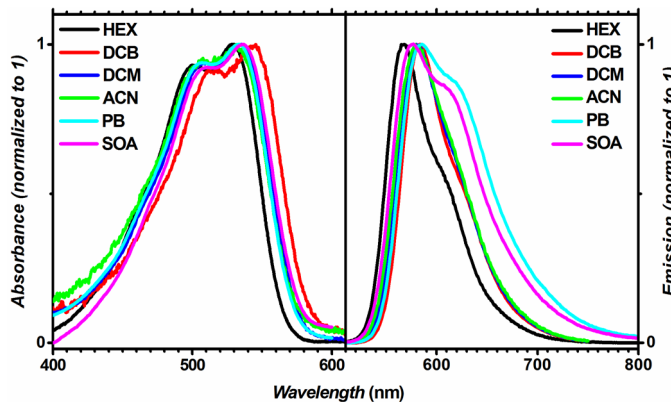


Figure S11. Absorption and emission spectra of **9** in HEX, DCB, DCM, ACN, PB and SOA. The emission spectra were recorded upon excitation at 500 nm.

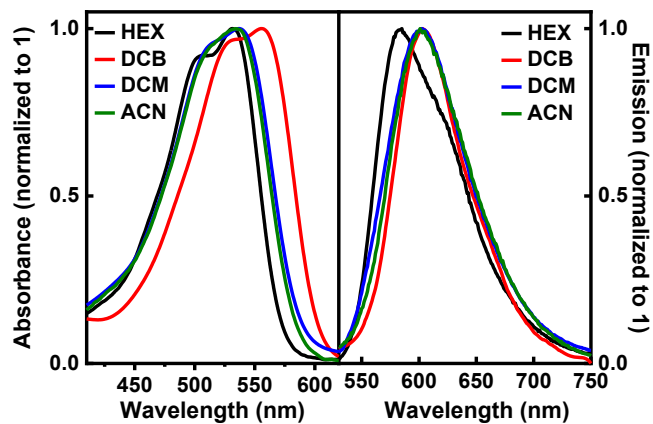


Figure S12. Absorption and emission spectra of **10** in HEX, DCB, DCM and ACN. The emission spectra of **10** were recorded upon excitation at 510 in DCB, DCM and ACN, and 500 nm in HEX.

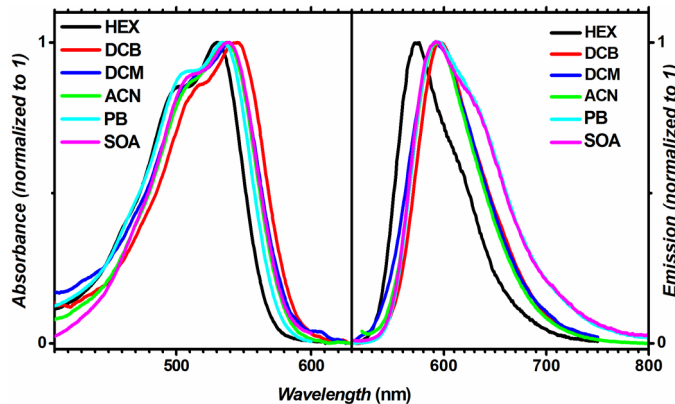


Figure S13. Absorption and emission spectra of **11** in HEX, DCB, DCM, ACN, PB and SOA. The emission spectra of **11** were recorded upon excitation at 500 in DCB, DCM and ACN, and 490 nm in HEX.

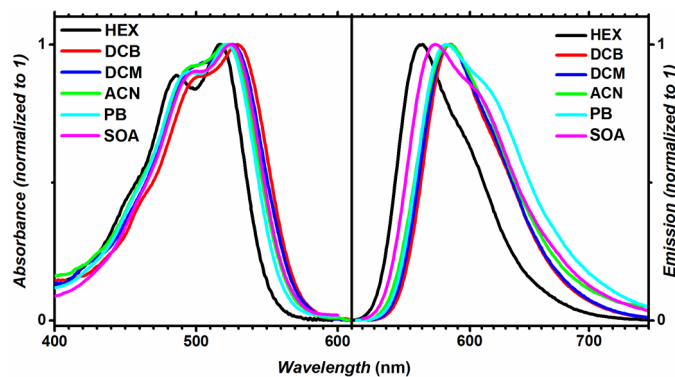


Figure S14. Absorption and emission spectra of **12** in HEX, DCB, DCM, ACN, PB and SOA. The emission spectra of **12** were recorded upon excitation at 505 in DCB, DCM and ACN, and 470 nm in HEX.

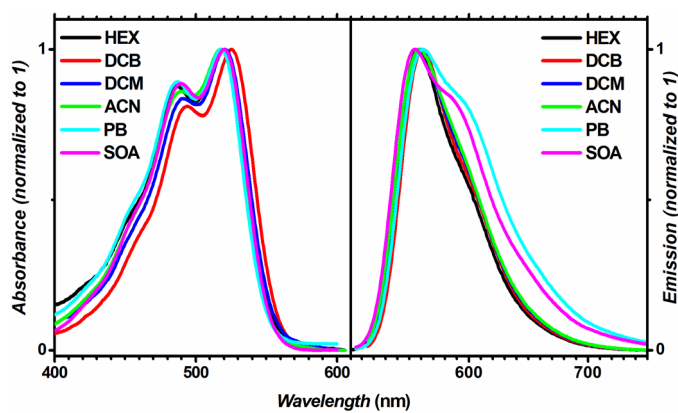


Figure S15. Absorption and emission spectra of **13** in HEX, DCB, DCM, ACN, PB and SOA. The emission spectra of **13** were recorded upon excitation at 505 in DCB, DCM and ACN, and 470 nm in HEX.

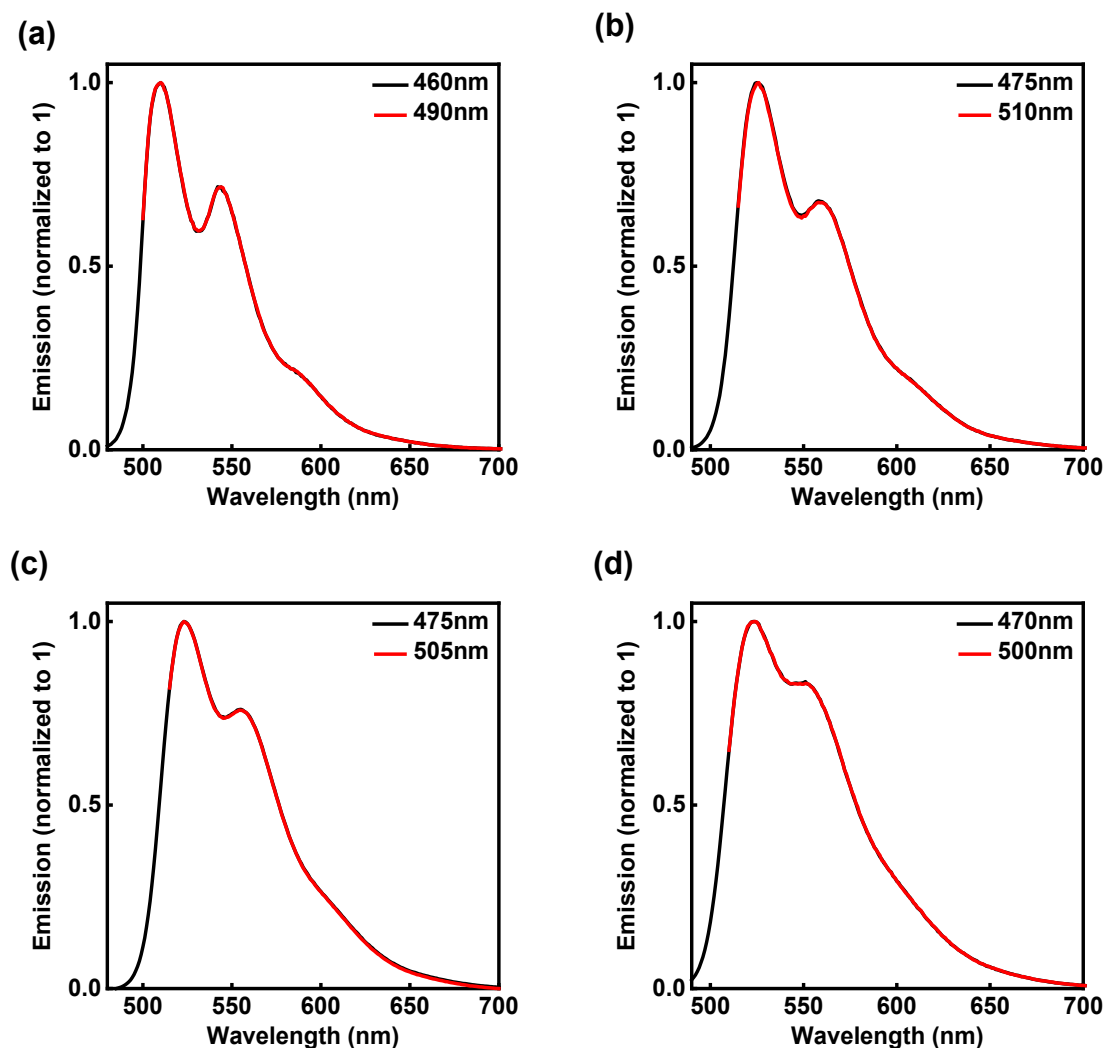


Figure S16. Emission spectra of **1** in (a) HEX, (b) DCB, (c) DCM and (d) ACN. The emission spectra of **1** were recorded upon excitation at the indicated wavelengths.

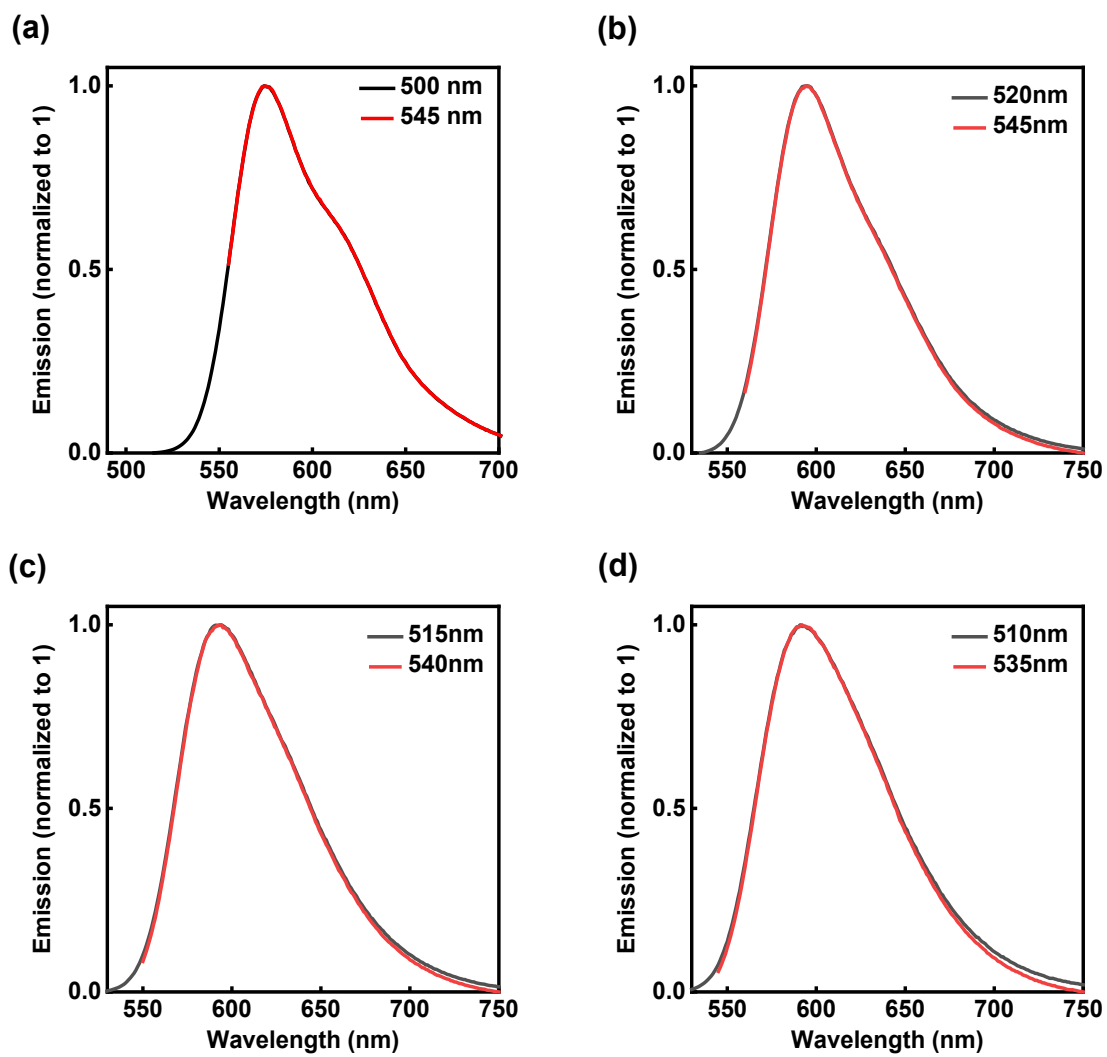


Figure S17. Emission spectra of **2** in (a) HEX, (b) DCB, (c) DCM and (d) ACN. The emission spectra of **2** were recorded upon excitation at the indicated wavelengths.

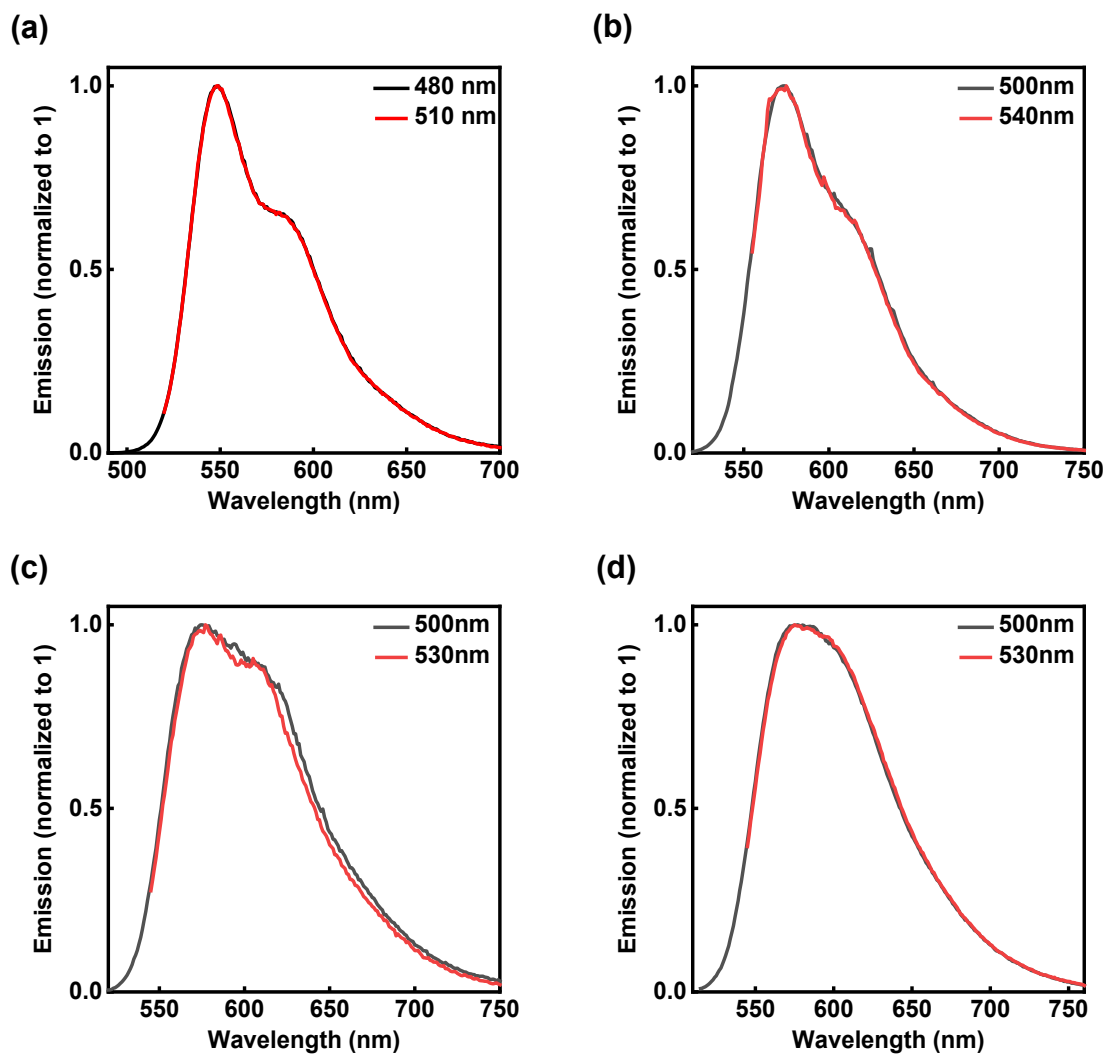


Figure S18. Emission spectra of **3** in (a) HEX, (b) DCB, (c) DCM and (d) ACN. The emission spectra of **3** were recorded upon excitation at the indicated wavelengths.

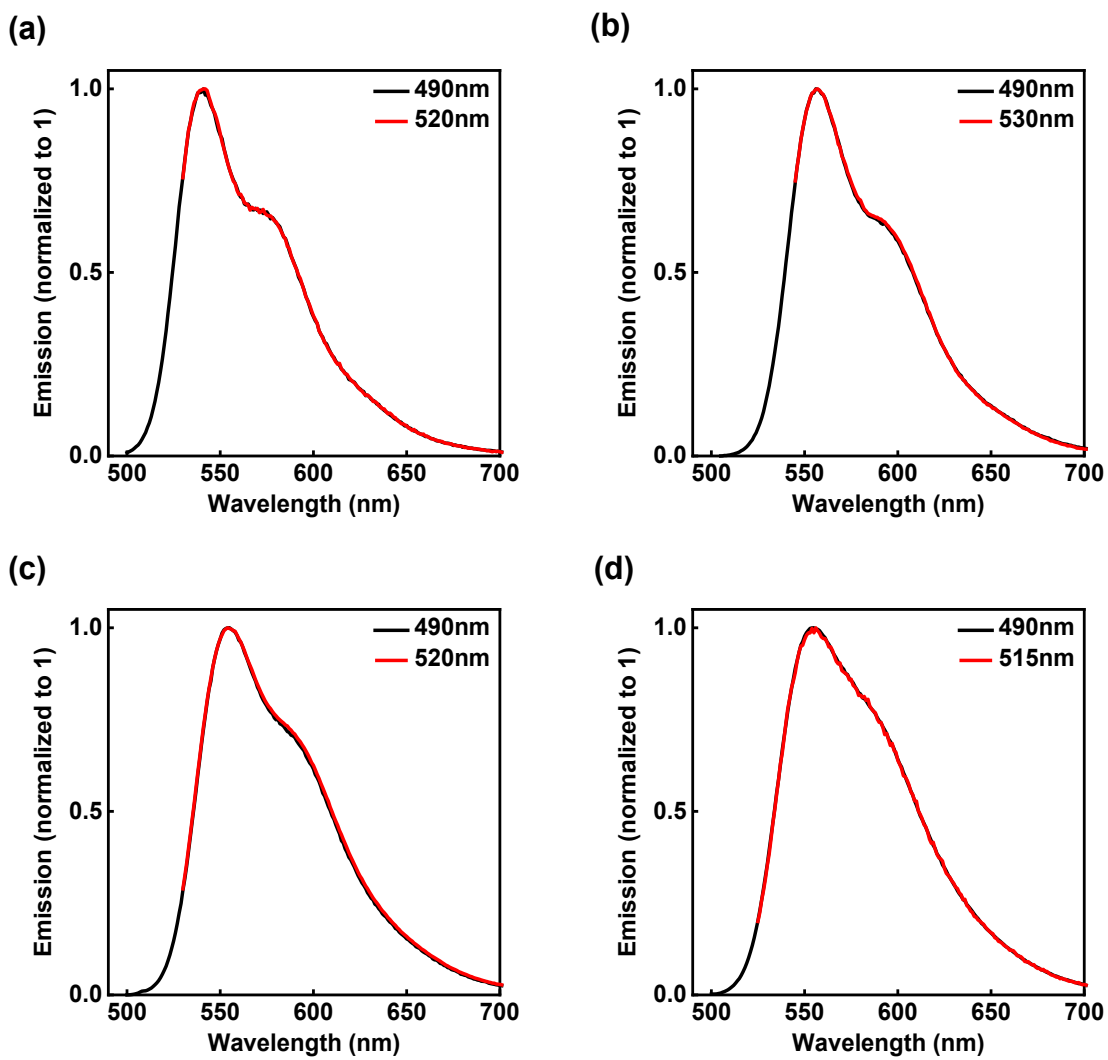


Figure S19. Emission spectra of **4** in (a) HEX, (b) DCB, (c) DCM and (d) ACN. The emission spectra of **4** were recorded upon excitation at the indicated wavelengths.

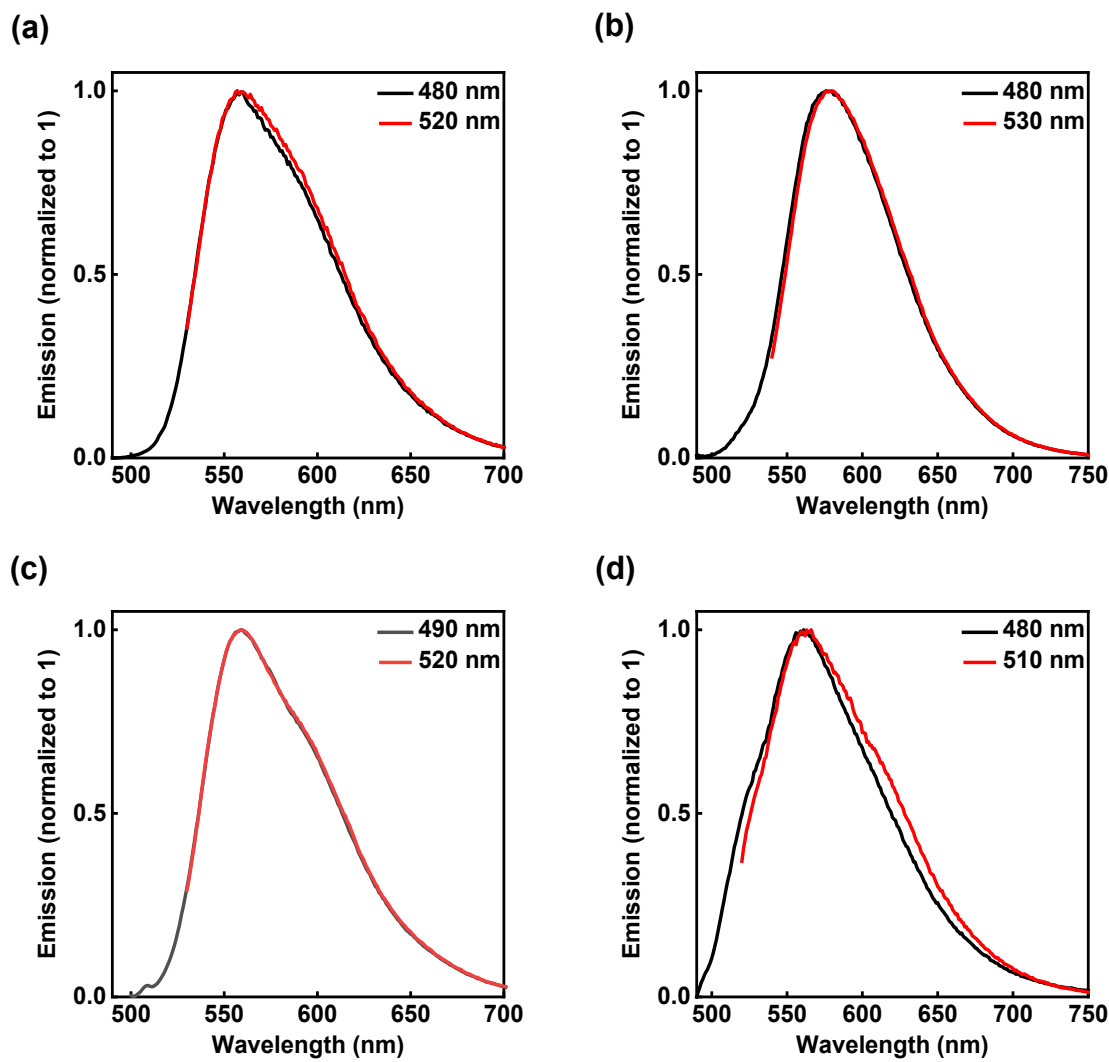


Figure S20. Emission spectra of **5** in (a) HEX, (b) DCB, (c) DCM and (d) ACN. The emission spectra of **5** were recorded upon excitation at the indicated wavelengths.

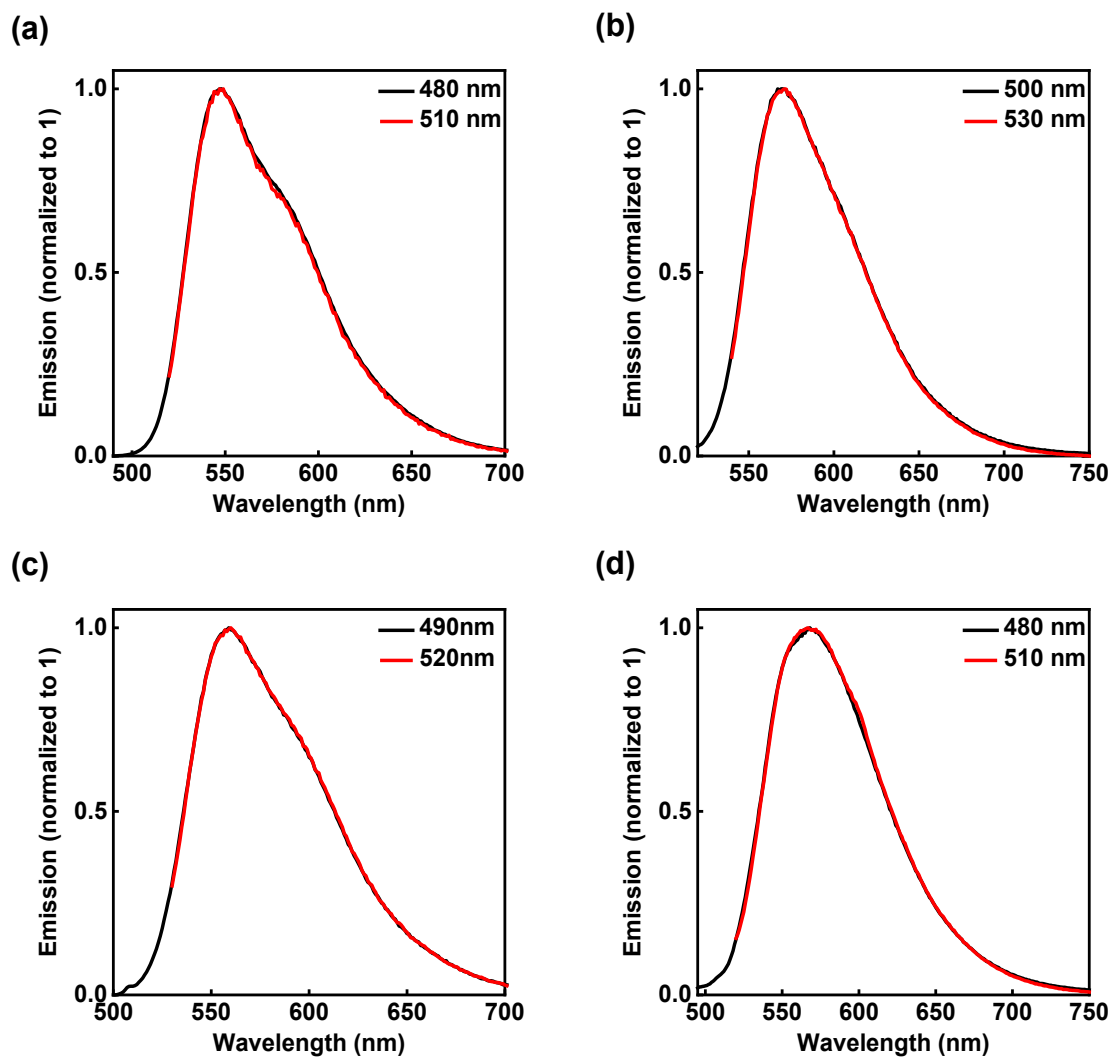


Figure S21. Emission spectra of **6** in (a) HEX, (b) DCB, (c) DCM and (d) ACN. The emission spectra of **6** were recorded upon excitation at the indicated wavelengths.

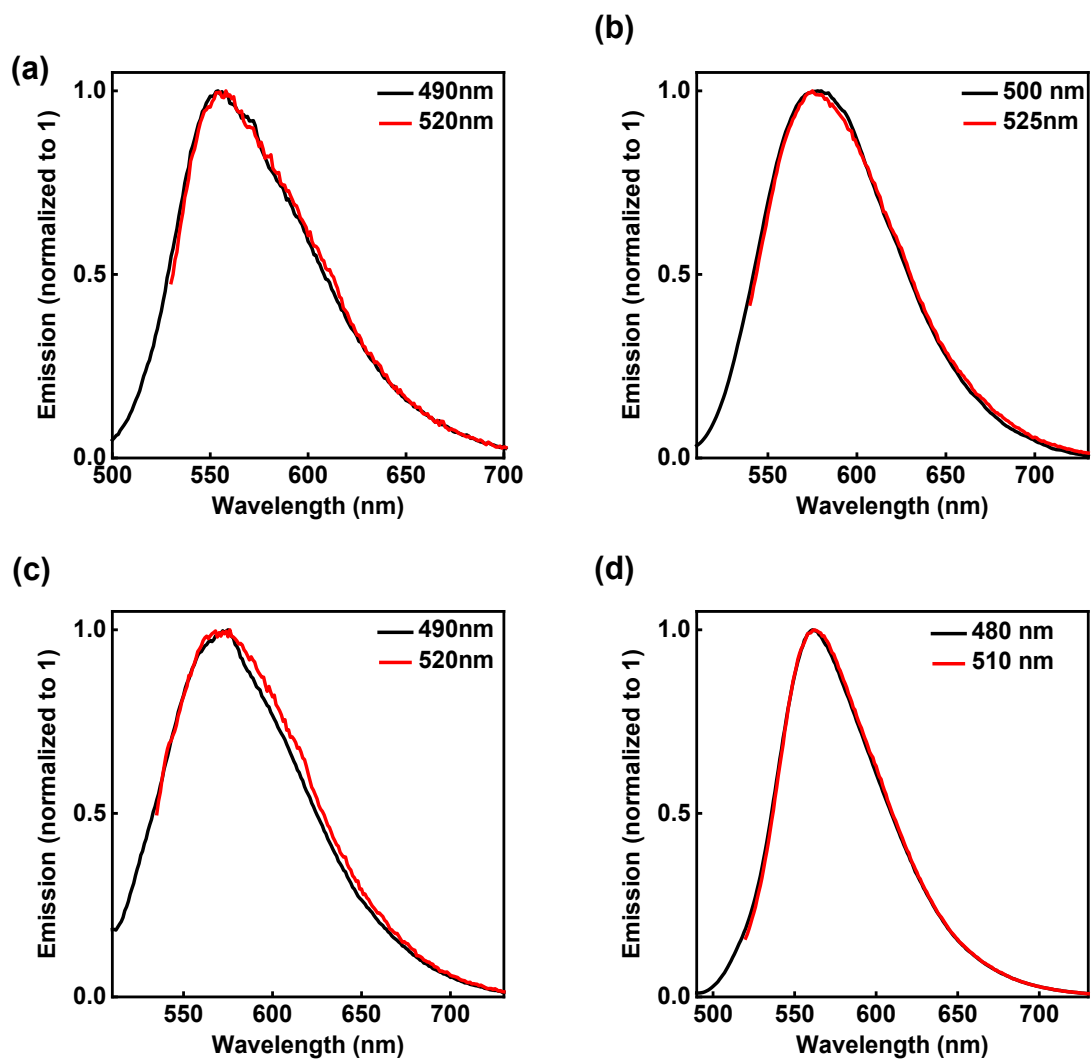


Figure S22. Emission spectra of 7 in (a) HEX, (b) DCB, (c) DCM and (d) ACN. The emission spectra of 7 were recorded upon excitation at the indicated wavelengths.

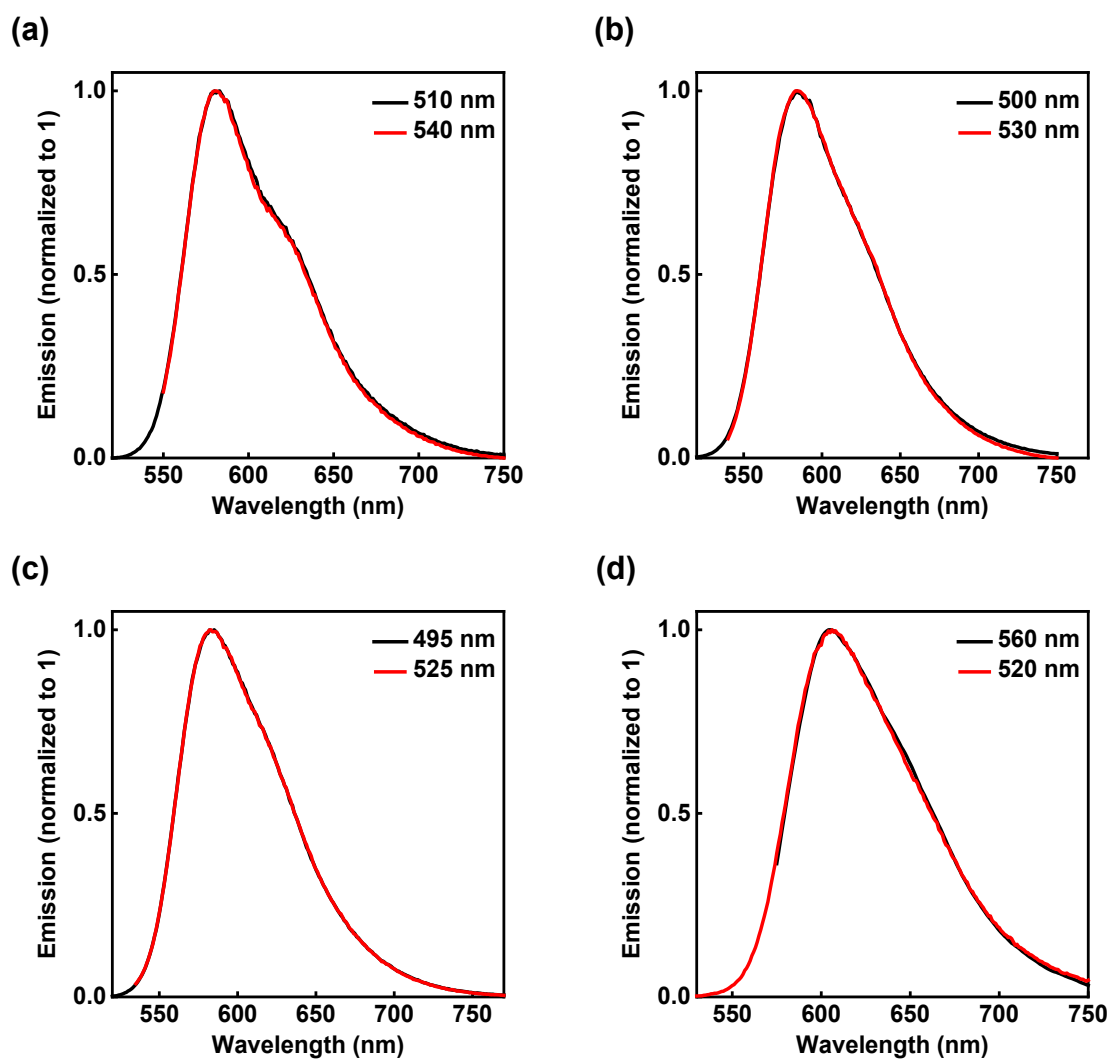


Figure S23. Emission spectra of **8** in (a) HEX, (b) DCB, (c) DCM and (d) ACN. The emission spectra of **8** were recorded upon excitation at the indicated wavelengths.

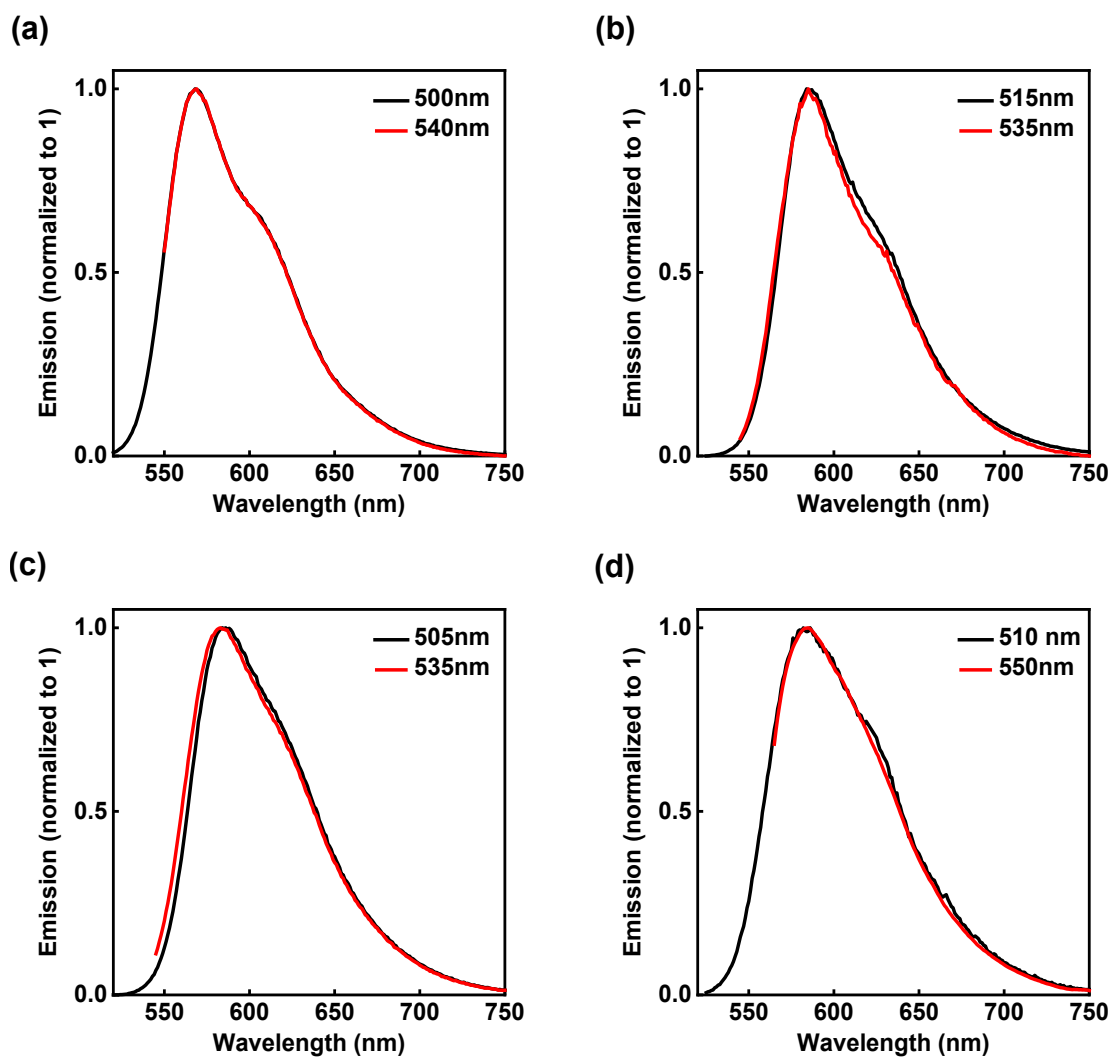


Figure S24. Emission spectra of **9** in (a) HEX, (b) DCB, (c) DCM and (d) ACN. The emission spectra of **9** were recorded upon excitation at the indicated wavelengths.

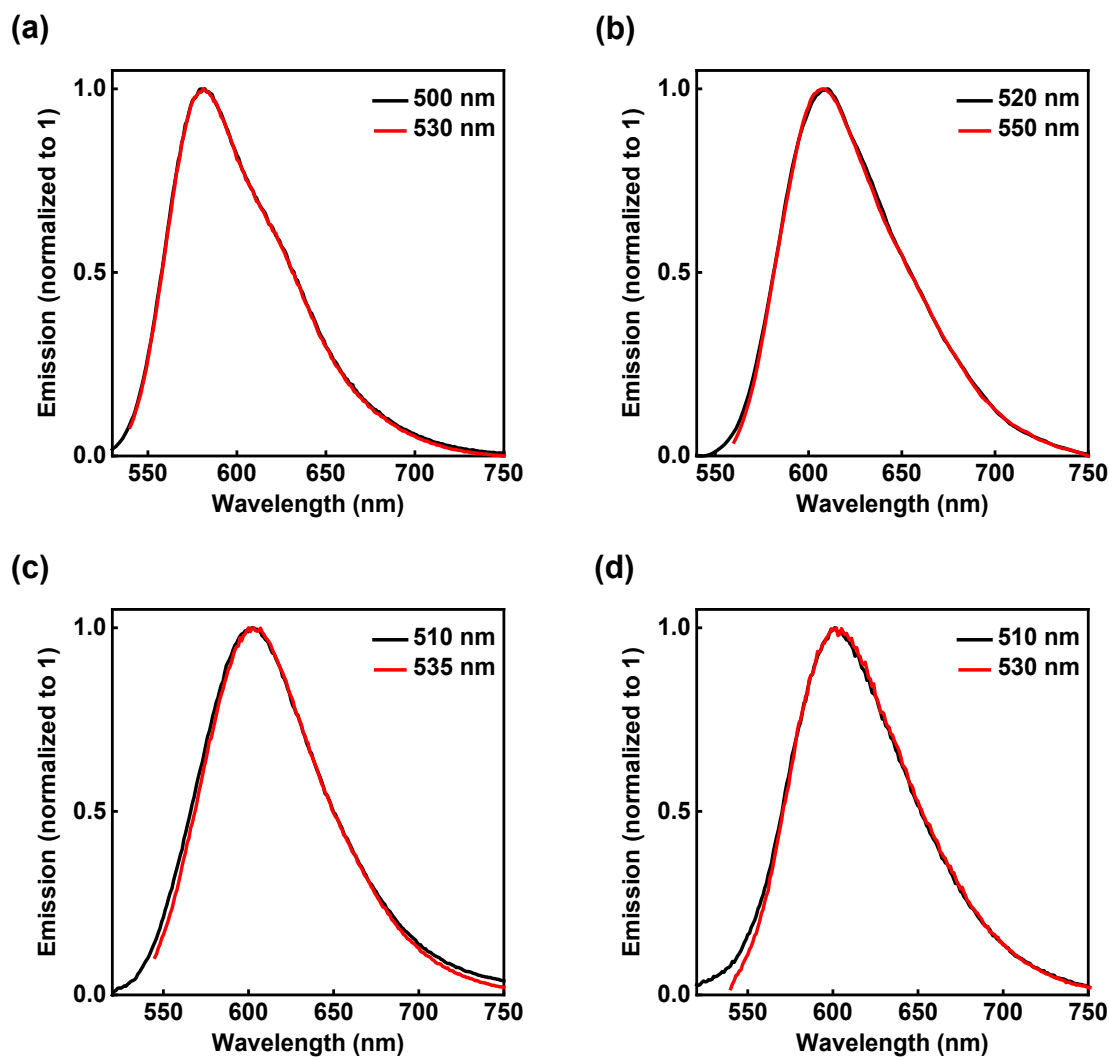


Figure S25. Emission spectra of **10** in (a) HEX, (b) DCB, (c) DCM and (d) ACN. The emission spectra of **10** were recorded upon excitation at the indicated wavelengths.

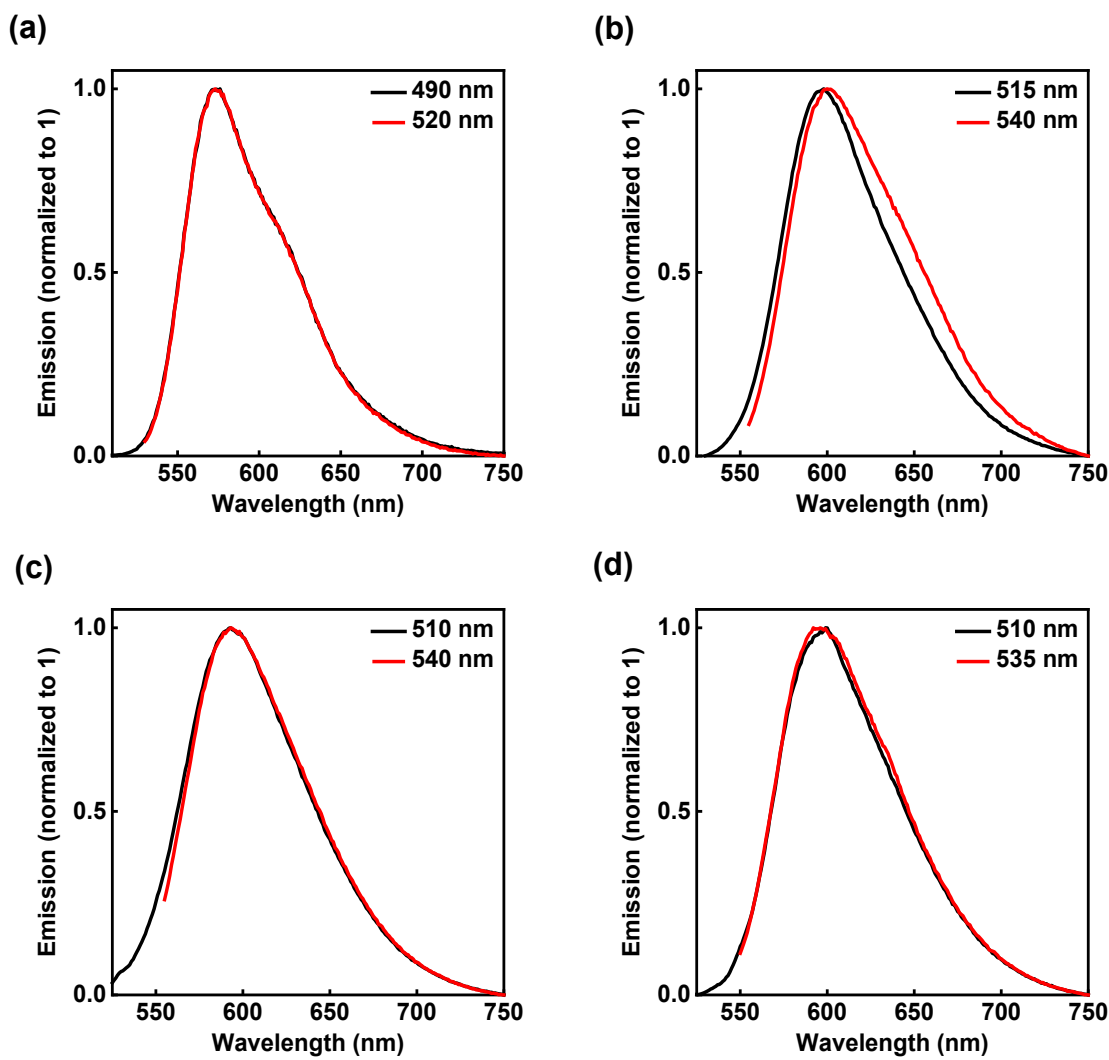


Figure S26. Emission spectra of **11** in (a) HEX, (b) DCB, (c) DCM and (d) ACN. The emission spectra of **11** were recorded upon excitation at the indicated wavelengths.

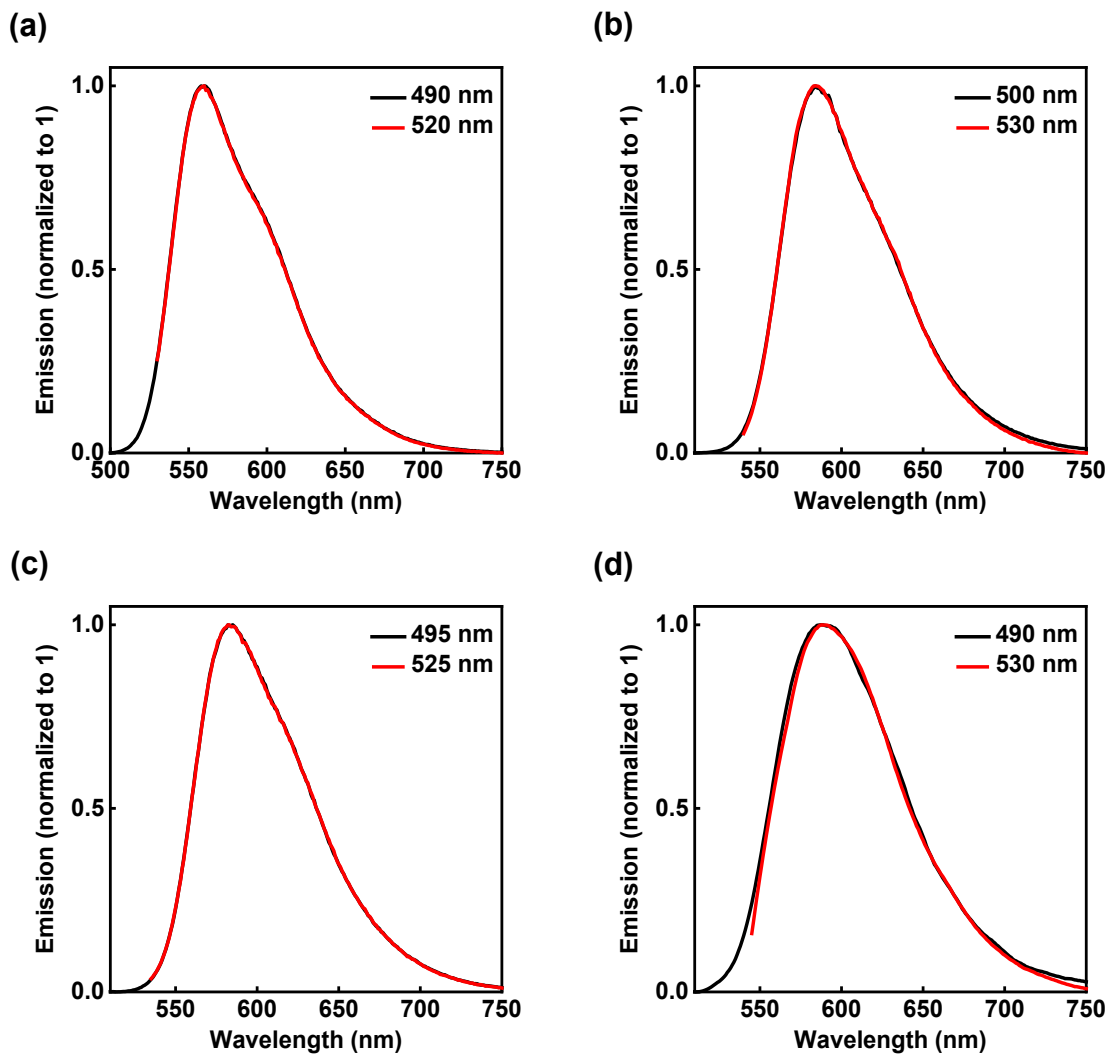


Figure S27. Emission spectra of **12** in (a) HEX, (b) DCB, (c) DCM and (d) ACN. The emission spectra of **12** were recorded upon excitation at the indicated wavelengths.

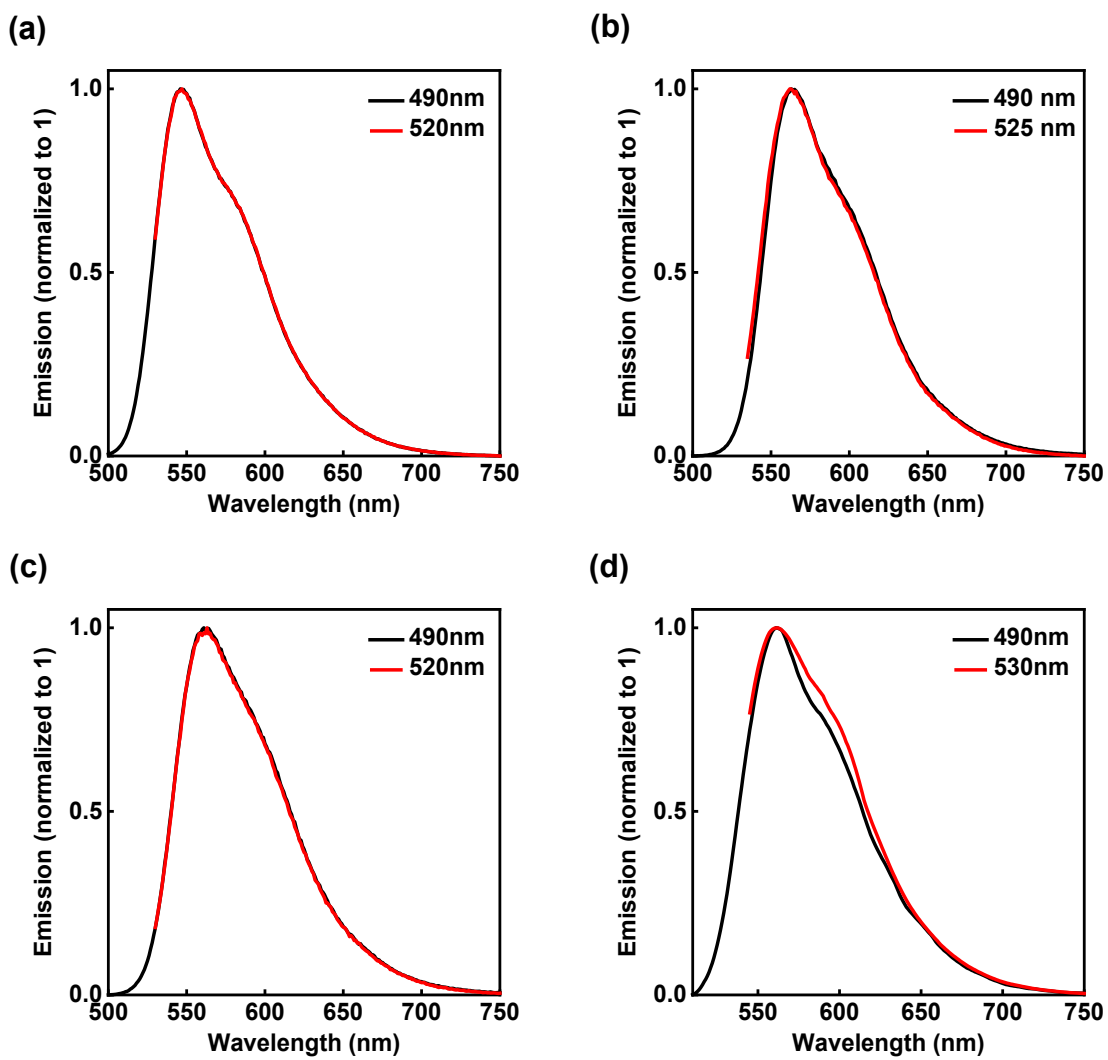


Figure S28. Emission spectra of **13** in (a) HEX, (b) DCB, (c) DCM and (d) ACN. The emission spectra of **13** were recorded upon excitation at the indicated wavelengths.

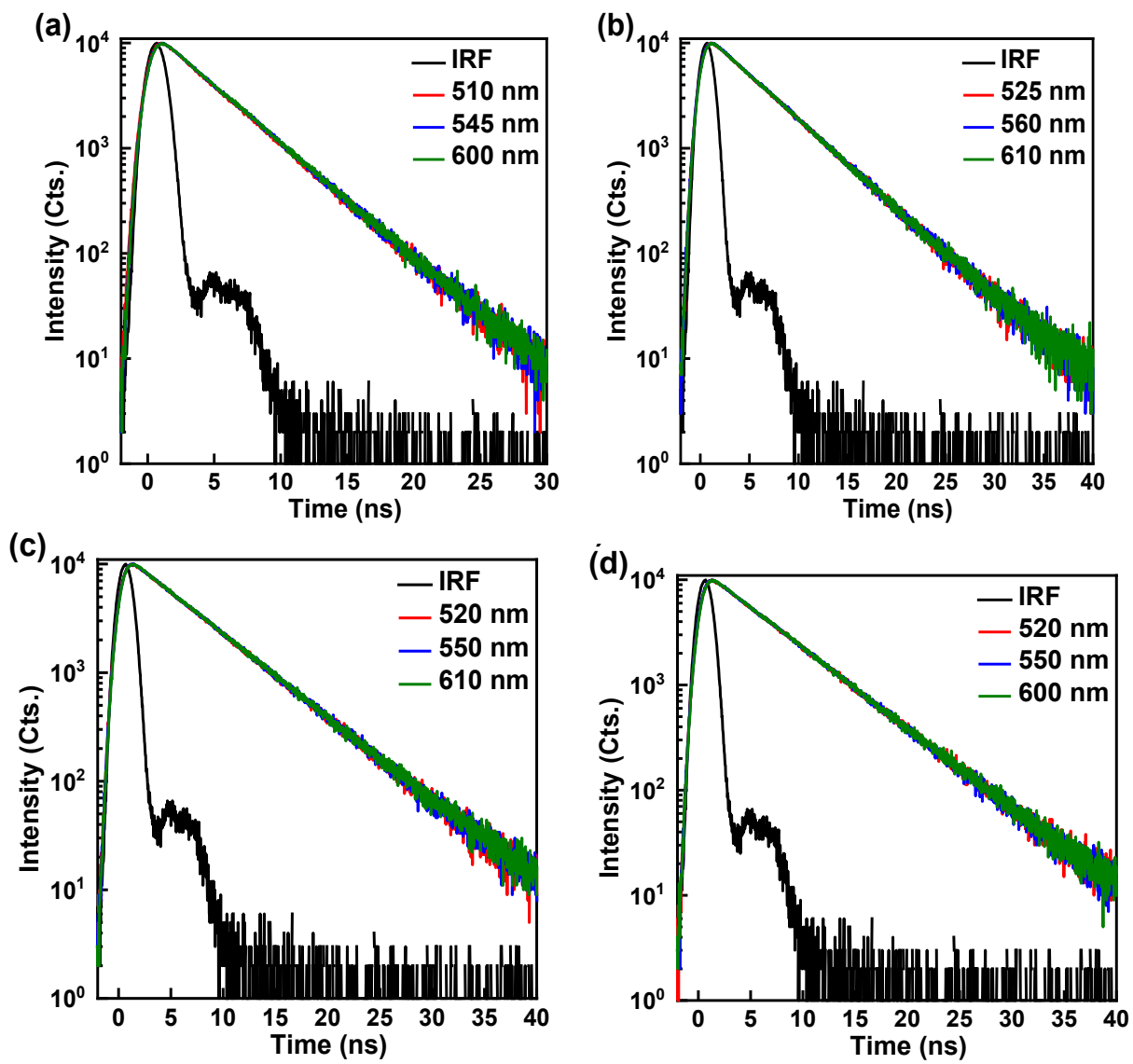


Figure S29. Emission decays of **1** in (a) HEX, (b) DCB, (c) DCM and (d) ACN upon excitation at 460 nm. The decays were gated at the indicated wavelengths.

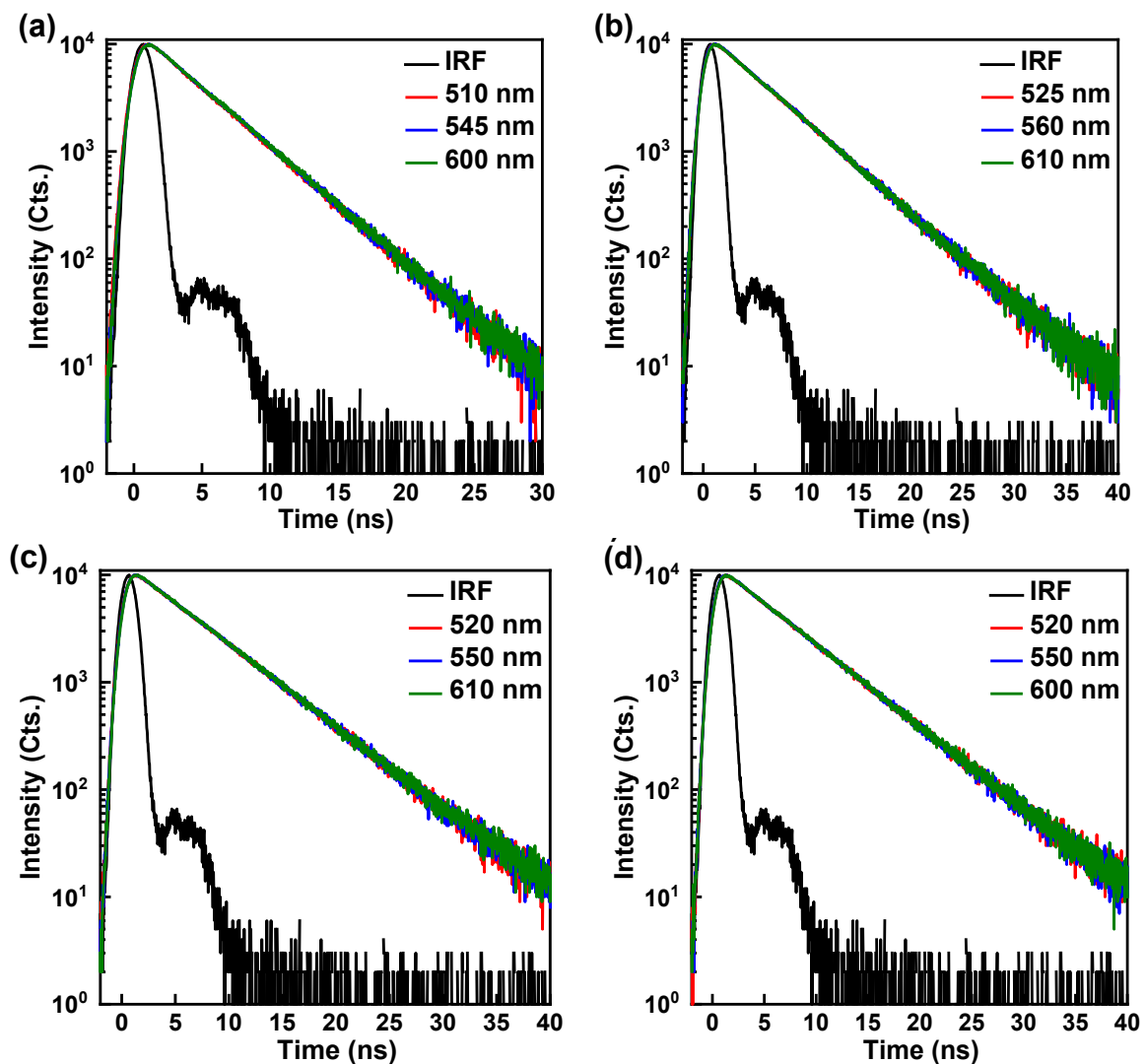


Figure S30. Emission decays of **2** in (a) HEX, (b) DCB, (c) DCM and (d) ACN upon excitation at 460 nm. The decays were gated at the indicated wavelengths.

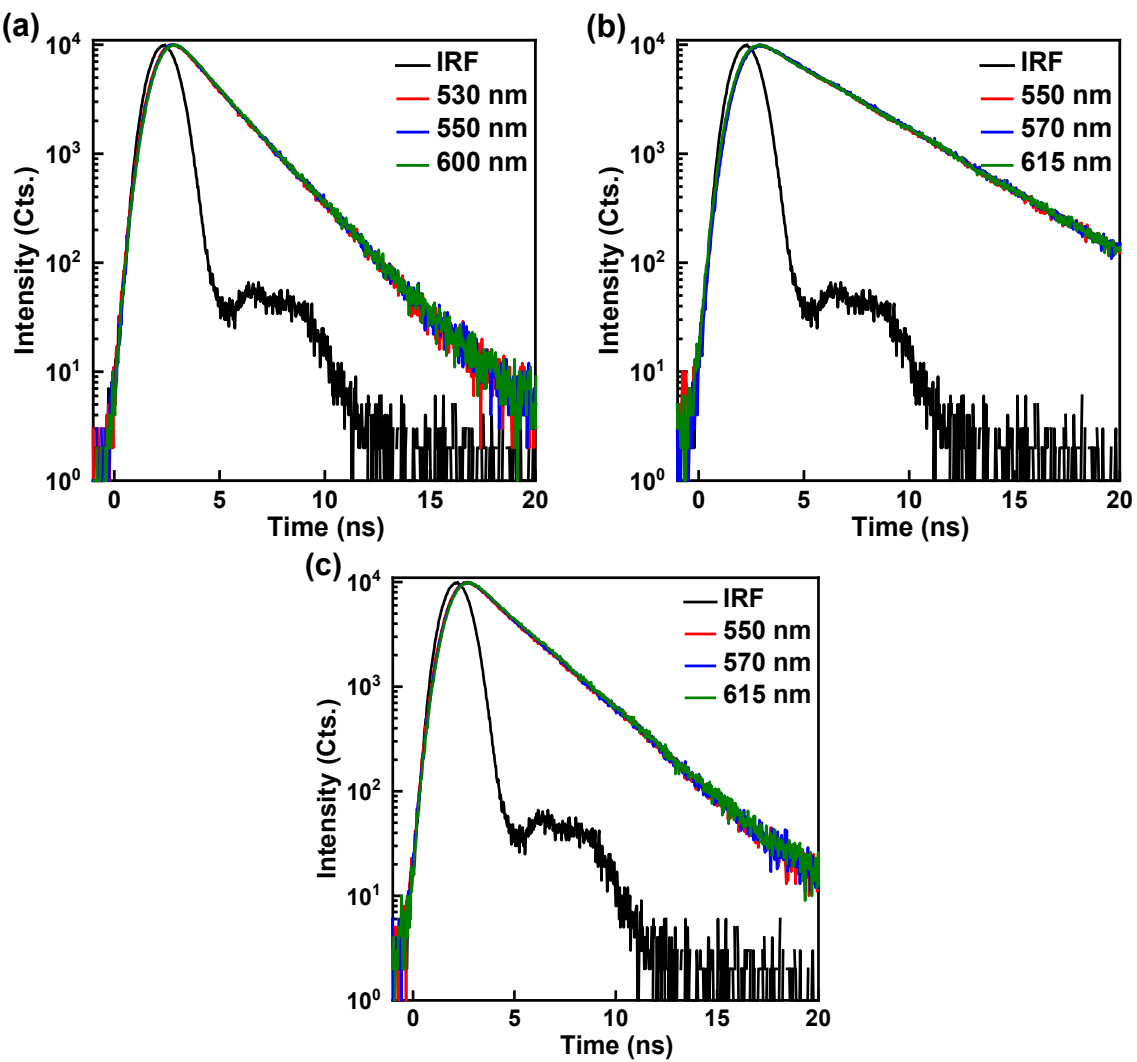


Figure S31. Emission decays of **3** in (a) HEX, (b) DCB, (c) DCM upon excitation at 460 nm. The decays were gated at the indicated wavelengths. The emission lifetime of **3** in ACN is below IRF (black curve, 1.5 ns), and thus the emission decays could not be recorded.

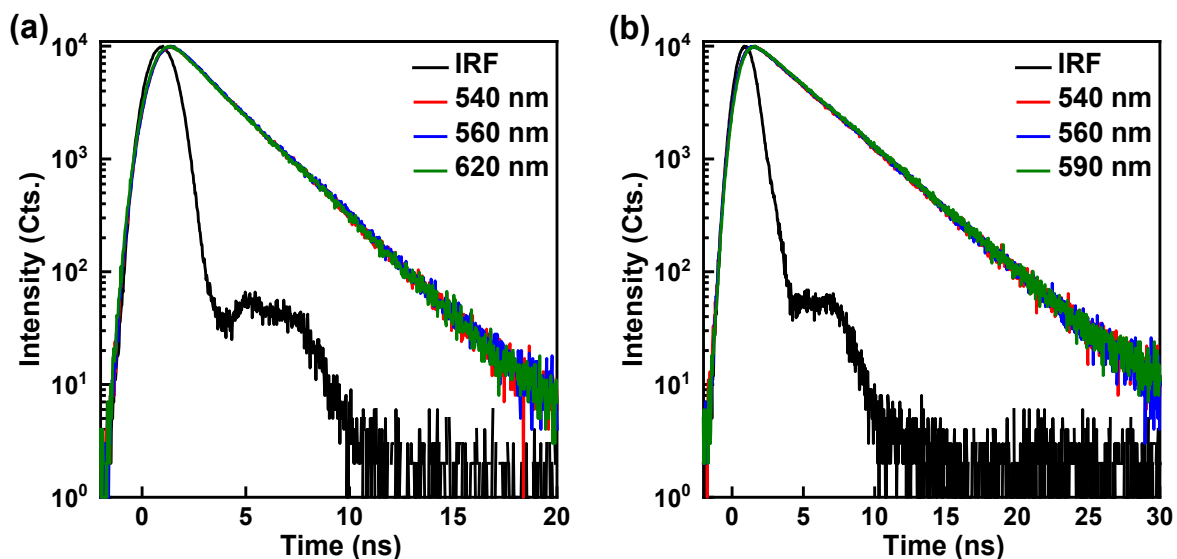


Figure S32. Emission decays of **4** in (a) HEX, (b) DCB, (c) DCM upon excitation at 460 nm. The decays were gated at the indicated wavelengths. The emission lifetimes of **3** in ACN and DCM are below IRF (black curve, 1.5 ns), and thus the emission decays could not be recorded.

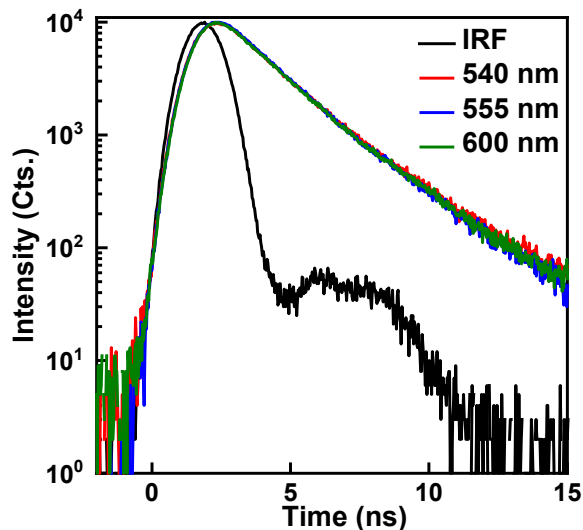


Figure S33. Emission decays of **6** in HEX upon excitation at 460 nm. The decays were gated at the indicated wavelengths. The emission lifetimes of **6** in DCB, DCM and ACN are below IRF (black curve, 1.5 ns), and thus the emission decays could not be recorded.

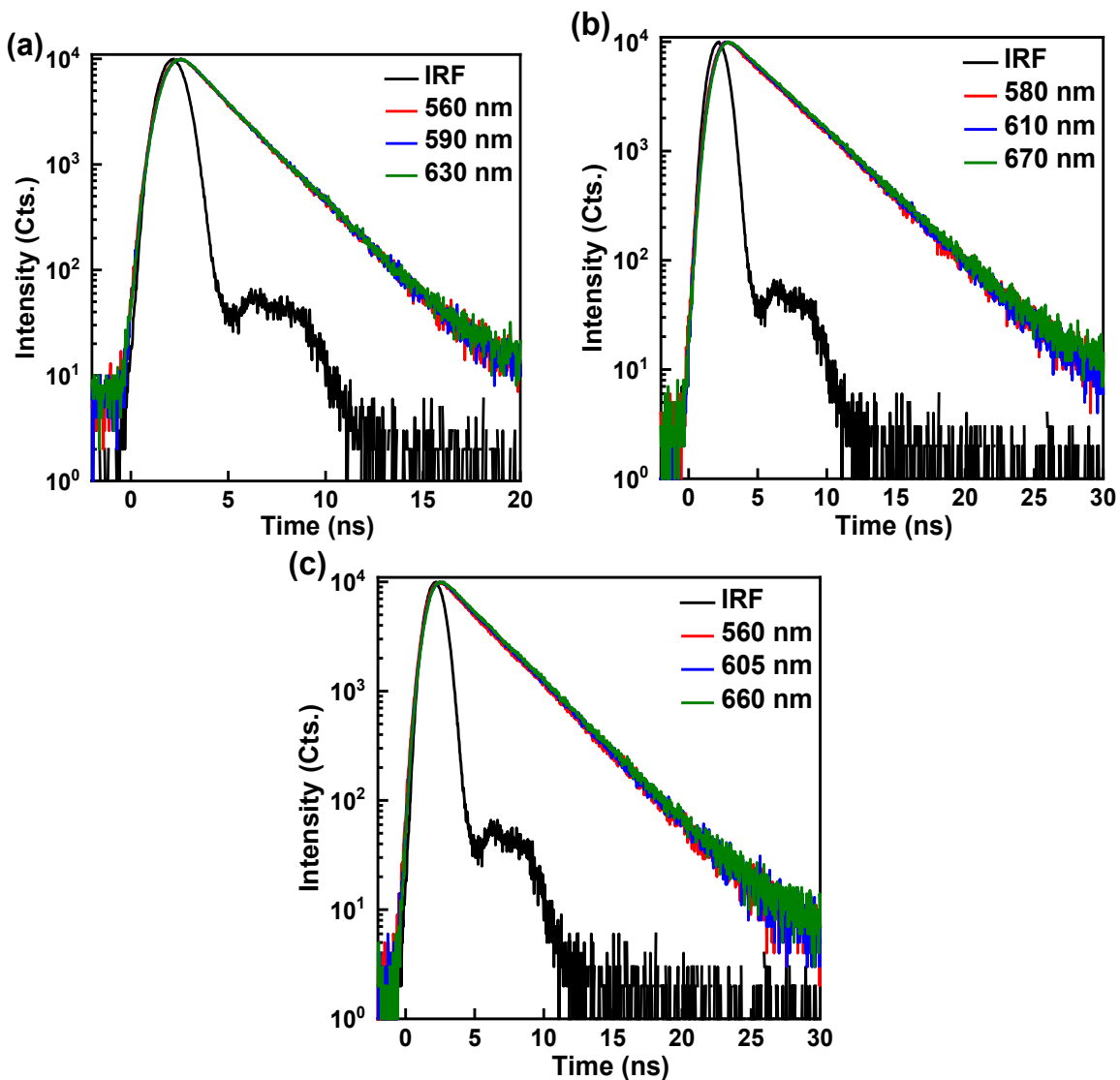


Figure S34. Emission decays of **8** in (a) HEX, (b) DCB, (c) DCM upon excitation at 460 nm. The decays were gated at the indicated wavelengths. The emission lifetime of **8** in ACN is below IRF (black curve, 1.5 ns), and thus the emission decays could not be recorded.

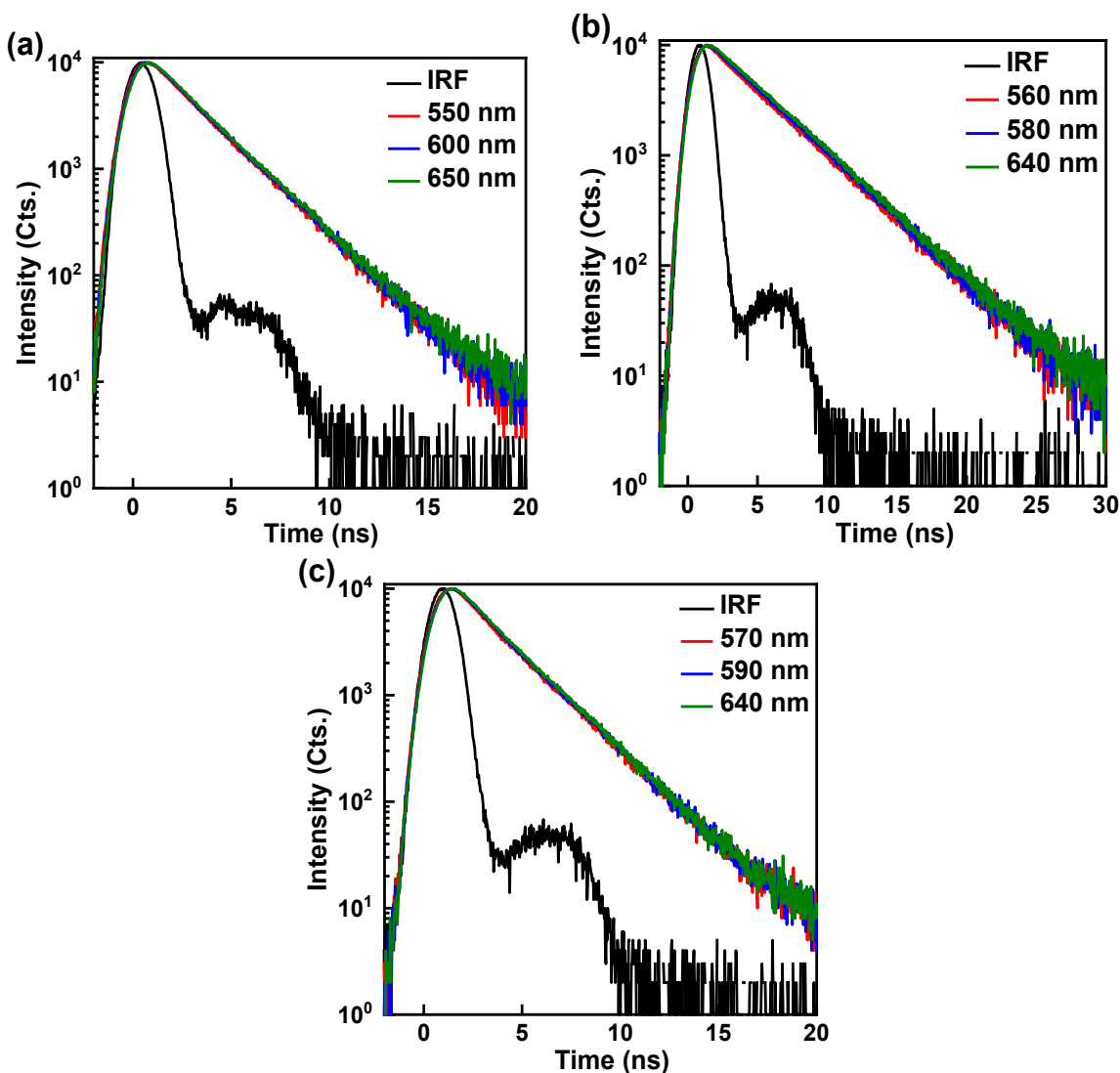


Figure S35. Emission decays of **9** in (a) HEX, (b) DCB, (c) DCM upon excitation at 460 nm. The decays were gated at the indicated wavelengths. The emission lifetime of **9** in ACN is below IRF (black curve, 1.5 ns), and thus the emission decays could not be recorded.

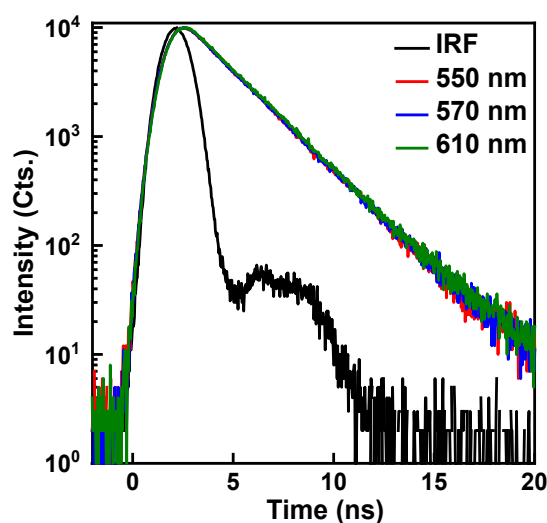


Figure S36. Emission decays of **11** in (a) HEX upon excitation at 460 nm. The decays were gated at the indicated wavelengths. The emission lifetime of **11** in DCB, DCM and ACN is below IRF (black curve, 1.5 ns), and thus the emission decays could not be recorded.

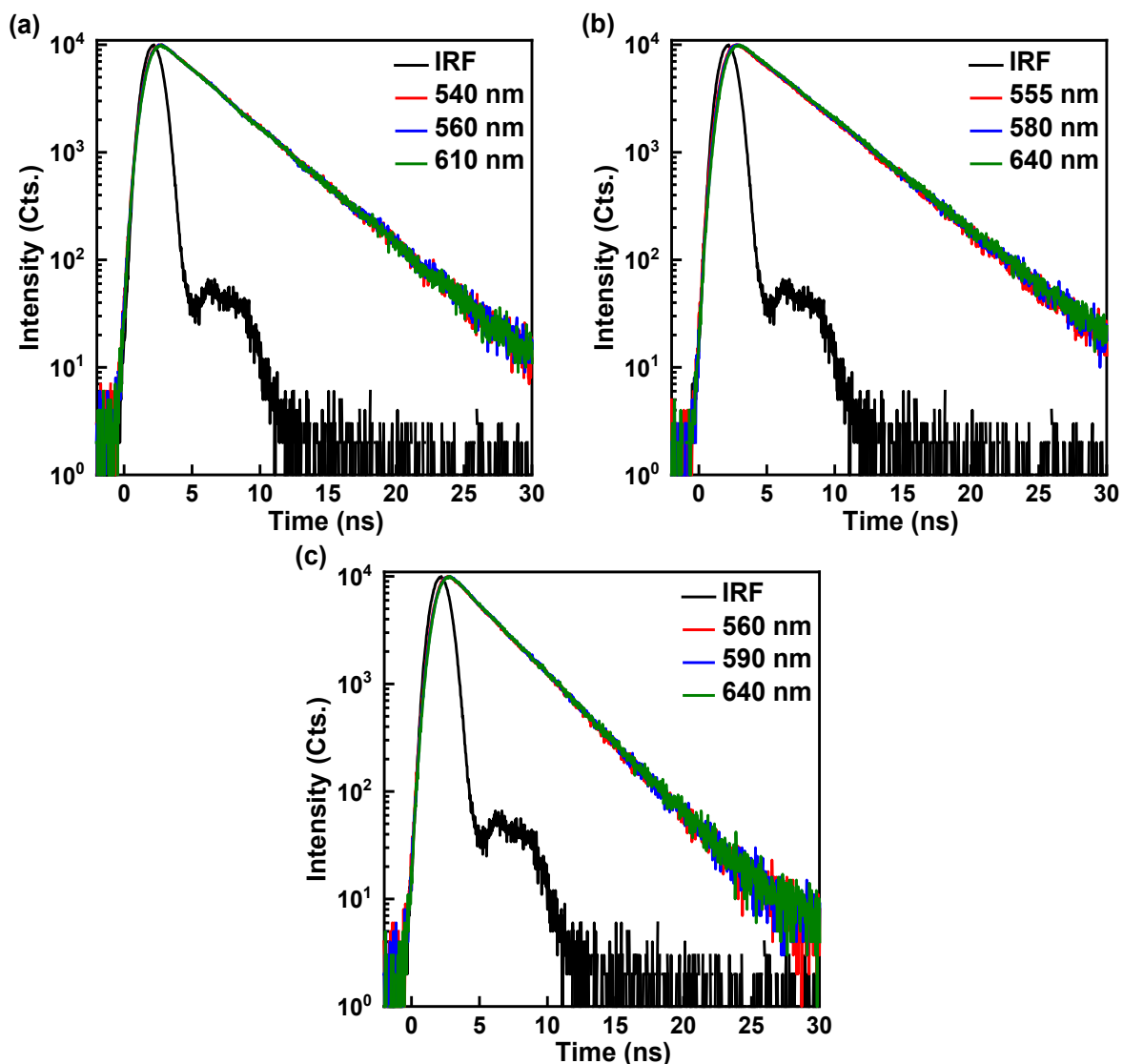


Figure S37. Emission decays of **12** in (a) HEX, (b) DCB, (c) DCM upon excitation at 460 nm. The decays were gated at the indicated wavelengths. The emission lifetime of **12** in ACN is below IRF (black curve, 1.5 ns), and thus the emission decays could not be recorded.

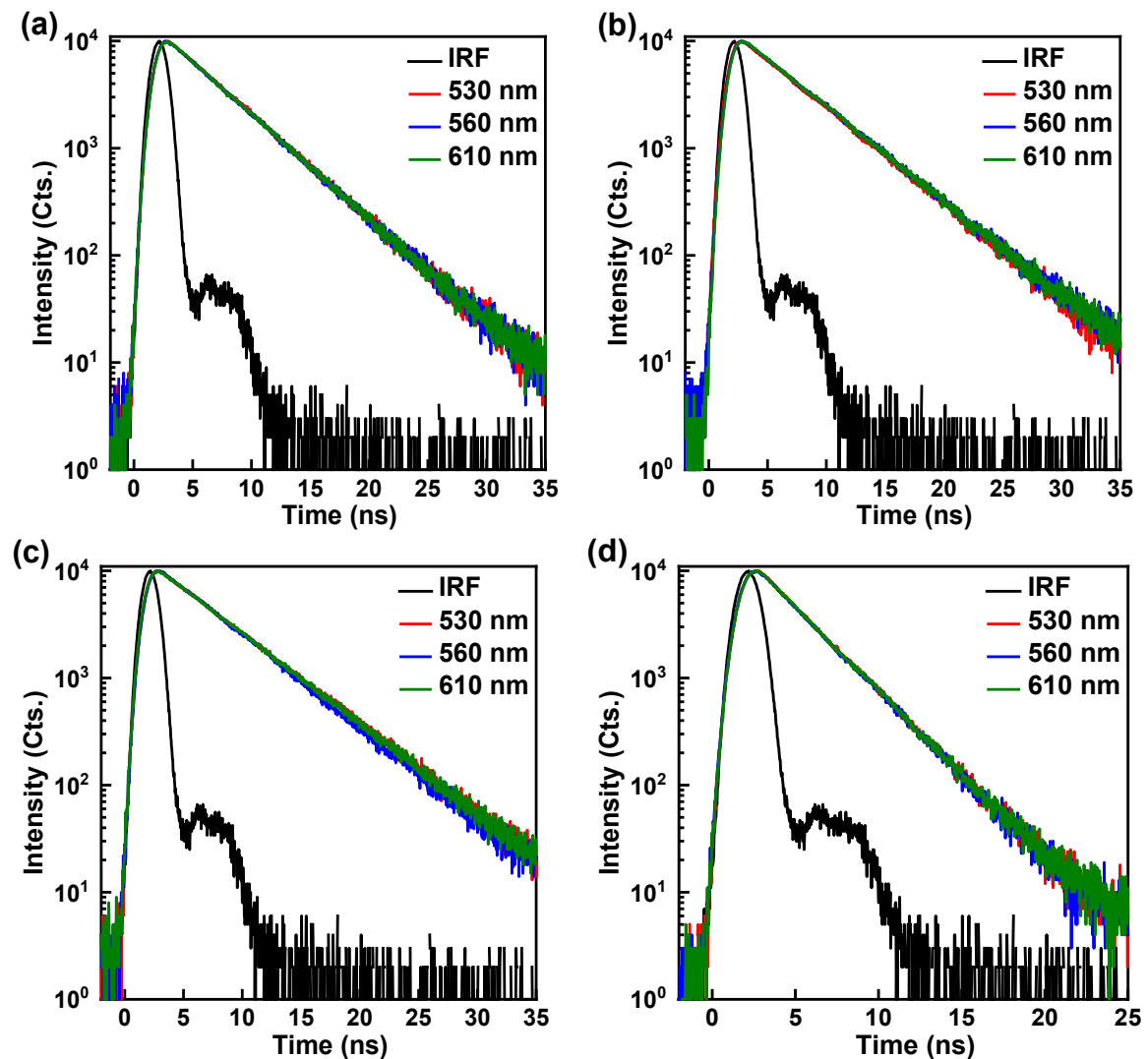


Figure S38. Emission decays of **13** in (a) HEX, (b) DCB, (c) DCM and (d) ACN upon excitation at 460 nm. The decays were gated at the indicated wavelengths.

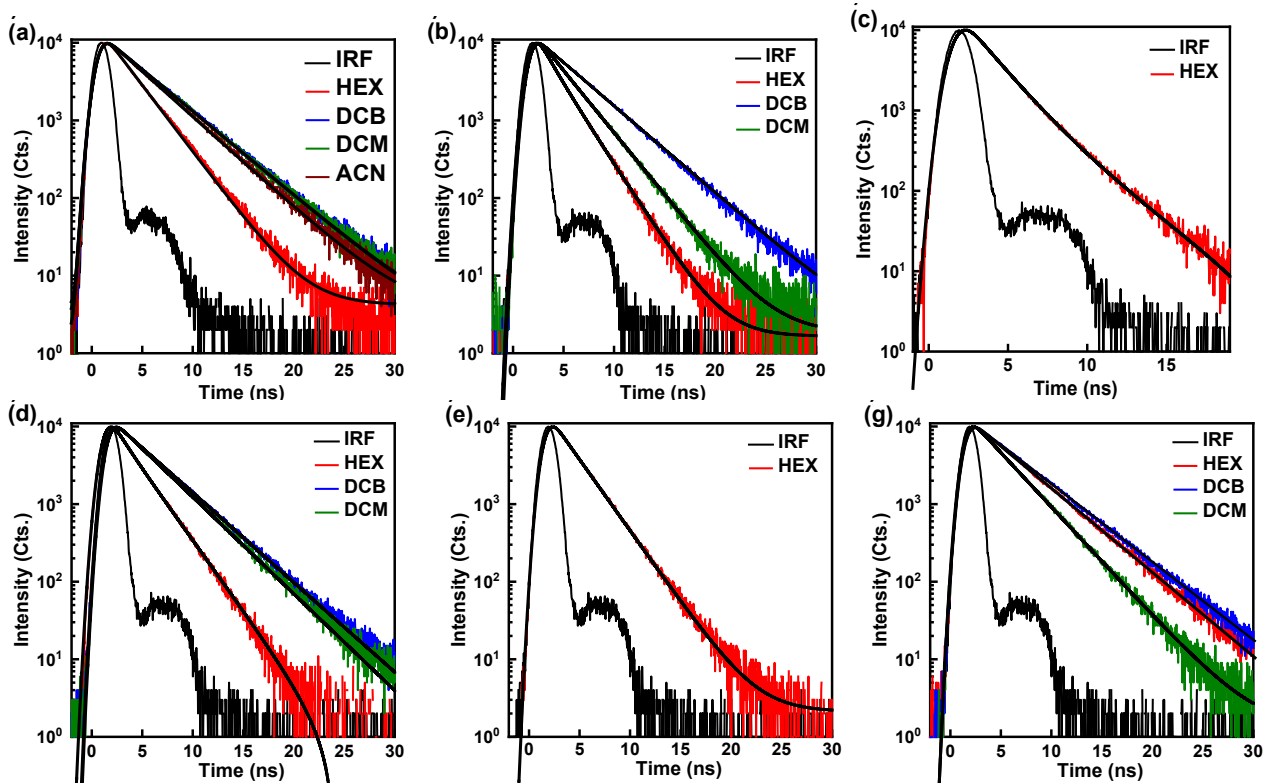


Figure S39. Emission decays of (a) 2, (b) 3, (c) 6, (d) 8, (e) 11 and (f) 12 upon excitation at 460 nm in various solvents. The observation wavelengths of the samples were located at maximum emission. The solid lines are from the best single-exponential fit to the experimental data. The emission lifetimes of **5**, **7**, **10** in all solvents as well as the emission lifetimes of presented dyes and in some solvents were below IRF (black curve, 1.5 ns), and thus the decays could not be recorded.

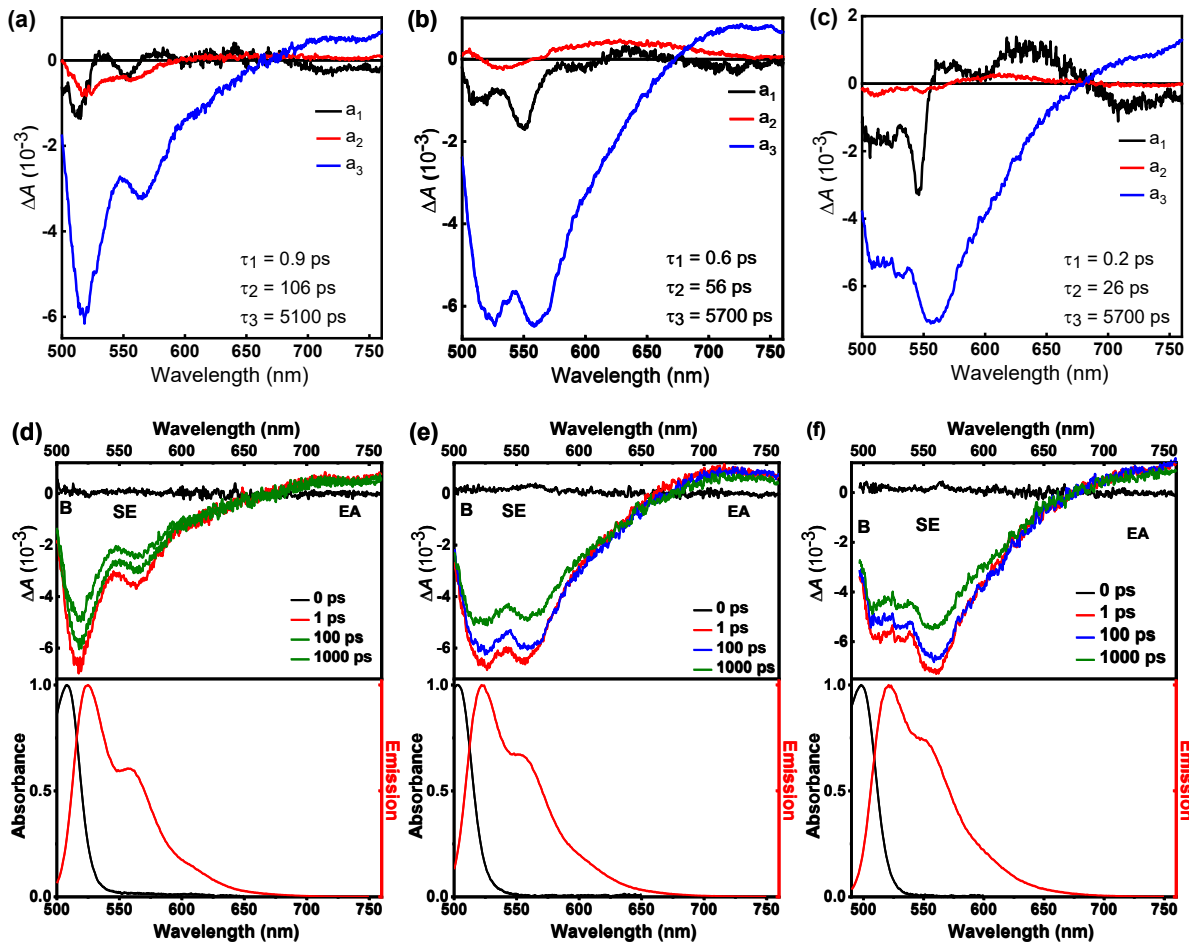


Figure S40. (a-c) Decay associated difference spectra (DADS) showing the distributions of amplitudes, $A_i(\lambda)$, along with the corresponding time constants, τ_i , obtained from multiexponential global fits (eq. S1) of transient absorption signals of **1** in (a) DCB, (b) DCM and (c) ACN. (d-f) Transient-absorption spectra, gated at different pump-probe delay times (upper panels) and time-integrated absorption and emission spectra, normalized to unity (lower panels) of **1** in (d) DCB, (e) DCM and (f) ACN. The transient absorption spectra were excited at 480 nm.

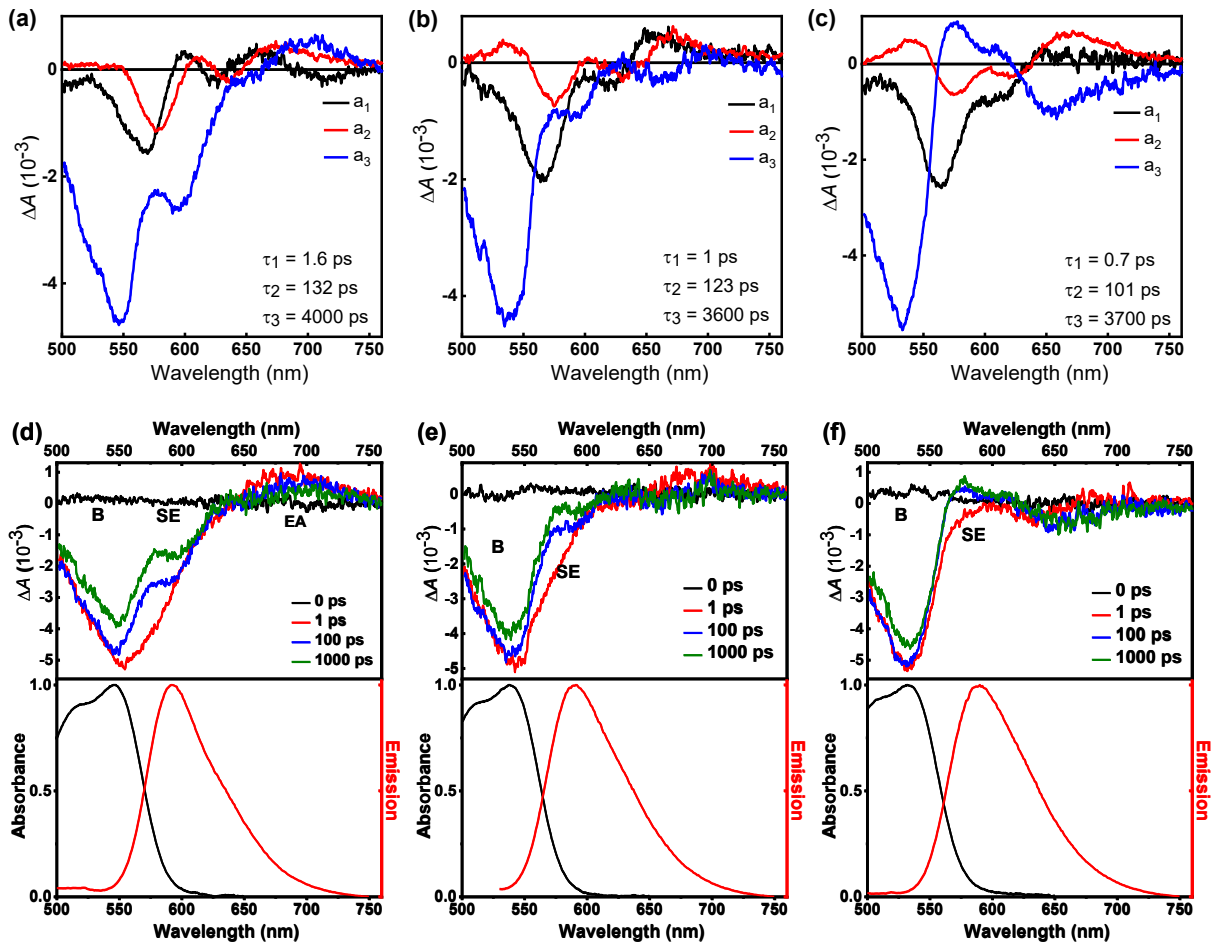


Figure S41. (a-c) DADS showing the distributions of amplitudes, $A_i(\lambda)$, along with the corresponding time constants, τ_i , obtained from multiexponential global fits (eq. S1) of transient absorption signals of **2** in (a) DCB, (b) DCM and (c) ACN. (d-f) Transient absorption spectra gated at different pump-probe delay times (upper panels) and time-integrated absorption and emission spectra, normalized to unity (lower panels) of **2** in (d) DCB, (e) DCM and (f) ACN. The transient absorption spectra were excited at 480 nm.

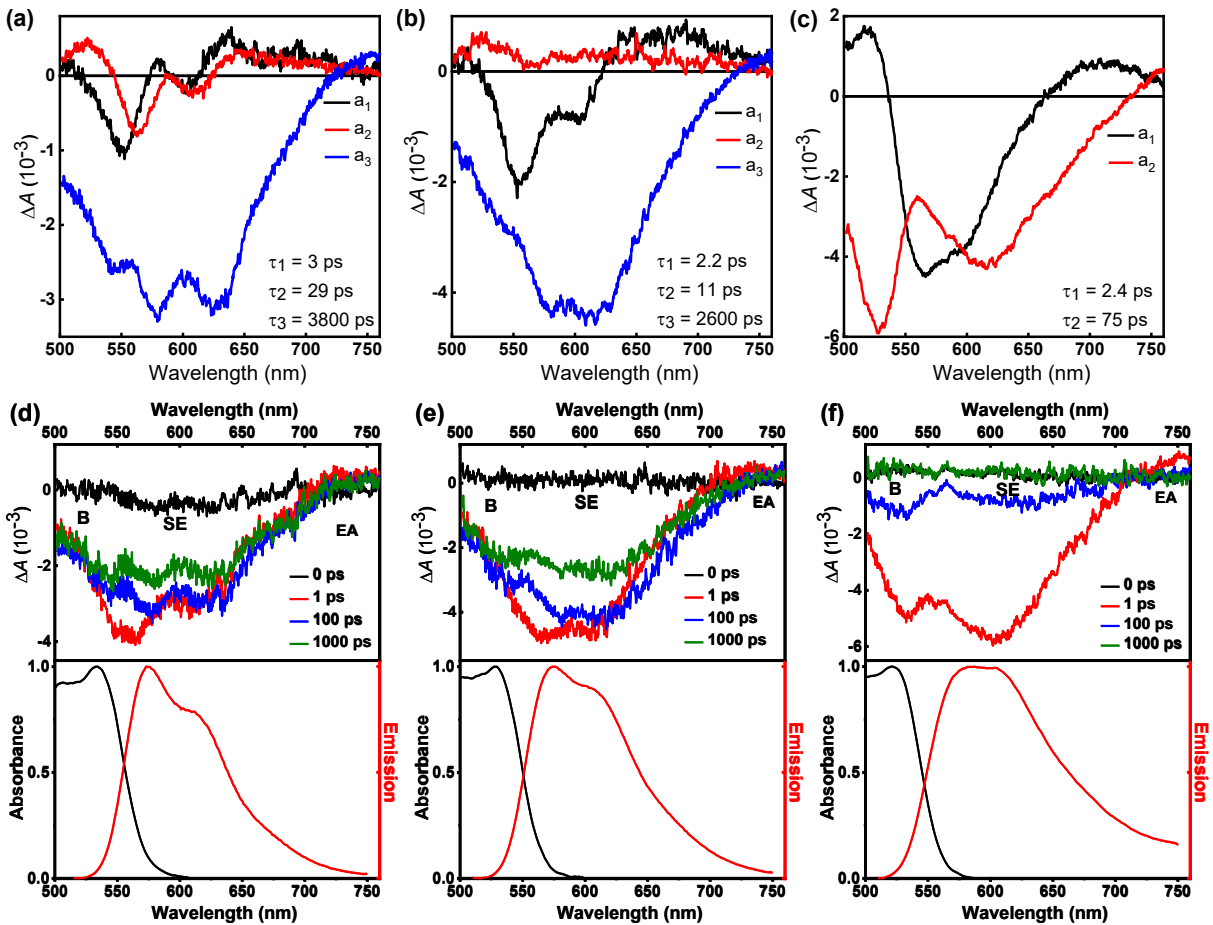


Figure S42. (a-c) DADS showing the distributions of amplitudes, $A_i(\lambda)$, along with the corresponding time constants, τ_i , obtained from multiexponential global fits (eq. S1) of transient absorption signals of **3** in (a) DCB, (b) DCM and (c) ACN. (d-f) Transient absorption spectra gated at different pump-probe delay times (upper panels) and time-integrated absorption and emission spectra, normalized to unity (lower panels) of **3** in (d) DCB, (e) DCM and (f) ACN. The transient absorption spectra were excited at 480 nm.

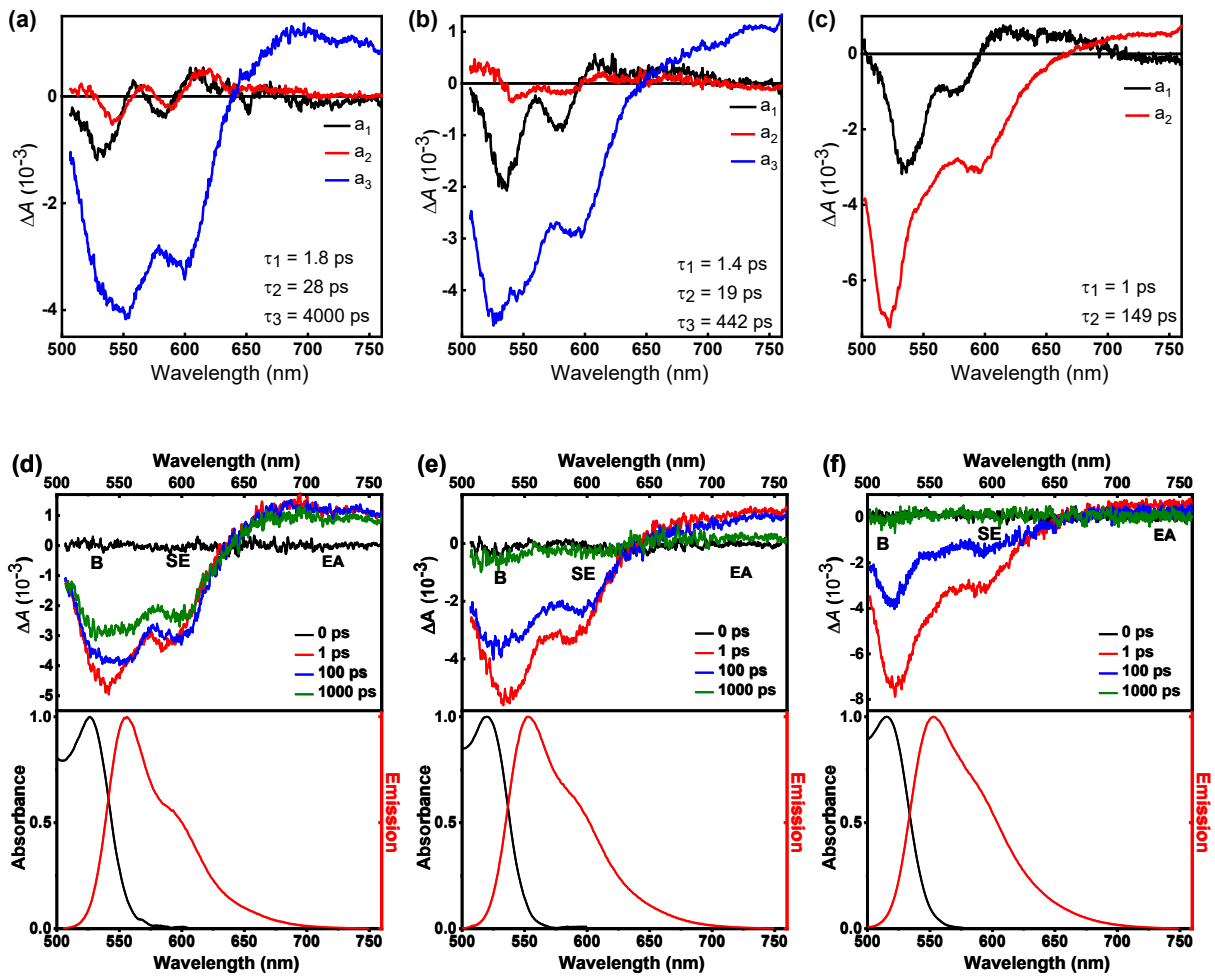


Figure S43. (a-c) DADS showing the distributions of amplitudes, $A_i(\lambda)$, along with the corresponding time constants, τ_i , obtained from multiexponential global fits (eq. S1) of transient absorption signals of **4** in (a) DCB, (b) DCM and (c) ACN. (d-f) Transient absorption spectra gated at different pump-probe delay times (upper panels) and time-integrated absorption and emission spectra, normalized to unity (lower panels) of **4** in (d) DCB, (e) DCM and (f) ACN. The transient absorption spectra were excited at 480 nm.

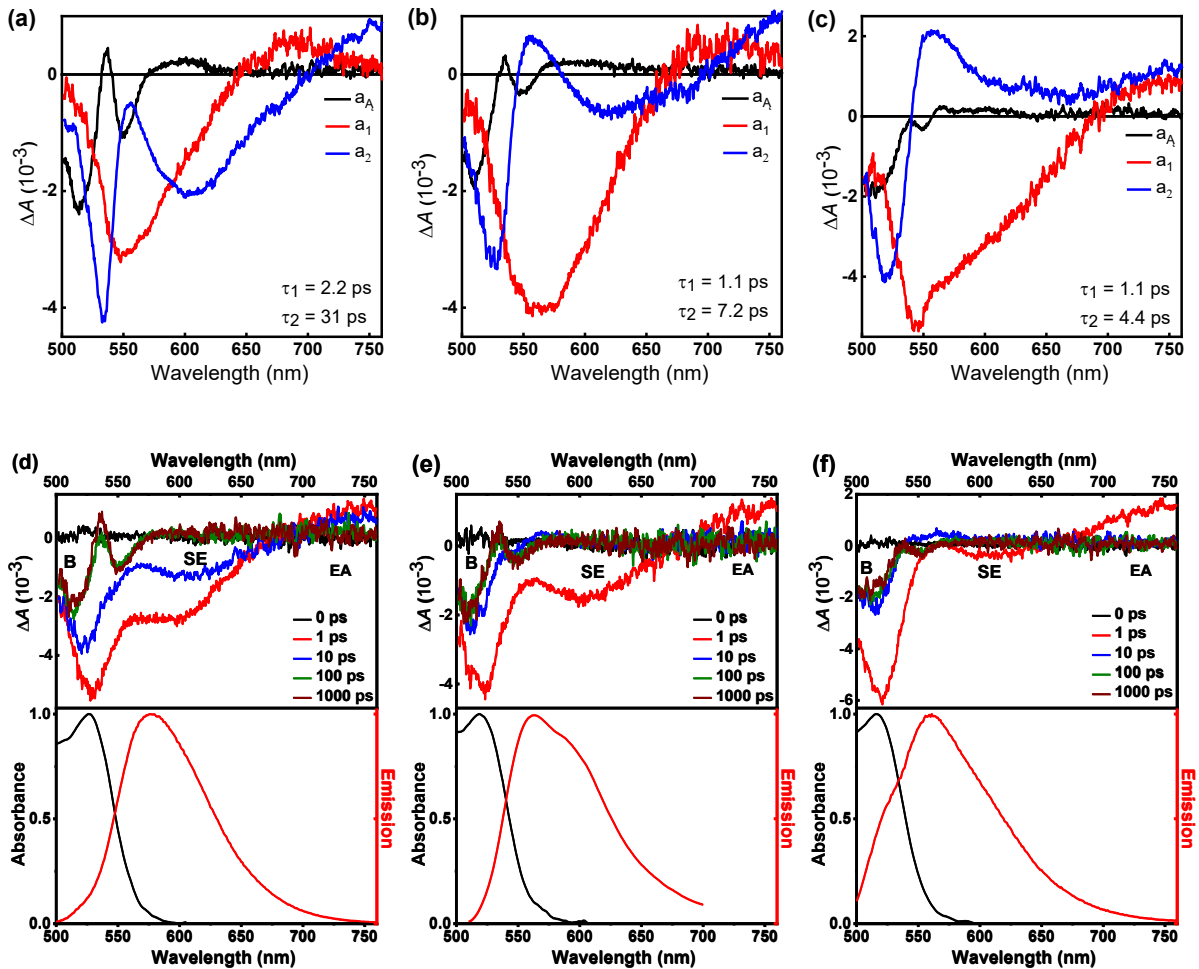


Figure S44. (a-c) DADS showing the distributions of amplitudes, $A_i(\lambda)$, along with the corresponding time constants, τ_i , obtained from multiexponential global fits (eq. S1) of transient absorption signals of **5** in (a) DCB, (b) DCM and (c) ACN. (d-f) Transient absorption spectra gated at different pump-probe delay times (upper panels) and time-integrated absorption and emission spectra, normalized to unity (lower panels) of **5** in (d) DCB, (e) DCM and (f) ACN. The transient absorption spectra were excited at 480 nm.

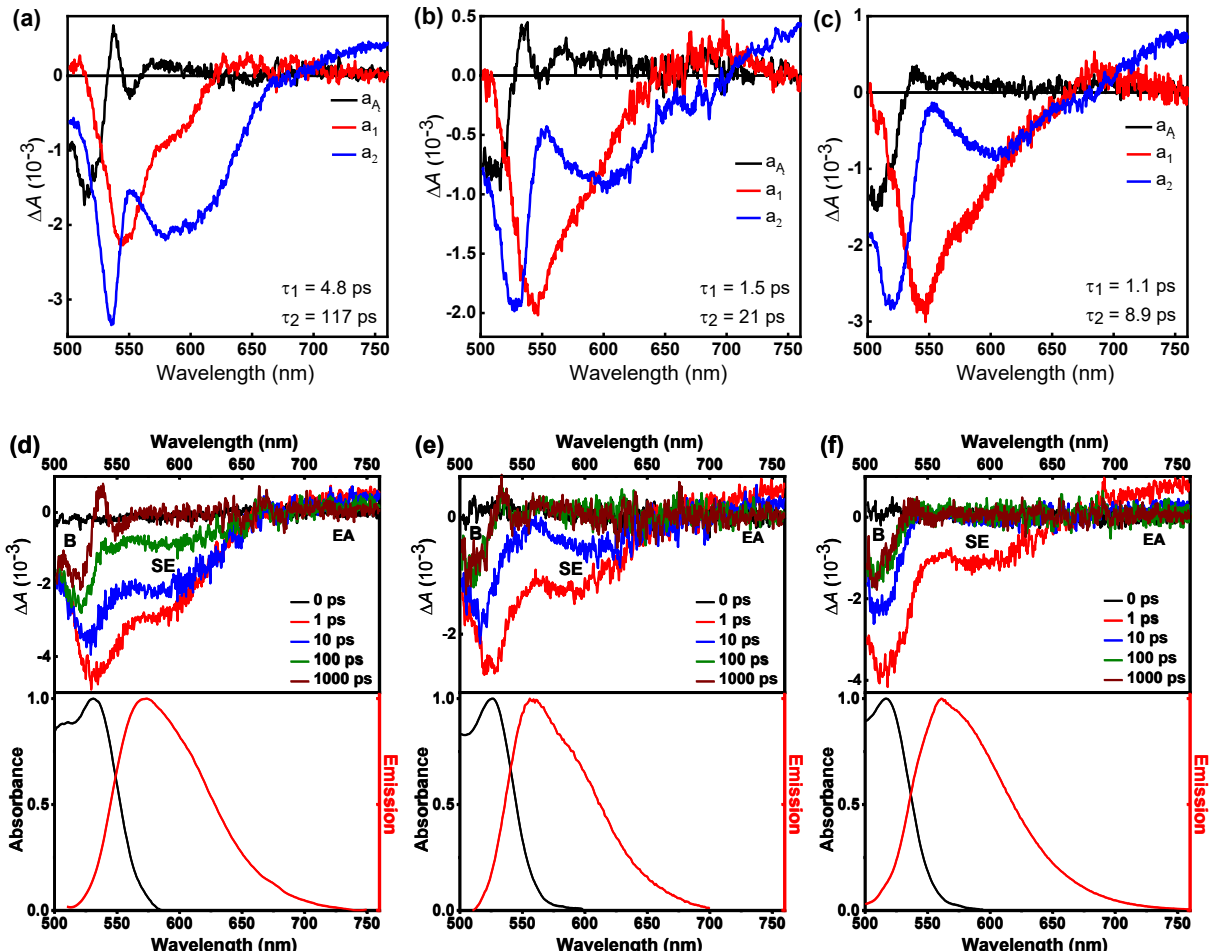


Figure S45. (a-c) DADS showing the distributions of amplitudes, $A_i(\lambda)$, along with the corresponding time constants, τ_i , obtained from multiexponential global fits (eq. S1) of transient absorption signals of **6** in (a) DCB, (b) DCM and (c) ACN. (d-f) Transient absorption spectra gated at different pump-probe delay times (upper panels) and time-integrated absorption and emission spectra, normalized to unity (lower panels) of **6** in (d) DCB, (e) DCM and (f) ACN. The transient absorption spectra were excited at 480 nm.

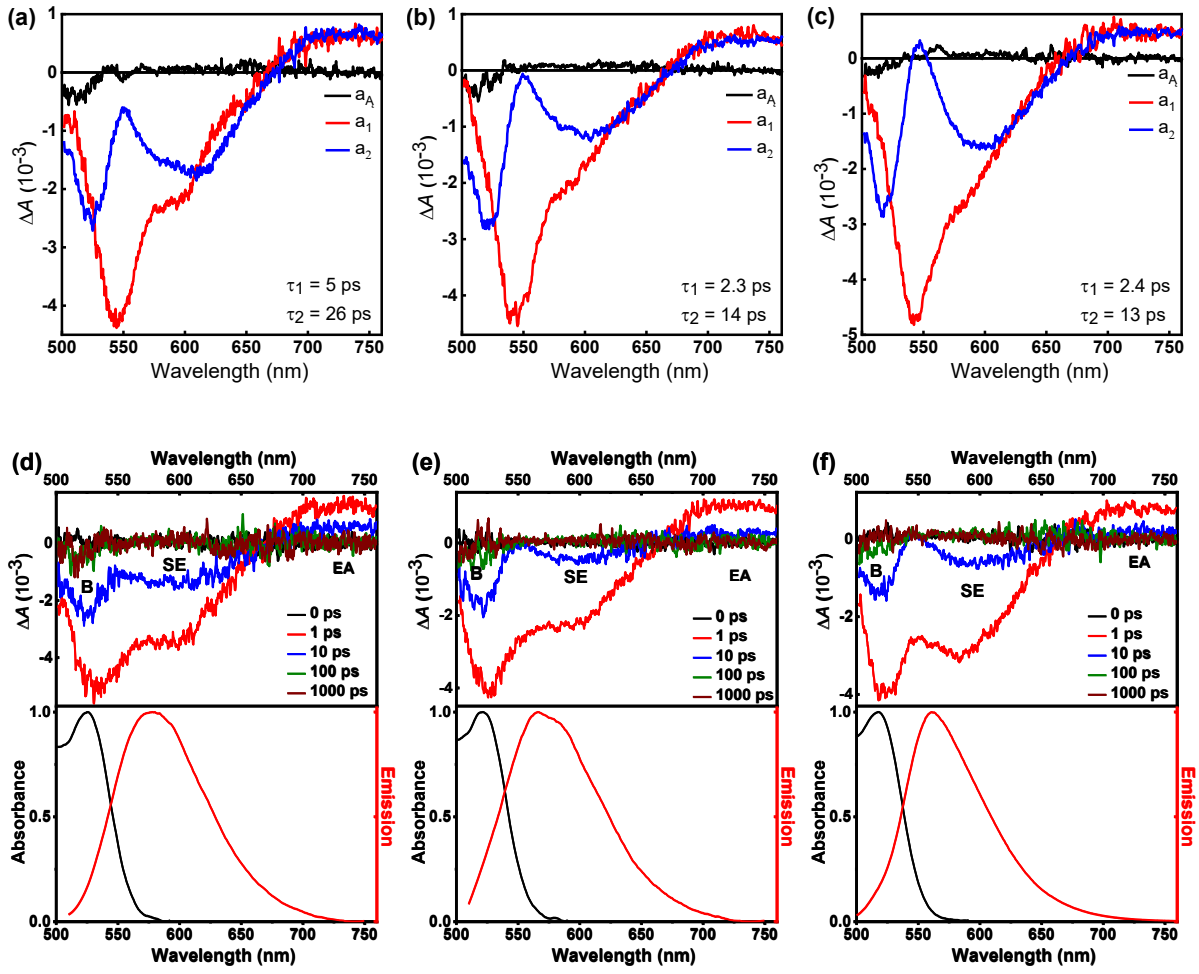


Figure S46. (a-c) DADS showing the distributions of amplitudes, $A_i(\lambda)$, along with the corresponding time constants, τ_i , obtained from multiexponential global fits (eq. S1) of transient absorption signals of 7 in (a) DCB, (b) DCM and (c) ACN. (d-f) Transient absorption spectra gated at different pump-probe delay times (upper panels) and time-integrated absorption and emission spectra, normalized to unity (lower panels) of 7 in (d) DCB, (e) DCM and (f) ACN. The transient absorption spectra were excited at 480 nm.

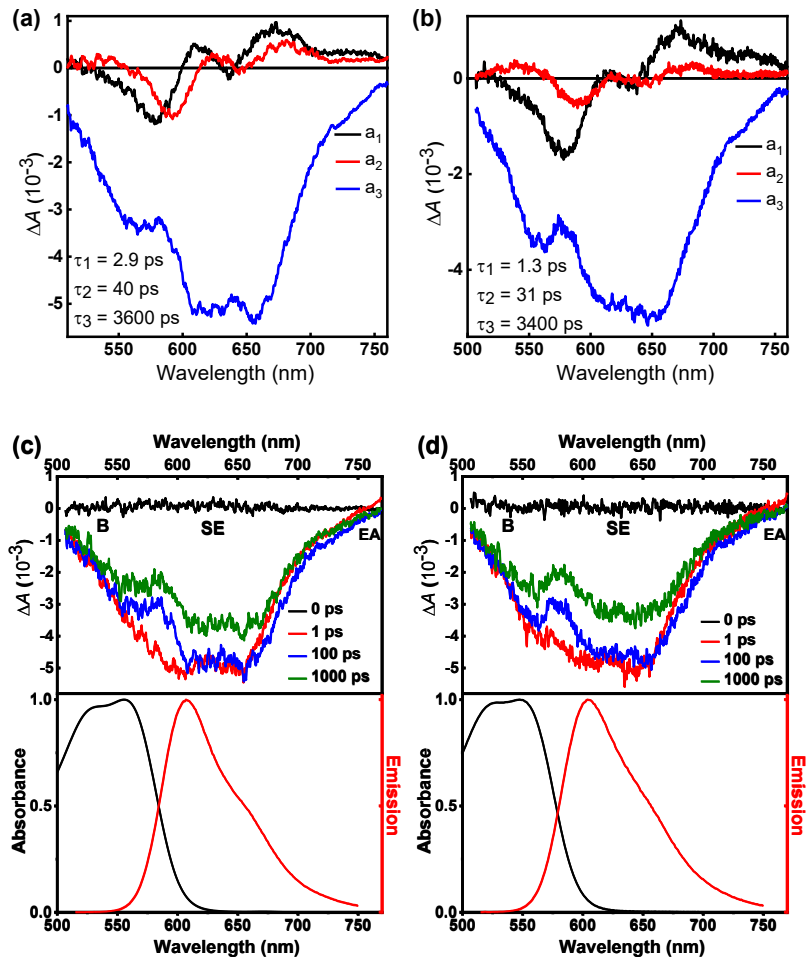


Figure S47. (a,b) DADS showing the distributions of amplitudes, $A_i(\lambda)$, along with the corresponding time constants, τ_i , obtained from multiexponential global fits (eq. S1) of transient absorption signals of **8** in (a) DCB and (b) DCM. (c,d) Transient absorption spectra gated at different pump-probe delay times (upper panels) and time-integrated absorption and emission spectra, normalized to unity (lower panels) of **8** in (c) DCB and (d) DCM. The transient absorption spectra were excited at 480 nm. Due to extremely low solubility of **8** in ACN the measurement of TA signal in the dye was not possible.

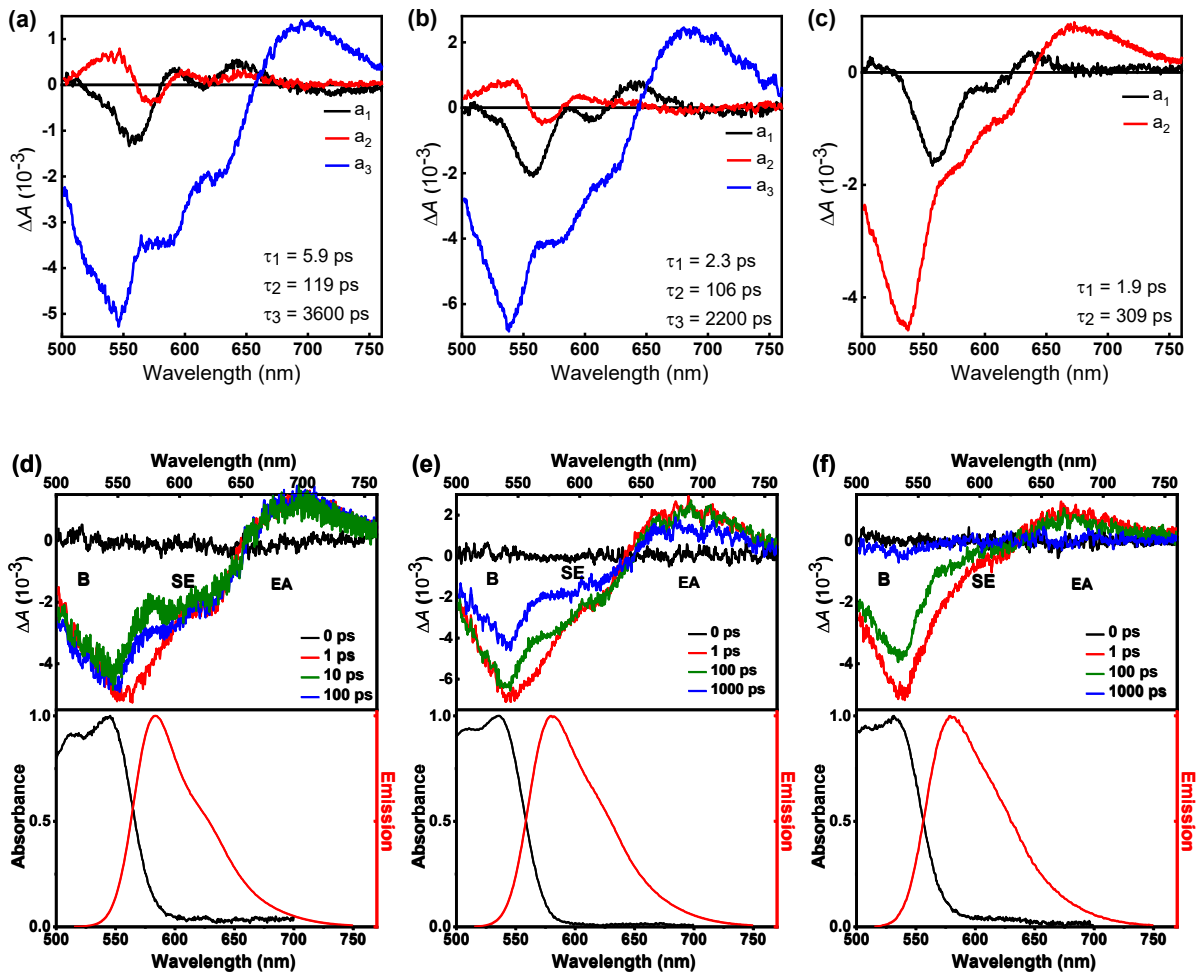


Figure S48. (a-c) DADS showing the distributions of amplitudes, $A_i(\lambda)$, along with the corresponding time constants, τ_i , obtained from multiexponential global fits (eq. S1) of transient absorption signals of **9** in (a) DCB, (b) DCM and (c) ACN. (d-f) Transient absorption spectra gated at different pump-probe delay times (upper panels) and time-integrated absorption and emission spectra, normalized to unity (lower panels) of **9** in (d) DCB, (e) DCM and (f) ACN. The transient absorption spectra were excited at 480 nm.

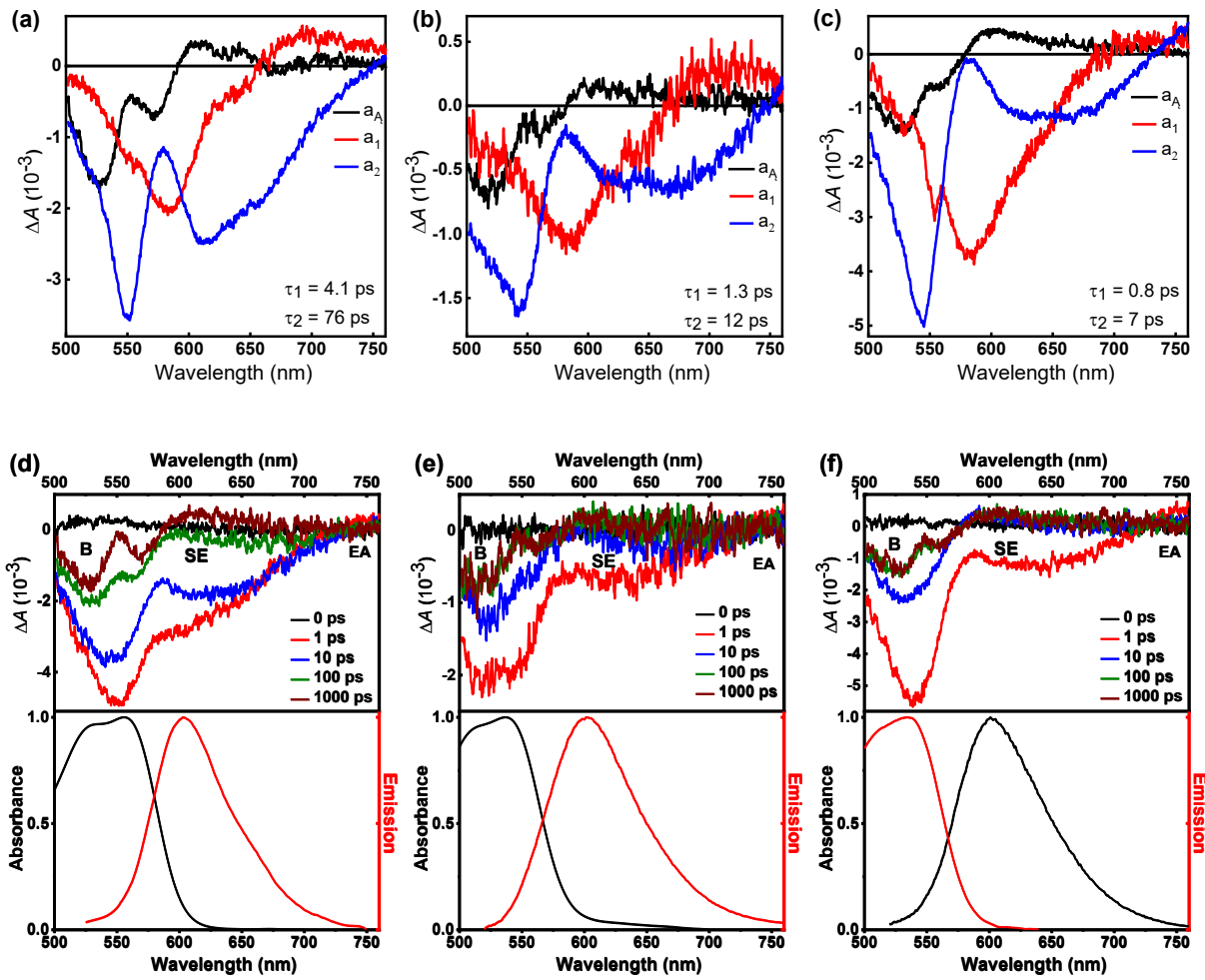


Figure S49. (a-c) DADS showing the distributions of amplitudes, $A_i(\lambda)$, along with the corresponding time constants, τ_i , obtained from multiexponential global fits (eq. S1) of transient absorption signals of **10** in (a) DCB, (b) DCM and (c) ACN. (d-f) Transient absorption spectra gated at different pump-probe delay times (upper panels) and time-integrated absorption and emission spectra, normalized to unity (lower panels) of **10** in (d) DCB, (e) DCM and (f) ACN. The transient absorption spectra were excited at 480 nm.

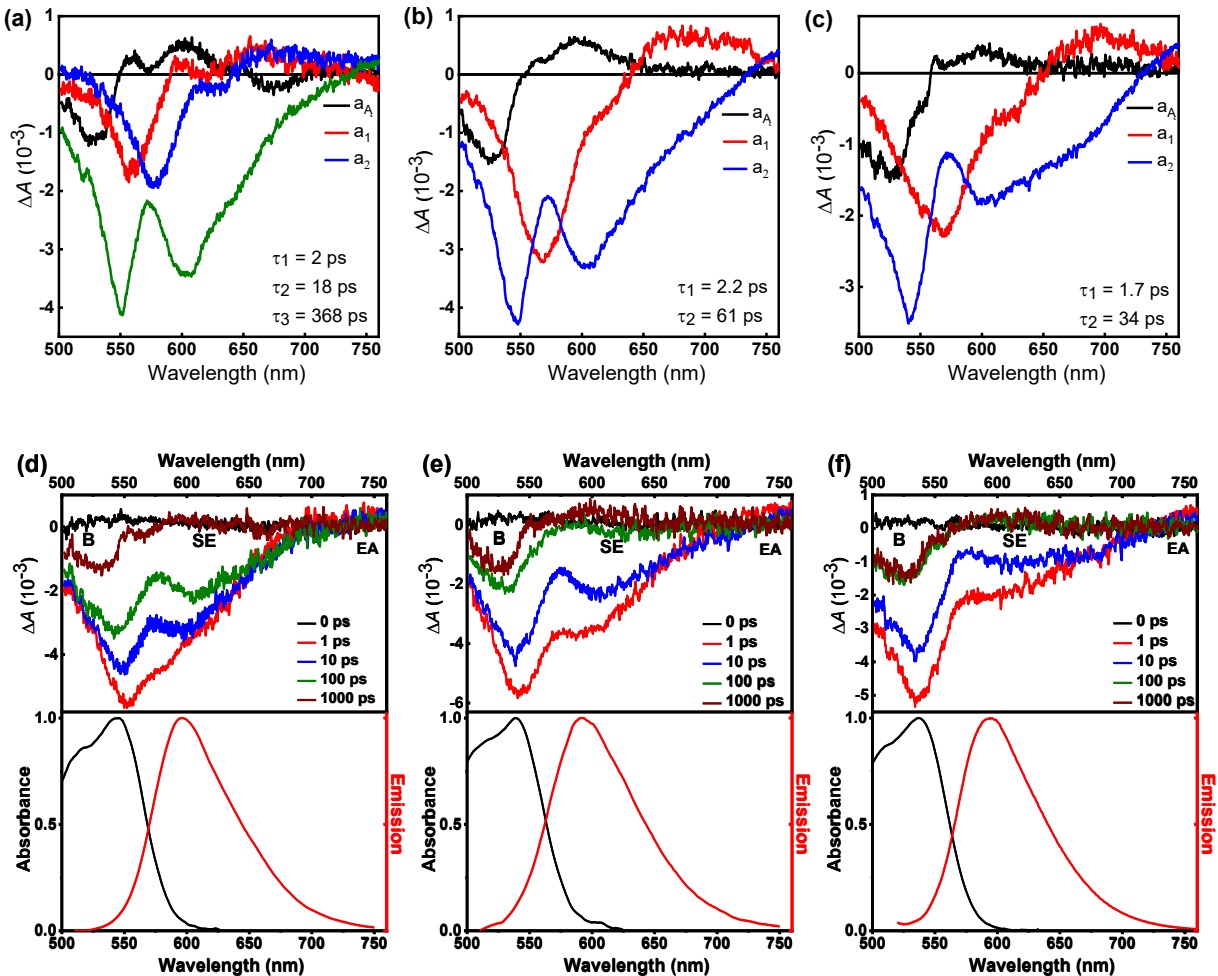


Figure S50. (a-c) DADS showing the distributions of amplitudes, $A_i(\lambda)$, along with the corresponding time constants, τ_i , obtained from multiexponential global fits (eq. S1) of transient absorption signals of **11** in (a) DCB, (b) DCM and (c) ACN. (d-f) Transient absorption spectra gated at different pump-probe delay times (upper panels) and time-integrated absorption and emission spectra, normalized to unity (lower panels) of **11** in (d) DCB, (e) DCM and (f) ACN. The transient absorption spectra were excited at 480 nm.

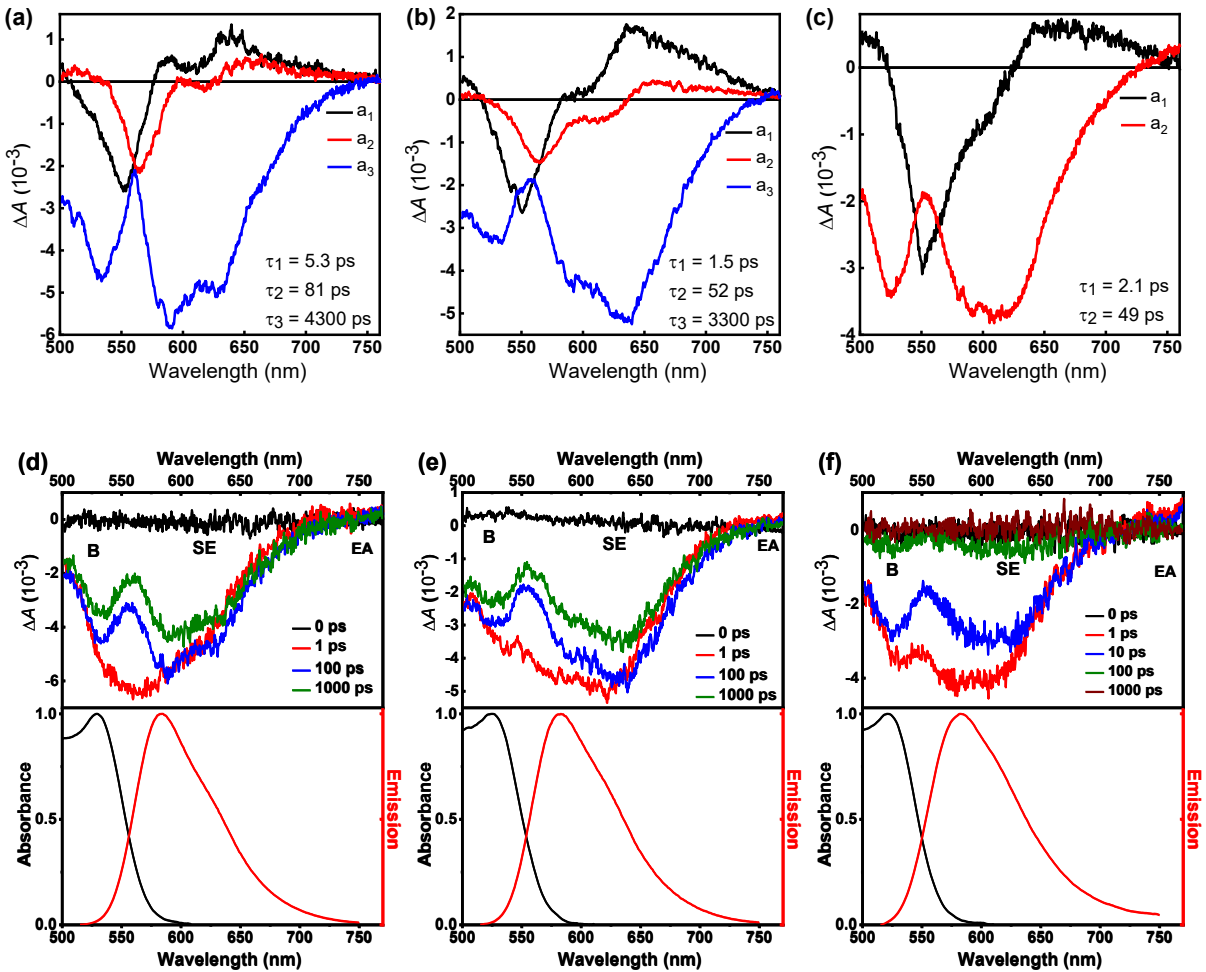


Figure S51. (a-c) DADS showing the distributions of amplitudes, $A_i(\lambda)$, along with the corresponding time constants, τ_i , obtained from multiexponential global fits (eq. S1) of transient absorption signals of **12** in (a) DCB, (b) DCM and (c) ACN. (d-f) Transient absorption spectra gated at different pump-probe delay times (upper panels) and time-integrated absorption and emission spectra, normalized to unity (lower panels) of **12** in (d) DCB, (e) DCM and (f) ACN. The transient absorption spectra were excited at 480 nm.

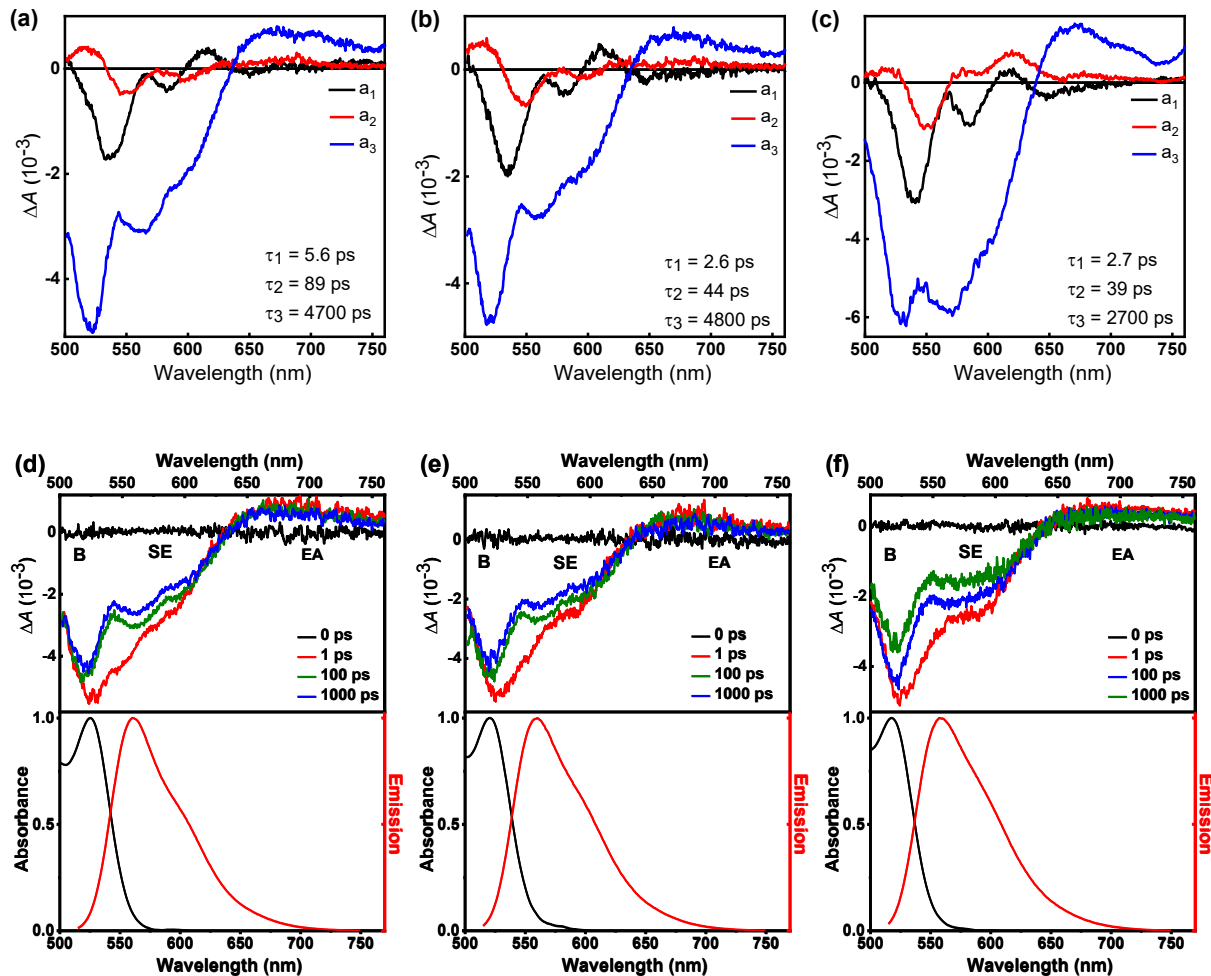
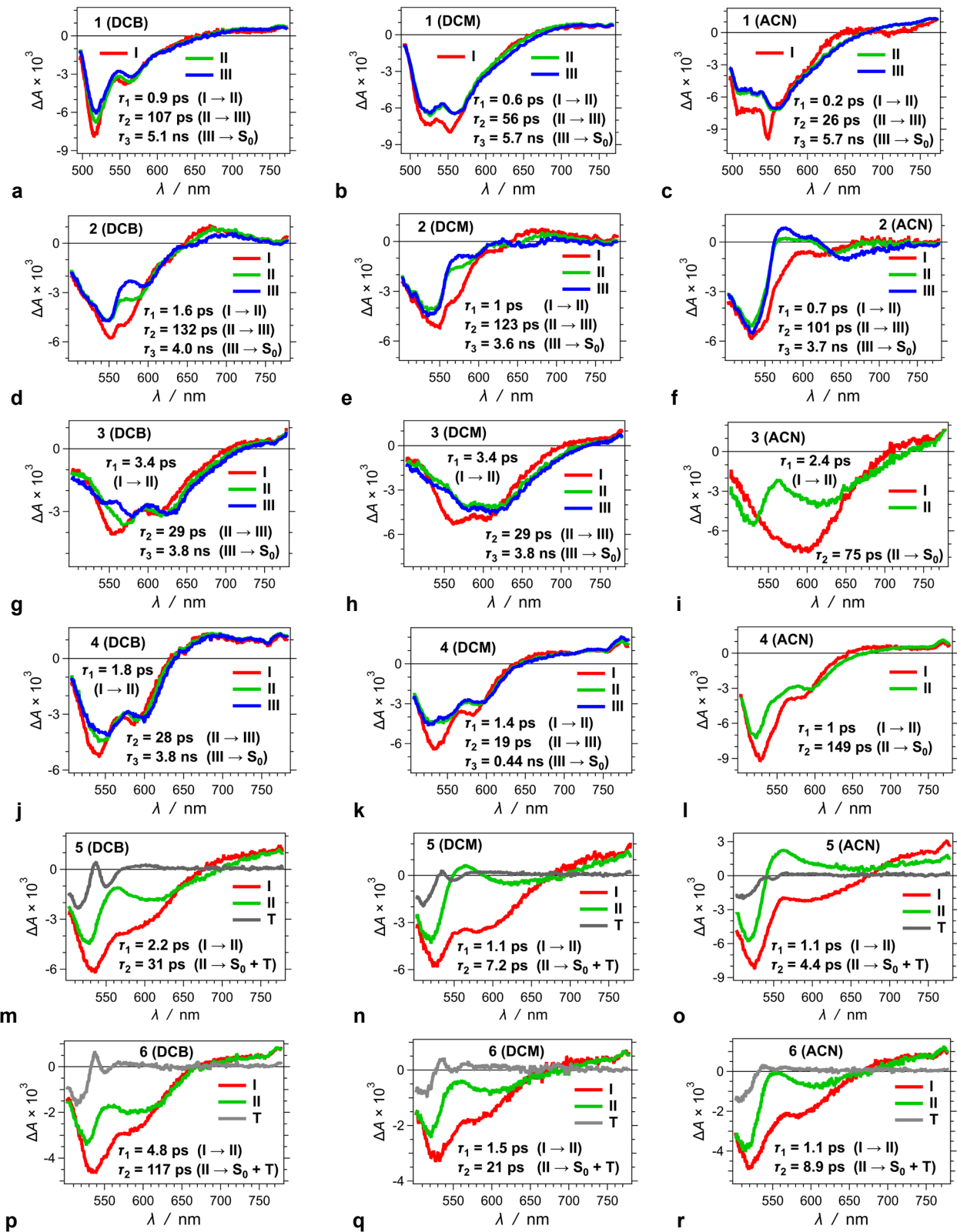


Figure S52. (a-c) DADS showing the distributions of amplitudes, $A_i(\lambda)$, along with the corresponding time constants, τ_i , obtained from multiexponential global fits (eq. S1) of transient absorption signals of **13** in (a) DCB, (b) DCM and (c) ACN. (d-f) Transient absorption spectra gated at different pump-probe delay times (upper panels) and time-integrated absorption and emission spectra, normalized to unity (lower panels) of **13** in (d) DCB, (e) DCM and (f) ACN. The transient absorption spectra were excited at 480 nm.



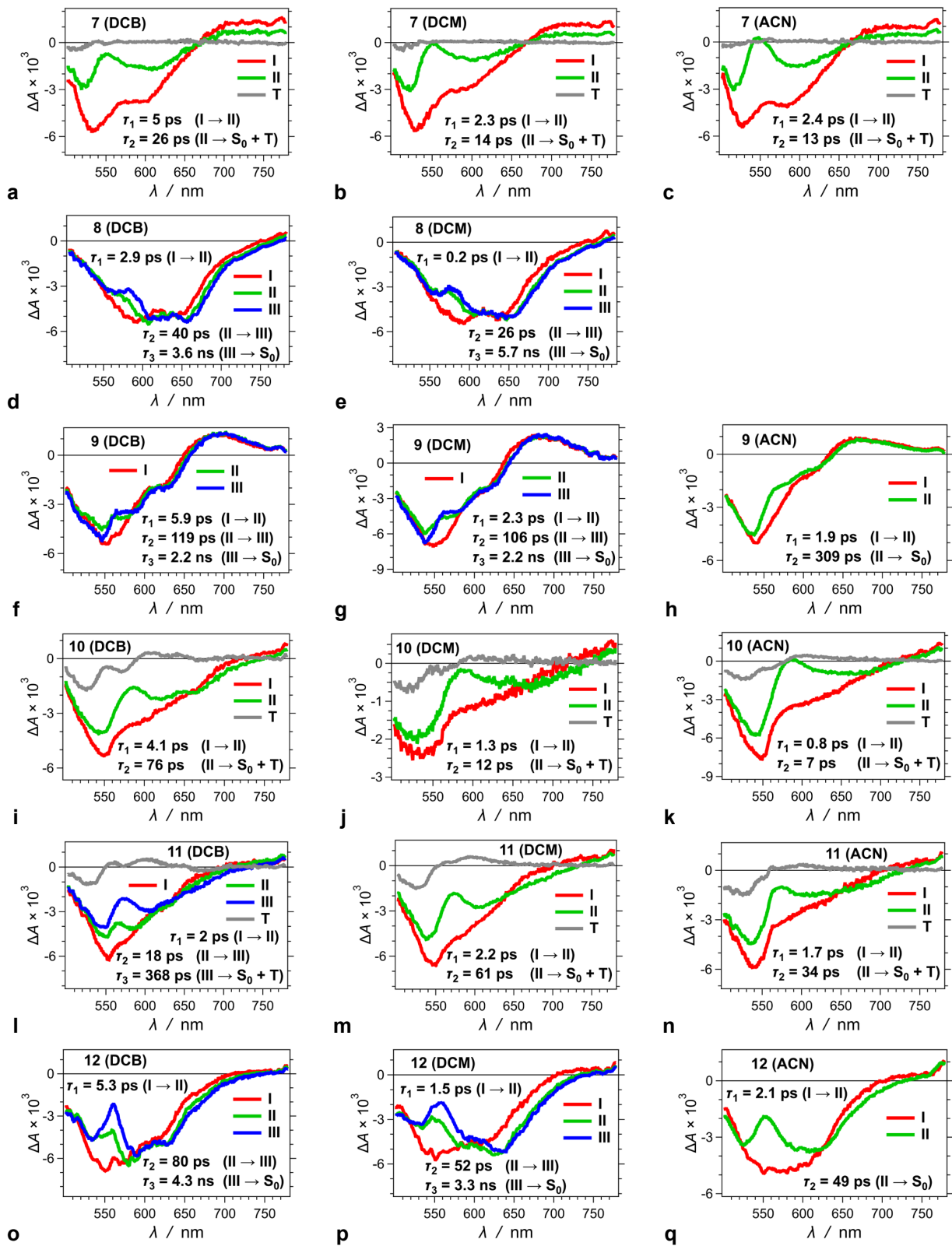


Figure S54. Spectra of **7**, **8**, **9**, **10**, **11** and **12**, for DCB, DCM and ACN, showing the transitions associated with the time constants, τ_i , that the global fits produce (eq. S1), reconstructed from DADS amplitude distributions, $A_i(\lambda)$, (Figure S46 – S51).

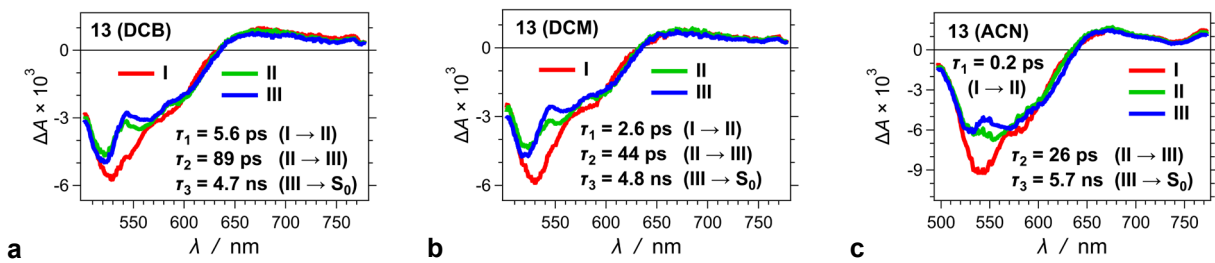


Figure S55. Spectra of **13**, for (a) DCB, (b) DCM and (c) ACN, showing the transitions associated with the time constants, τ_i , that the global fits produce (eq. S1), reconstructed from DADS amplitude distributions, $A_i(\lambda)$, (Figure S52a-c).

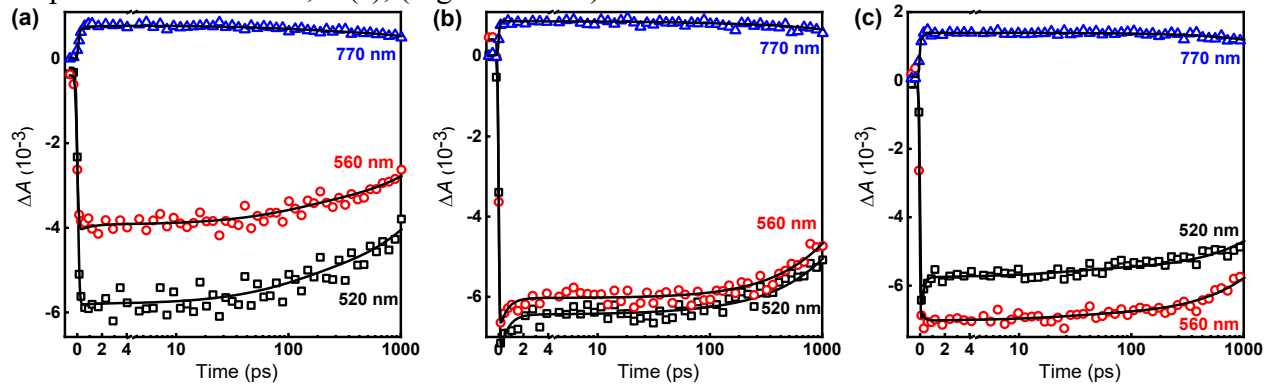


Figure S56. TA decays of **1** in (a) DCB, (b) DCM and (c) ACN excited at 480 nm and gated at different observation wavelengths. The solid lines are from the best global multiexponential fits to the experimental data.

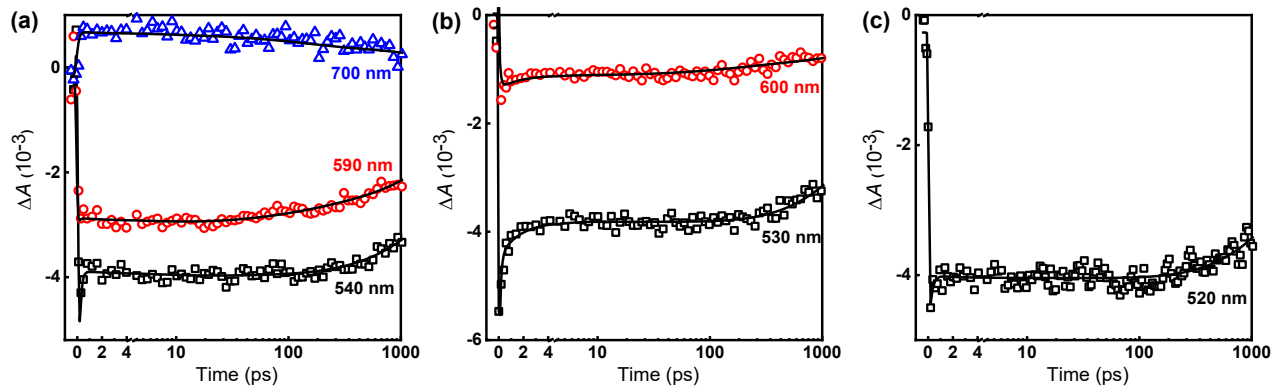


Figure S57. TA decays of **2** in (a) DCB, (b) DCM and (c) ACN excited at 480 nm and gated at different observation wavelengths. The solid lines are from the best global multiexponential fits to the experimental data.

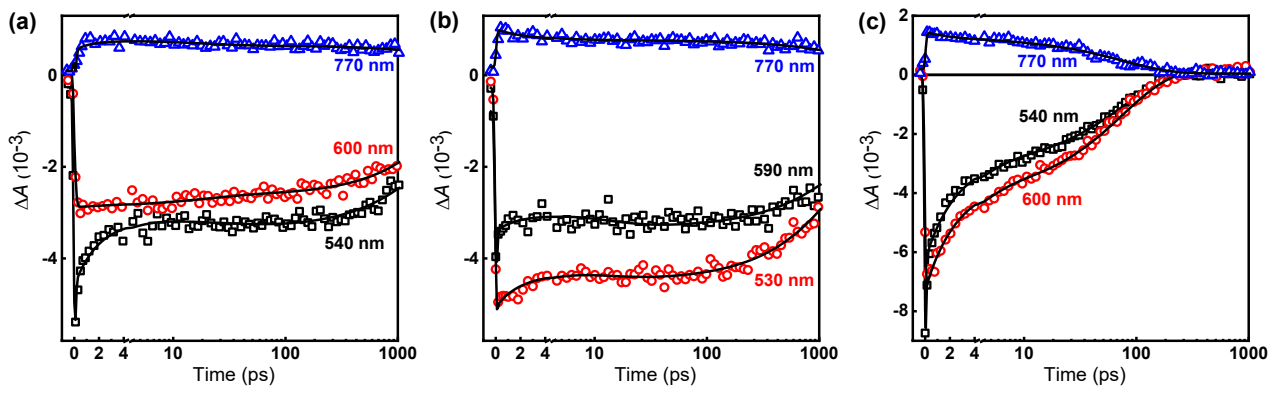


Figure S58. TA decays of **3** in (a) DCB, (b) DCM and (c) ACN excited at 480 nm and gated at different observation wavelengths. The solid lines are from the best global multiexponential fits to the experimental data.

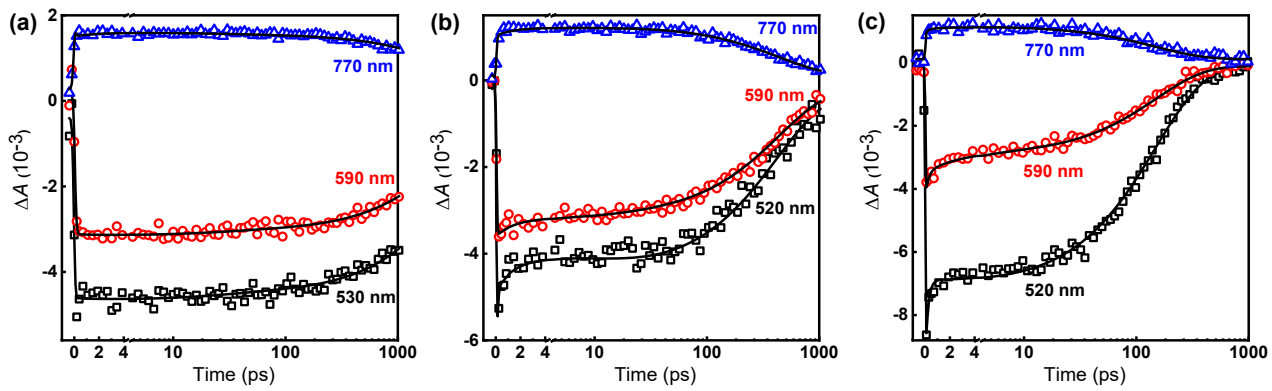


Figure S59. TA decays of **4** in (a) DCB, (b) DCM and (c) ACN excited at 480 nm and gated at different observation wavelengths. The solid lines are from the best global multiexponential fits to the experimental data.

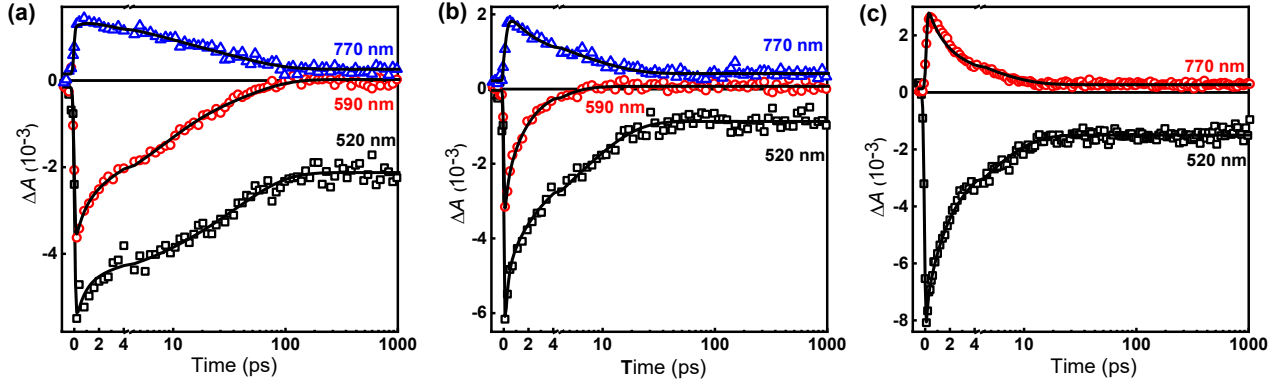


Figure S60. TA decays of **5** in (a) DCB, (b) DCM and (c) ACN excited at 480 nm and gated at different observation wavelengths. The solid lines are from the best global multiexponential fits to the experimental data.

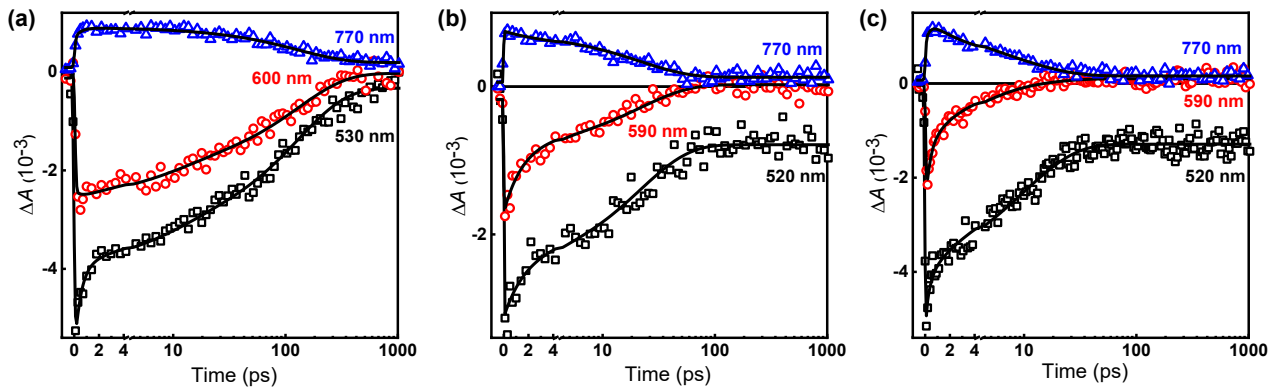


Figure S61. TA decays of **6** in (a) DCB, (b) DCM and (c) ACN excited at 480 nm and gated at different observation wavelengths. The solid lines are from the best global multiexponential fits to the experimental data.

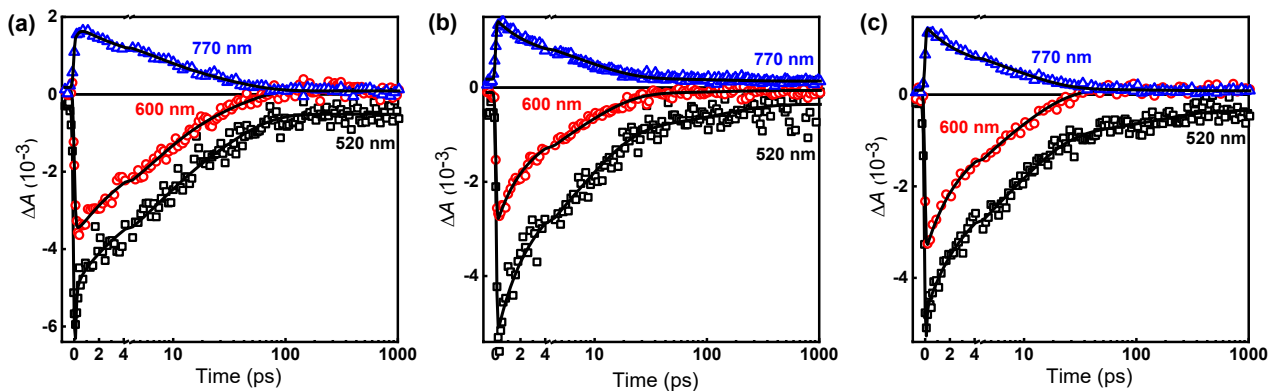


Figure S62. TA decays of **7** in (a) DCB, (b) DCM and (c) ACN excited at 480 nm and gated at different observation wavelengths. The solid lines are from the best global multiexponential fits to the experimental data.

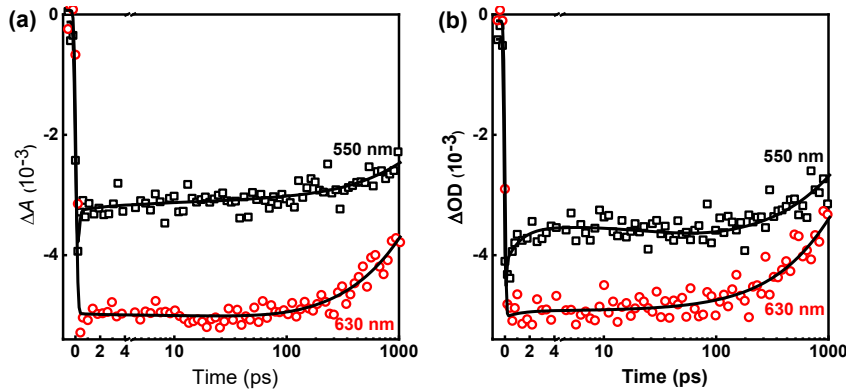


Figure S63. TA decays of **8** in (a) DCB and (b) DCM excited at 480 nm and gated at different observation wavelengths. The solid lines are from the best global multiexponential fits to the experimental data. Due to extremely low solubility of **8** in ACN the measurement of TA signal in the dye was not possible.

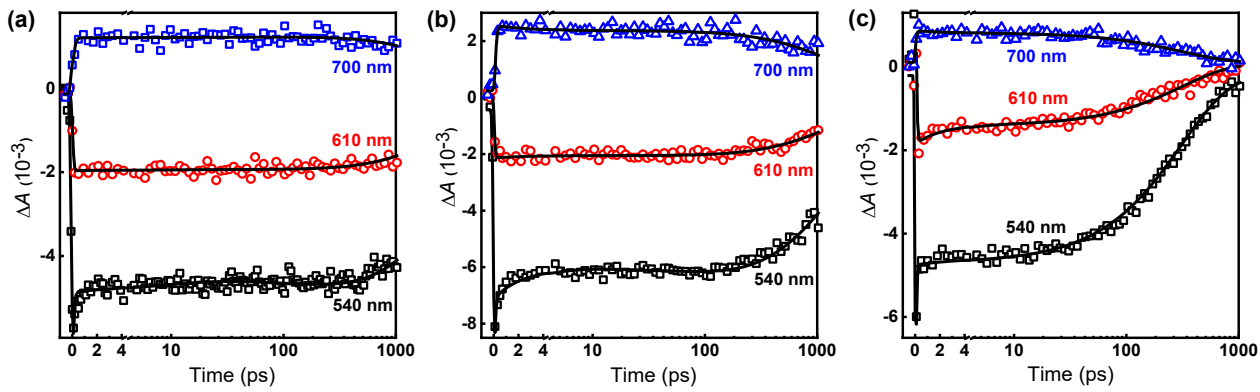


Figure S64. TA decays of **9** in (a) DCB, (b) DCM and (c) ACN excited at 480 nm and gated at different observation wavelengths. The solid lines are from the best global multiexponential fits to the experimental data.

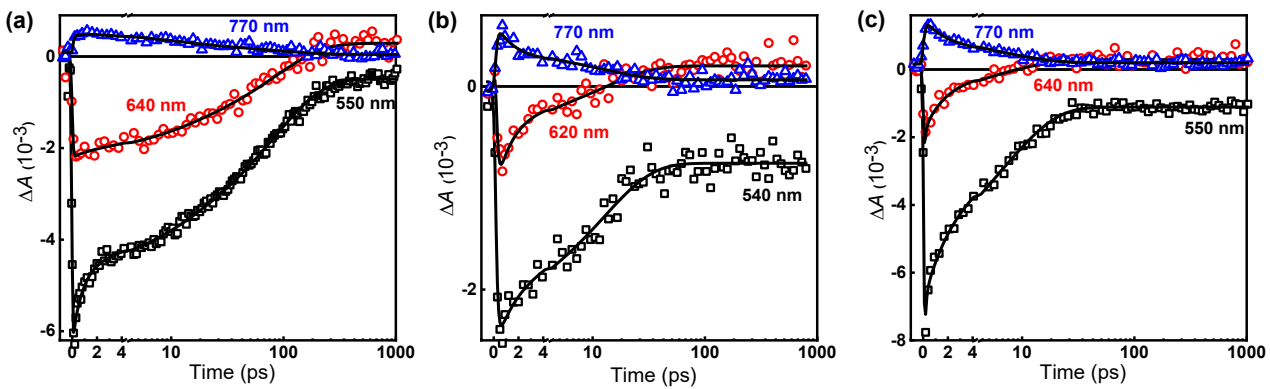


Figure S65. TA decays of **10** in (a) DCB, (b) DCM and (c) ACN excited at 480 nm and gated at different observation wavelengths. The solid lines are from the best global multiexponential fits to the experimental data.

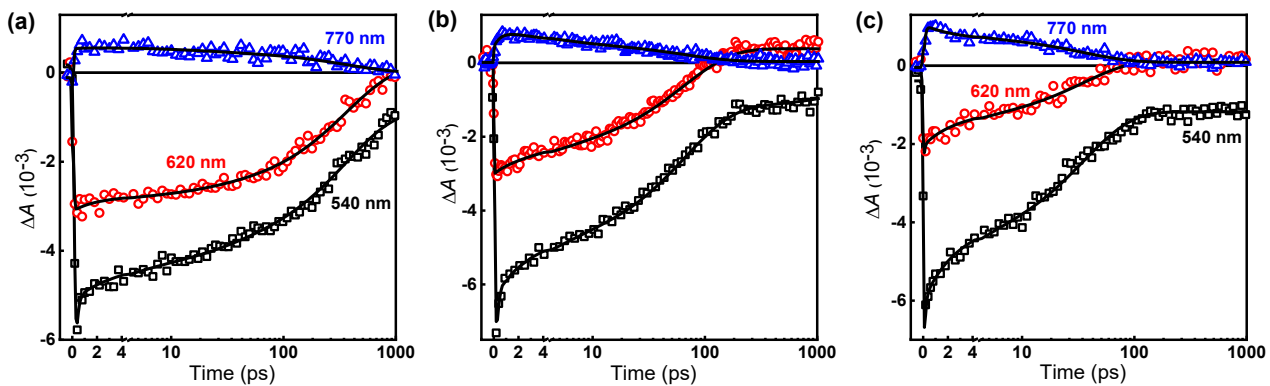


Figure S66. TA decays of **11** in (a) DCB, (b) DCM and (c) ACN excited at 480 nm and gated at different observation wavelengths. The solid lines are from the best global multiexponential fits to the experimental data.

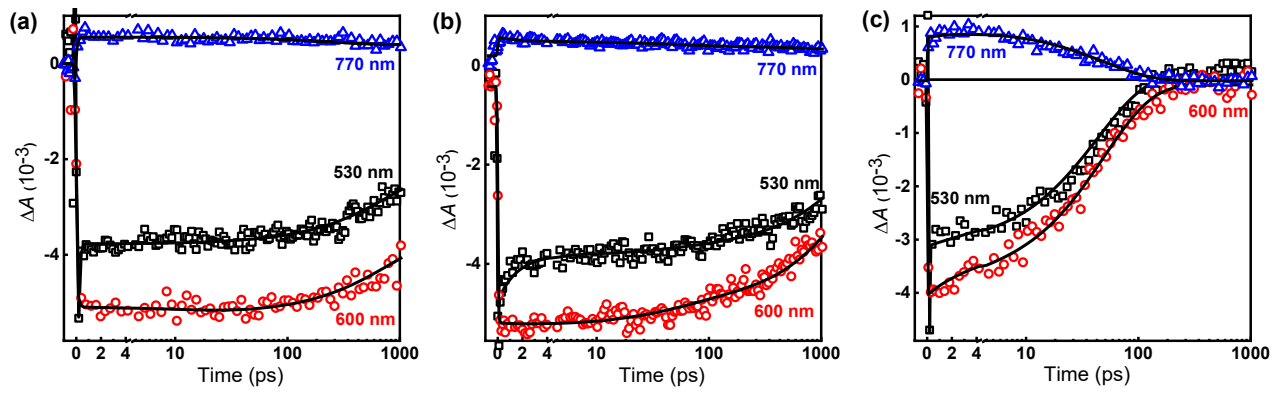


Figure S67. TA decays of **12** in (a) DCB, (b) DCM and (c) ACN excited at 480 nm and gated at different observation wavelengths. The solid lines are from the best global multiexponential fits to the experimental data.

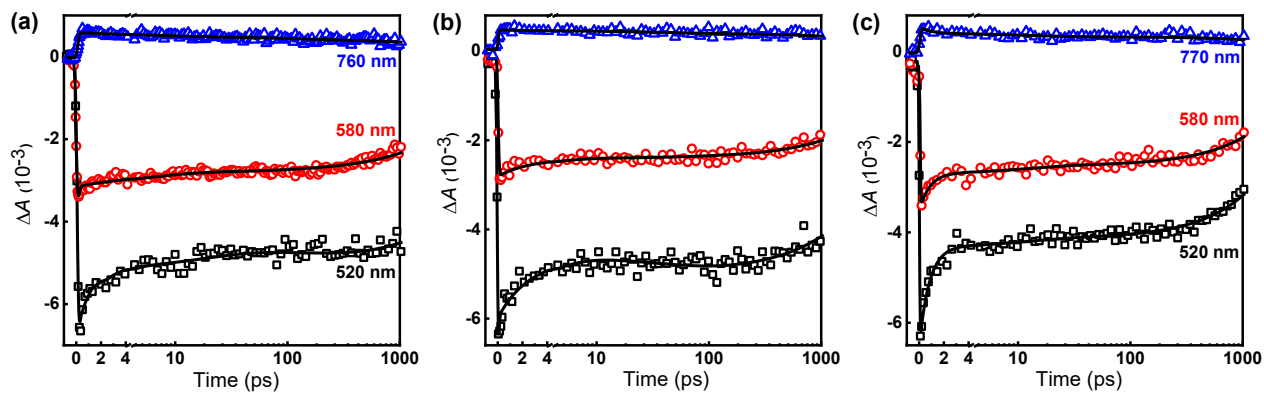


Figure S68. TA decays of **13** in (a) DCB, (b) DCM and (c) ACN excited at 480 nm and gated at different observation wavelengths. The solid lines are from the best global multiexponential fits to the experimental data.

Lippert–Mataga–Ooshika analysis

To estimate the increase in the electric dipole moments of the DPND dyes upon optical excitation, we examine the dependence of their Stokes' shifts, $\Delta\mathcal{E}$, on the medium polarity, as implemented by the Lippert–Mataga–Ooshika formalism (Figure 4C):^{17,18,19}

$$\Delta\mathcal{E} = \frac{(\mu^* - \mu_0)^2}{2 \varepsilon_0 r^3} \Delta f_O(\varepsilon, n^2) + \Delta\mathcal{E}_0 \quad (\text{S2})$$

Where μ_0 and μ^* are the permanent electric dipole moments of the relaxed S_0 and the fluorescent S_1 state; ε_0 is the vacuum permittivity ($5.526 \times 10^{-3} e^2 V^{-1}\text{\AA}^{-1}$); and r is the molecular radius estimated from the longest distance between non-hydrogen atoms in the optimized ground-state geometries. The Onsager polarity, $f_O(x) = 2(x - 1)/(2x + 1)$, $f_O(\varepsilon, n^2) = f_O(\varepsilon) - f_O(n^2)$, accounts for the media effects from the dipolar / orientational, P_μ , and nuclear, P_v , polarizations,²⁰ i.e., the difference between the total Onsager polarity, $f_O(\varepsilon)$, and the polarity originating from the electronic polarization only, $f_O(n^2)$. The intercepts, ΔE_0 , correspond to the Stokes' shifts for non-polar media, i.e., for solvents with $f_O(\varepsilon, n^2) = 0$.

The slopes of the linear fits of $\Delta\mathcal{E}$ vs. $f_O(\varepsilon, n^2)$ are proportional to the square of the vector difference between the dipole of the emissive excited state and the relaxed ground state, i.e., $\Delta\mu = |\mu^* - \mu_0| = (2 \varepsilon_0 r^3 \text{ slope})^{1/2}$. For PB and SOA, the values of $\Delta\mathcal{E}$ appear as outliers (Figure 4C). These ester solvents slightly perturb the vibronic amplitudes of the emission bands causing about 0.2-eV shifts in the spectral maxima (Figure 4A,B). In the recorded fluorescence spectra of these DPNDs against abscissas in wavelength scales, the maxima correspond usually the most hypsochromic vibronic peak (Figures S3 – S15). Converting of the spectra to energy scales, i.e., $F(\mathcal{E}) = F(\lambda) \mathcal{E}^{-5}$, increases

¹⁷ Lippert, E. *Z. Naturforsch. A* **1955**, *10a*, 541-545.

¹⁸ Mataga, N.; Kaifu, Y.; Koizumi, M. *Bull. Chem. Soc. Jpn.* **1956**, *29*, 465-470.

¹⁹ Ooshika, Y. *J. Phys. Soc. Jpn.* **1954**, *9*, 594-602.

²⁰ Upadhyayula, S.; Bao, D.; Millare, B.; Sylvia, S. S.; Masum Habib, K. M.; Ashraf, K.; Ferreira, A.; Bishop, S.; Bonderer, R.; Baqai, S.; Jing, X.; Penchev, M.; Ozkan, M.; Ozkan, C. S.; Lake, R. K.; Vullev, V. *I.J. Phys. Chem. B* **2011**, *115*, 9473-9490.

the amplitude of the most hypsochromic vibronic peak to a lesser extent than of the other peaks. When the second most hypsochromic vibronic peak is only slightly less intense than the first one, it becomes the spectral maximum for $F(\mathcal{E})$, which is the case for the ester solvents. The 0.2-eV differences between the two most hypsochromic peaks correspond the deviations from the linearity of \mathcal{E}_{fl} and $\Delta\mathcal{E}$ vs. $f_0(\varepsilon, n^2)$ for the PB and SOA (Figure 4A-C).

Therefore, our initial analysis includes only HEX, DCB, DCM and ACN, yielding $slope_1$ and $\Delta\mu_1$ (Table S4). The expression for propagation of errors in power relations allows for estimating the uncertainty of the values of $\Delta\mu$ estimated from these *slopes*, i.e., for $y = (C x)^n$, where C is a constant, $x = x \pm \delta x$ and $y = y \pm \delta y$, $\delta y = n C^n x^{1-n} \delta x$. The values of $\Delta\mu_1$ do not exceed 4.5 D, with uncertainties that are comparable and even larger than $\Delta\mu_1$ for some of the compounds (Table S4).

The exclusion of PB and SOA from this analysis, while well-reasoned, is still arbitrary. Linear fits including all six solvents, HEX, SOA, PB, DCB, DCM and CAN, produce estimates that are smaller than $slope_1$ and $\Delta\mu_1$, but with larger uncertainties for most of the compounds, see, $slope_2$ and $\Delta\mu_2$ (Table S4), which is expected for plots of $\Delta\mathcal{E}$ vs. $f_0(\varepsilon, n^2)$, with scattered values, i.e., for the ester solvents.

For **1**, **4**, **9**, **11** and **13** in PB and SOA, the two vibronic maxima are well resolved. For these samples in PB and SOA, the second maxima, $\mathcal{E}_{\text{fl}}^{(2)}$, corresponding to the most hypsochromic vibronic peaks, are in line with the trends of \mathcal{E}_{fl} vs. $f_0(\varepsilon, n^2)$ for the other solvents (Figures 4A,B). Furthermore, Stokes' shifts estimated from these second maxima at the most hypsochromic vibronic peaks, $\Delta\mathcal{E}^{(2)} = \mathcal{E}_{\text{abs}} - \mathcal{E}_{\text{fl}}^{(2)}$, follow well the linearity of the Lippert–Mataga–Ooshika relationship, eq. S2 (Figure 4C), reproducing the values of $\Delta\mu_1$.

These small estimates of $\Delta\mu$ are consistent with the small differences between the computed dipoles of the optimized S_0 and the relaxed emissive S_1 states of the DPND conjugates (Table S4). In this

type of analysis it is important to consider possible overestimations of $\Delta\mu$ obtained from ΔE vs. $fo(\epsilon, n^2)$ linear correlations. Based on the Onsager solvation theory, Lippert–Mataga–Ooshika formalism assumes spherical solvation cavities, which is not the case for planer and elongated chromophores. Therefore, the used molecular radii are often larger than the effective radii for such systems, resulting in overestimates of the dipole changes, since $\Delta\mu \propto r^{3/2}$. At the same time, challenges to account for long-range electrostatic interactions, inherent to DFT (especially for excited states), may render possibilities for underestimation of dipole values of compounds with strongly polarizing groups, such as -NO₂.

Overall, this analysis yields small values for $\Delta\mu$ of the DPND conjugates, and suggests that their fluorescent S₁ states do not acquire a charge-transfer character.

Table S4. Results from Lippert–Mataga–Ooshika analysis and comparison with DFT-calculated dipoles.

<i>compd</i>	<i>r</i> / Å ^a	<i>slope</i> ₁ / eV ^b	<i>slope</i> ₂ / eV ^c	$\Delta\mu_1$ / D ^b	$\Delta\mu_2$ / D ^c	μ_0 / D ^d	$\mu^{(FC)}$ / D ^d	μ^* / D ^d
1	5.7	0.10 ± 0.03	0.029 ± 0.200	2.2 ± 0.3	1.2 ± 4.0	0.00	0.00	0.00
2	8.4	0.11 ± 0.04	0.048 ± 0.172	4.1 ± 0.8	2.7 ± 4.8	—	—	—
3	7.1	0.13 ± 0.06	0.13 ± 0.05	3.4 ± 0.8	3.4 ± 0.6	5.76	6.15	6.91
4	7.2	0.059 ± 0.044	-0.009 ± 0.187	2.3 ± 0.9	-0.9 ± 9.7	5.77	5.41	6.50
5	6.4	0.083 ± 0.099	0.018 ± 0.189	2.4 ± 1.4	1.1 ± 5.8	3.53	2.80	3.32
6	7.1	0.15 ± 0.10	0.067 ± 0.189	3.8 ± 1.2	2.8 ± 3.1	—	—	—
7	6.1	0.051 ± 0.106	0.019 ± 0.121	1.7 ± 1.8	1.0 ± 3.4	4.73	4.70	4.11
8	9.6	0.90 ± 0.034	0.035 ± 0.156	4.5 ± 0.8	2.8 ± 6.2	0.00	0.00	0.00
9	8.6	0.071 ± 0.089	0.019 ± 0.159	3.4 ± 2.1	1.7 ± 7.2	—	—	—
10	8.2	0.060 ± 0.102	0.060 ± 0.102	2.9 ± 2.5	—	0.00	0.00	0.00
11	8.6	0.10 ± 0.02	0.044 ± 0.159	4.1 ± 0.4	2.6 ± 4.7	—	—	—
12	9.6	0.15 ± 0.01	0.10 ± 0.14	5.7 ± 0.2	4.7 ± 3.3	—	—	—
13	8.6	0.029 ± 0.029	-0.030 ± 0.153	2.2 ± 1.1	-2.2 ± 5.6	0.00	0.00	0.00

^a Molecular radii obtained from the halves of the longest distances between non-hydrogen atoms in the DFT-optimized ground-state geometries. ^b The values of *slope*₁ are obtained from linear fits of $\Delta\mathcal{E}$ vs. $fo(\epsilon, n^2)$ for HEX, DCB, DCM and ACN, and $\Delta\mu_1 = (2 \epsilon_0 r^3 slope_1)^{1/2}$. ^c The values of *slope*₂ are obtained from linear fits of $\Delta\mathcal{E}$ vs. $fo(\epsilon, n^2)$ for HEX, PB, SOA, DCB, DCM and ACN, and $\Delta\mu_2$

$= (2 \varepsilon_0 r^3 slope_2)^{1/2}$. ^d Magnitudes of dipole moments of DFT-computed structures: μ_0 – of the ground-state optimized geometries; $\mu^{(FC)}$ – of the Franck-Condon (FC) excited states, i.e., of S₁ electronic states with the geometry of the energy-minimized S₀ state; μ^* – of the relaxed S₁ structures, that manifest radiative deactivation to S₀ with large oscillator strengths.

4. Computational details

General Remarks. The equilibrium geometries of investigated molecular systems were determined by minimizing the energy of the electronic ground-state using second-order Møller–Plesset (MP2) perturbation theory.²¹ Vertical excitation energies, oscillator strengths and dipole moments of excited states were evaluated at the ground-state equilibrium geometries with the second-order algebraic-diagrammatic-construction (ADC(2)) method²², which is a computationally efficient single-reference propagator method. The ADC(2) method provides a balanced description of the energies of locally-excited ($^1\pi\pi^*$) states of the chromophore and intramolecular charge-transfer (CT) states which is essential for a reliable characterization of the potential-energy (PE) surfaces of photo-induced reactions. The ADC(2) method was also used for geometry optimization of the lowest excited singlet state in order to determine spectral properties of the fluorescing state. The geometries were optimized without symmetry constraint.

As the driving coordinate for the construction of the minimum-energy reaction path (relaxed scan) for the ring-closing reaction, the CO bond length (R_{CO}) formed between carbon atom of pyrrole and oxygen atom of nitrobenzene was chosen. For one-dimensional relaxed scans, R_{CO} was fixed, while the energy of a given electronic state was minimized with respect to all other nuclear degrees of freedom. The ‘vertical’ energy of the electronic ground state was determined by single-point energy calculations at these optimized geometries. Dunning’s correlation-consistent double- ζ basis set (cc-pVDZ)²³ was employed for single-structure geometry optimizations. For more time-consuming excited-state minimum-energy reaction path construction, a more compact, def-SV(P)²⁴, basis set

²¹ C. Møller, M. S. Plesset, *Phys. Rev.* **1934**, *46*, 618-622.

²² A. B. Trofimov, J. Schirmer, *J. Phys. B: At., Mol. Opt. Phys.* **1995**, *28*, 2299-2324.

²³ T. H. Dunning Jr., *J. Chem. Phys.* **1989**, *90*, 1007-1023.

²⁴ A. Schäfer, H. Horn, R. Ahlrichs, *J. Chem. Phys.* **1992**, *97*, 2571.

was used. The electronic-structure calculations were performed with the TURBOMOLE²⁵ program package, using the resolution-of-the-identity (RI) approximation.²⁶

Quadrupolar-type di-nitroaryl DPNDs, such as **10** and **13** (Figure 2) can exist in two isomeric forms with either C_i or C_2 symmetry, depending on the mutual orientation of the aryl substituents. Compound **8**, with only one possible conformer symmetry, C_i , presents an exception. These rotamers, with C_i and C_2 symmetry, are almost isoenergetic and manifest similar spectroscopic properties.³ From here on and in the manuscript, discussion will focus solely on the structures with C_i symmetry. For the theoretical studies, we truncated the aliphatic groups of the DPND core to methyl substituents. While this change has only a marginal effect on the electronic properties of these systems, it significantly expedites excited-state explorations at the *ab initio* theoretical level.

Table S5. Average dihedral angles between peripheral nitroaryl moieties and the DPND core for theoretically considered derivatives. Values in parentheses refer to twist angle of the nitro group relative to an aryl ring. Optimization of the molecular geometry in the ground electronic state (S_0) and lowest excited state (S_1) were performed with MP2/cc-pVDZ and ADC(2)/cc-pVDZ methods, respectively.

Compound/State	S_0	S_1
3	45.0° (0.3°)	32.8° (1.0°)
4	45.9° (1.5°)	33.2° (1.7°)
5	45.6° (31.5°)	33.0° (19.3°)
7	53.9° (54.5°)	38.1° (46.8°)
8	45.3° (0.35°)	34.3° (0.94°)
10	45.3° (32.2°)	35.0° (26.1°)
13	62.1° (36.8°)	49.6° (37.0°)

²⁵ TURBOMOLE(V7.2), a development of University of Karlsruhe and Forschungszentrum Karlsruhe GmbH, 1989–2007, TURBOMOLE GmbH, since 2007.

²⁶ C. Hättig, F. Weigend, *J. Chem. Phys.* **2000**, *113*, 5154–5161.

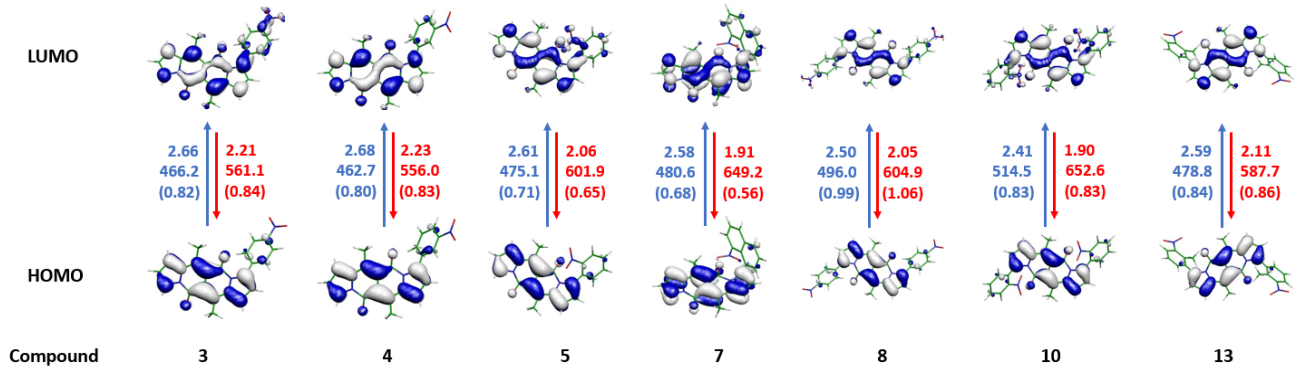
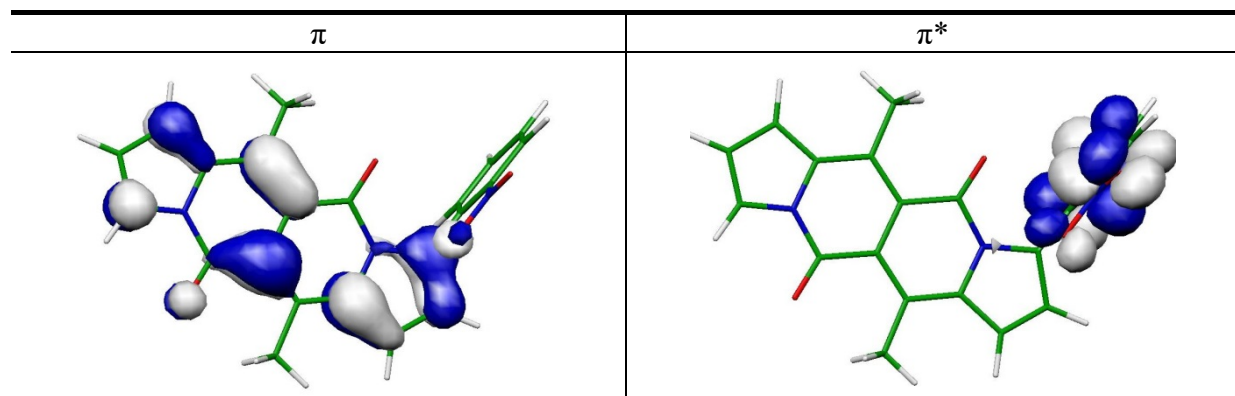


Figure S69. $S_0 \rightarrow S_1$ absorption (blue) and $S_1 \rightarrow S_0$ fluorescence (red) energies (ΔE in eV), corresponding transition wavelengths (λ in nm), oscillator strength (f) (given in brackets for the respective transition) and molecular orbitals involved in the electronic transition computed with the ADC(2)/cc-pVDZ method at the MP2/ADC(2) equilibrium geometry of the S_0/S_1 state, respectively. All longer alkyl chains were replaced with methyl groups.

Table S6. Hartree-Fock molecular orbitals involved into the ^1CT transition (compound 5, Figure 9 in the manuscript) at $R_{\text{Co}} = 1.85 \text{ \AA}$.



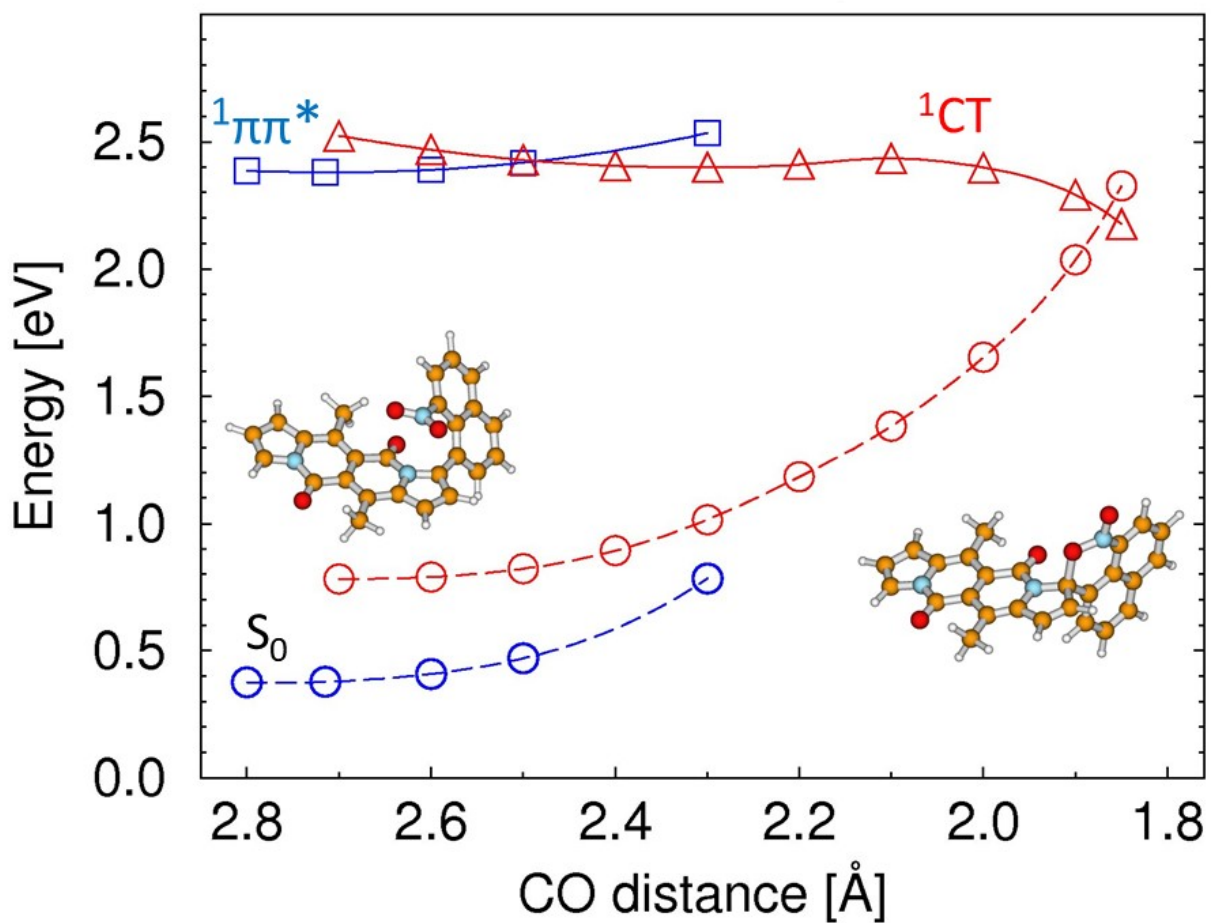


Figure S70. Potential-energy profiles of compound 7 optimized with the aid of the ADC(2)/def-SV(P) method in the lowest excited singlet state of the locally-excited ($^1\pi\pi^*$ – blue squares) and the charge-transfer (^1CT – red triangles) character along the CO distance. Circles connected by dashed line denote vertical energy of the ground state computed at the geometry of the respective excited state.

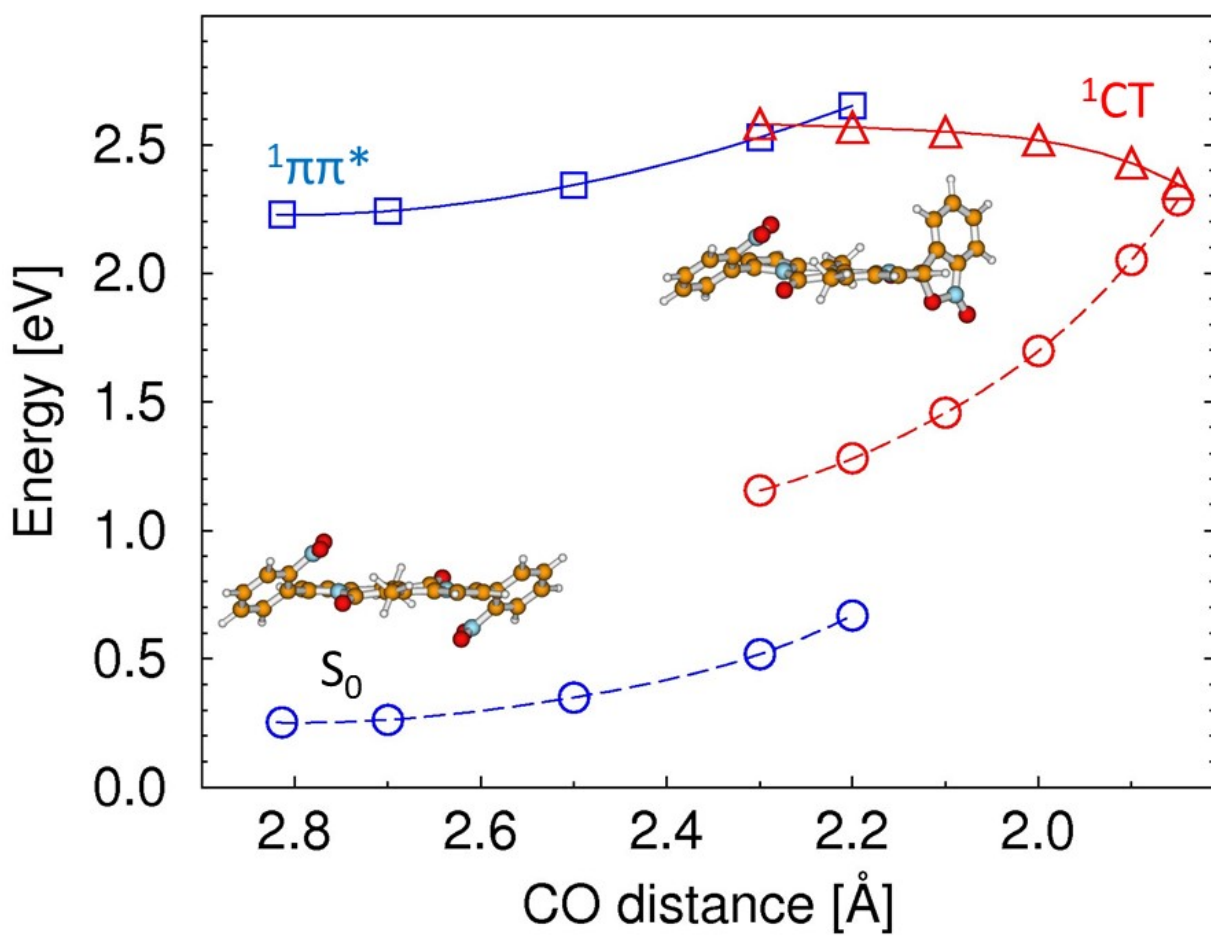


Figure S71. Potential-energy profiles of compound **10** optimized with the aid of the ADC(2)/def-SV(P) method for the locally-excited lowest singlet state ($^1\pi\pi^*$ – blue squares) and the charge-transfer (^1CT – red triangles) character along the CO distance. Circles connected by dashed lines denote the vertical energy of the ground state computed at the geometry of the respective excited state.

Table S7. Selected structural parameters (bond lengths in Å and torsional angles in degrees) and adiabatic energy (ΔE), oscillator strength (f), dipole moment (μ), electronic character of the lowest locally-excited singlet state of compound **10** determined with the ADC(2)/def-SV(P) method at $R_{CO} = 2.3\text{Å}$.

$^1\pi\pi^*$ state				
	State	E/eV	f	μ/Debye
S_0	0.52 ^a	-	3.24(0.73,0.38,-0.97)	(131a) ²
$^1\pi\pi^*$	2.53	0.788	4.24(0.81,-1.26,-0.73)	0.96(131a-132a)

^a Vertical energy.

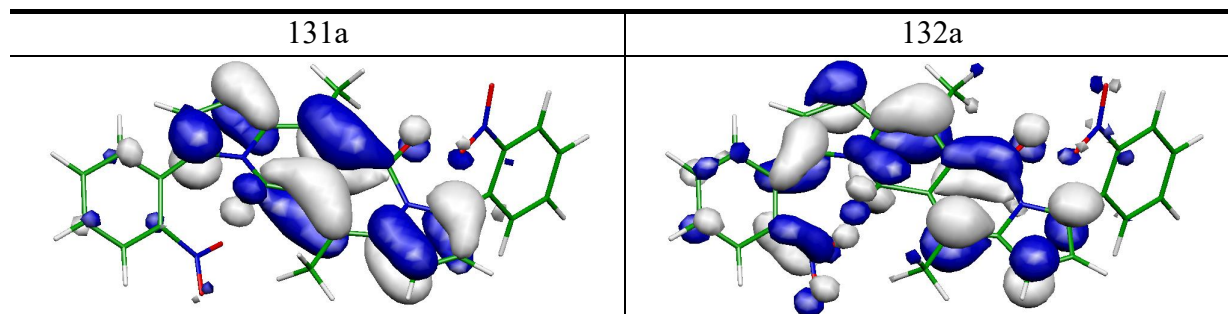


Table S8. Selected structural parameters (bond lengths in Å and torsional angles in degrees) and adiabatic energy (ΔE), oscillator strength (f), dipole moment (μ), electronic character of the lowest charge-transfer singlet state of compound **10** determined with the ADC(2)/def-SV(P) method at $R_{CO} = 2.3 \text{ \AA}$.

^1CT state				
	State	E/eV	f	μ/Debye
S_0	1.16 ^a	-	4.21(1.29,0.10,-1.03)	(131a) ²
^1CT	2.58	0.014	6.51(-0.83,2.06,-1.27)	0.46(131a-132a)+0.45(117a-132a)

^a Vertical energy.

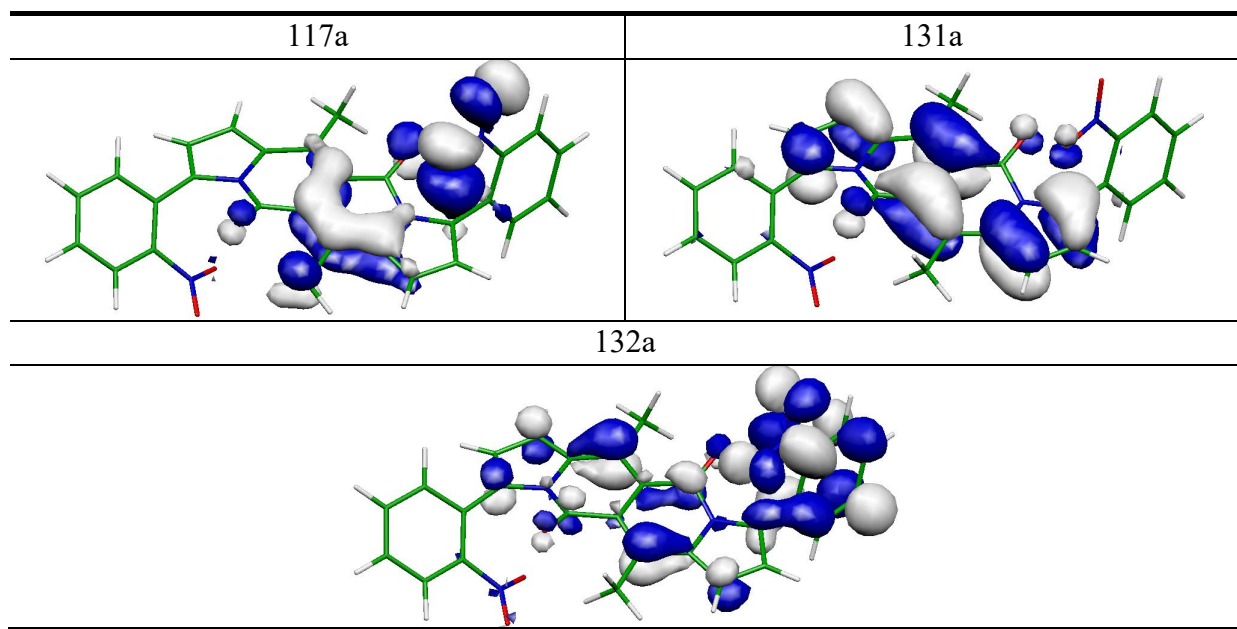


Table S9. Adiabatic energy (computed at the equilibrium geometry of a given state) in electron volts, and dipole moment in Debye (in brackets) determined at the MP2/ADC(2)/cc-pVDZ level of theory for exemplary, dipolar DPND molecules.

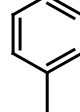
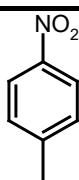
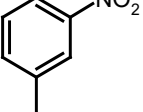
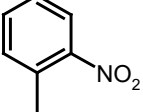
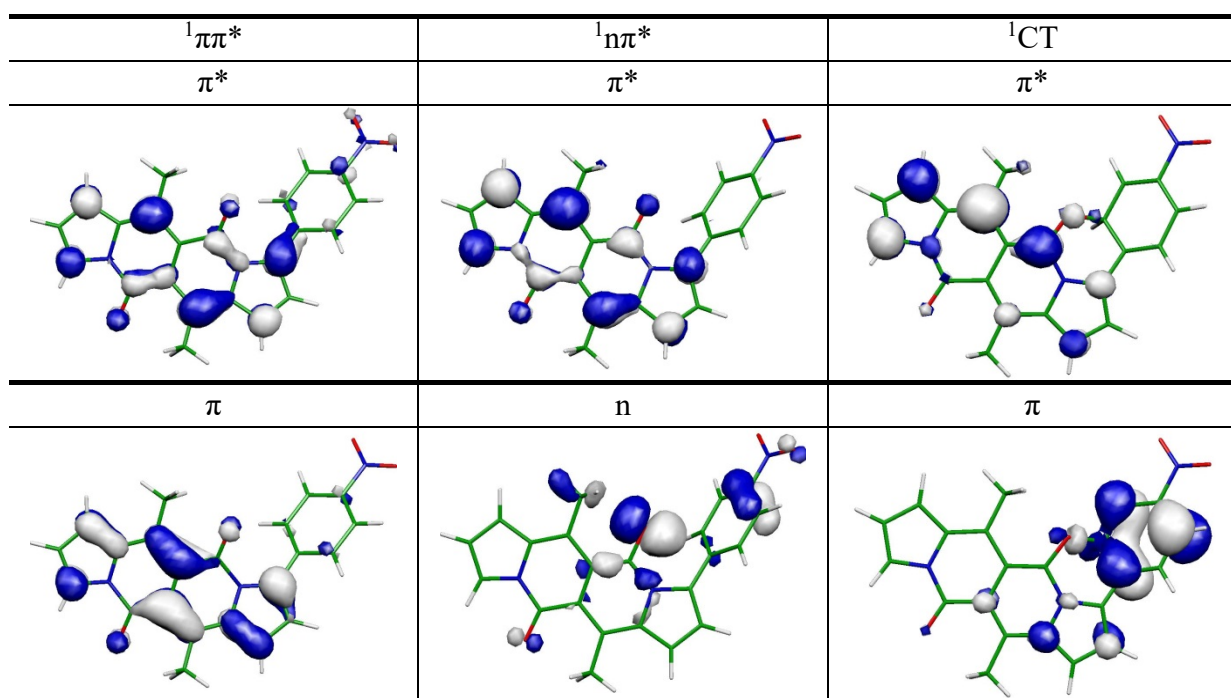
Compound					
	-	(3)	(4) <i>syn</i>	(4) <i>anti</i>	(5) <i>syn</i>
State					
S ₀	0.0 [0.92]	0.0 [5.76]	0.0 [4.06]	0.015 [5.77]	0.0 [3.53]
¹ $\pi\pi^*$	2.436 [3.99]	2.431 [6.25]	2.435 [3.45]	2.455 [6.50]	2.646 [3.93]
¹ n π^*	2.451 [9.76]	2.511 [3.71]	2.536 [8.69]	2.559 [5.22]	2.692 [8.93]
¹ n π^* - ¹ $\pi\pi^*$	0.015	0.079	0.101	0.104	0.045
¹ CT	2.657 [10.77]	2.689 [7.34]	2.602 [11.20]	2.685 [3.66]	2.793 [7.89]
¹ CT - ¹ $\pi\pi^*$	0.222	0.257	0.167	0.230	0.307

Table S10. Hartree-Fock molecular orbitals involved into the relevant electronic transitions of compound **3** determined at the equilibrium geometry of the respective state.



Cartesian coordinates:

Compound **3**, S₀:

44

C	3.737786	-3.413264	0.782455
C	4.273865	-2.413433	-0.062563
C	5.382857	-2.733751	-0.878956
C	5.944121	-4.018057	-0.865418
C	5.380940	-4.983214	-0.021554
C	4.285801	-4.700254	0.807695
C	3.791015	-1.027366	-0.043471
N	2.461624	-0.609497	-0.003100
C	2.404395	0.783552	0.127910
C	3.737651	1.250148	0.175857
C	4.584050	0.128693	0.072314
C	1.316400	-1.408090	-0.322367
C	0.020911	-0.715897	-0.151859
C	-0.026856	0.724038	0.071227
C	1.153729	1.470842	0.178274
C	-1.152878	-1.478203	-0.237489
C	-2.409003	-0.808508	-0.103725
N	-2.455550	0.569446	0.092736
C	-1.323517	1.424963	0.188352
C	-3.764793	0.997444	0.179785

C	-4.583430	-0.123161	0.037111
C	-3.748573	-1.256668	-0.140059
O	-1.498837	2.626133	0.359009
C	-1.187975	-2.968734	-0.462992
C	1.188991	2.967570	0.362878
O	1.468191	-2.566380	-0.689213
H	-3.981597	2.052481	0.334545
N	5.961282	-6.342759	-0.001228
O	6.928408	-6.556693	-0.735669
O	5.439029	-7.169966	0.749576
H	3.886338	-5.481062	1.458013
H	2.898306	-3.173929	1.440986
H	6.793154	-4.282322	-1.499019
H	5.793628	-1.969191	-1.546714
H	5.673875	0.120249	0.126755
H	4.046438	2.287586	0.297834
H	0.680002	3.258012	1.295220
H	2.224429	3.332465	0.388590
H	0.645500	3.476189	-0.447835
H	-5.673525	-0.114022	0.059561
H	-4.073750	-2.286157	-0.286493
H	-2.210928	-3.350657	-0.341306
H	-0.823440	-3.220878	-1.471327
H	-0.521158	-3.492992	0.238220

Compound 3, S₁:

C	3.580407	-3.412259	0.587559
C	4.254340	-2.375479	-0.114595
C	5.492755	-2.679269	-0.743560
C	6.035841	-3.965944	-0.691520
C	5.337059	-4.963085	0.007242
C	4.118910	-4.698805	0.655170
C	3.776928	-1.008063	-0.138919
N	2.454433	-0.587915	-0.056813
C	2.406860	0.818992	0.061249
C	3.773359	1.279286	0.070662
C	4.590962	0.169353	-0.062163
C	1.303033	-1.363209	-0.427375
C	0.019498	-0.702438	-0.160811
C	-0.023117	0.702713	0.089929
C	1.193840	1.496548	0.121326
C	-1.183022	-1.507976	-0.221807
C	-2.408525	-0.847871	-0.054642
N	-2.438578	0.530782	0.197392
C	-1.296346	1.374708	0.339757
C	-3.733993	0.955827	0.345520
C	-4.576895	-0.160050	0.173966
C	-3.774403	-1.285489	-0.072278
O	-1.473337	2.559423	0.638123

C	-1.188881	-2.999738	-0.430592
C	1.197724	3.000604	0.213521
O	1.453995	-2.489654	-0.900520
H	-3.938396	2.004384	0.557166
N	5.900963	-6.321852	0.070276
O	6.983827	-6.513954	-0.491032
O	5.253809	-7.177930	0.681040
H	3.617255	-5.499755	1.202477
H	2.649932	-3.194584	1.117760
H	6.976443	-4.213229	-1.188035
H	6.013590	-1.898419	-1.308041
H	5.682129	0.152160	-0.038763
H	4.087266	2.311862	0.223594
H	0.861340	3.340765	1.206101
H	2.206827	3.392930	0.018338
H	0.497854	3.440751	-0.512999
H	-5.666094	-0.133341	0.232780
H	-4.109643	-2.305101	-0.262871
H	-2.191228	-3.405189	-0.226453
H	-0.892847	-3.262885	-1.459350
H	-0.463063	-3.498661	0.230138

Compound **4**, S₀:

44

C	-3.746688	-1.259732	-0.150155
---	-----------	-----------	-----------

C	-2.407770	-0.810162	-0.109532
N	-2.456422	0.567215	0.091521
C	-3.766315	0.993240	0.177291
C	-4.583339	-0.127893	0.029360
C	-1.325738	1.423923	0.192363
C	-0.027349	0.725037	0.074600
C	0.022379	-0.714304	-0.152495
C	-1.150504	-1.477648	-0.242689
C	1.151110	1.473220	0.185056
C	2.403726	0.787590	0.132920
N	2.461985	-0.603968	-0.000879
C	1.319075	-1.404110	-0.322161
C	3.735927	1.256537	0.179376
C	4.583942	0.135584	0.071537
C	3.792184	-1.019218	-0.044783
C	4.277644	-2.406525	-0.063485
C	3.758921	-3.401913	0.796194
C	4.319613	-4.686098	0.811542
C	5.406807	-5.010088	-0.018737
C	5.911975	-4.007619	-0.854185
C	5.373382	-2.717172	-0.896689
N	7.058867	-4.324634	-1.738531
O	7.496320	-5.476297	-1.705274
O	1.474147	-2.561346	-0.690625
C	1.184656	2.969397	0.374674

C -1.182728 -2.967632 -0.472388
 O -1.502810 2.623972 0.367278
 O 7.497873 -3.414475 -2.444341
 H -3.984767 2.047557 0.334654
 H 3.910440 -5.447768 1.483027
 H 2.926077 -3.161022 1.462667
 H 5.792394 -1.975930 -1.580712
 H 5.674096 0.128064 0.118749
 H 4.043675 2.294360 0.300151
 H 0.674916 3.256436 1.307668
 H 2.219777 3.335006 0.402286
 H 0.641449 3.480310 -0.434800
 H -5.673478 -0.120170 0.049848
 H -4.070336 -2.289026 -0.301311
 H -2.205244 -3.351611 -0.353191
 H -0.816358 -3.216035 -1.480999
 H -0.515629 -3.492350 0.228159
 H 5.859411 -6.003340 -0.025542

Compound 4, S₁:

44

C -3.770761 -1.293377 -0.051545
 C -2.407060 -0.850052 -0.053228
 N -2.438181 0.523816 0.221900
 C -3.733571 0.943328 0.396497

C	-4.573374	-0.174557	0.224382
C	-1.297804	1.373373	0.346399
C	-0.027637	0.705447	0.090383
C	0.015808	-0.695435	-0.185024
C	-1.180030	-1.503064	-0.247687
C	1.195616	1.501520	0.117035
C	2.406996	0.825154	0.049543
N	2.452854	-0.581832	-0.079089
C	1.302365	-1.350097	-0.465544
C	3.774609	1.284351	0.049480
C	4.590692	0.171539	-0.075110
C	3.773592	-1.001944	-0.155256
C	4.253772	-2.372202	-0.113826
C	3.584565	-3.404358	0.596389
C	4.139217	-4.687583	0.667187
C	5.359547	-4.990233	0.035818
C	6.010675	-3.956788	-0.651816
C	5.491856	-2.664235	-0.740276
N	7.299415	-4.246051	-1.325253
O	7.720394	-5.402639	-1.263751
O	1.453951	-2.466668	-0.959027
C	1.196570	3.004461	0.213575
C	-1.184539	-2.990190	-0.490462
O	-1.478609	2.559755	0.643301
O	7.863114	-3.310470	-1.896752

H -3.939118 1.987902 0.625717
 H 3.615565 -5.470187 1.226004
 H 2.650831 -3.187159 1.120674
 H 6.033460 -1.907482 -1.312302
 H 5.681659 0.151093 -0.046538
 H 4.090942 2.318990 0.182205
 H 0.821072 3.339298 1.193546
 H 2.211110 3.399447 0.056474
 H 0.520999 3.444993 -0.535862
 H -5.662087 -0.153093 0.294522
 H -4.106624 -2.311653 -0.247550
 H -2.189070 -3.399297 -0.305358
 H -0.879339 -3.231698 -1.521615
 H -0.467400 -3.505840 0.167621
 H 5.804760 -5.986279 0.072255

Compound **5**, S₀:

44

C -3.671896 -3.529714 0.661616
 C -4.221008 -2.461371 -0.085555
 C -5.372860 -2.758047 -0.854256
 C -5.950912 -4.035494 -0.865436
 C -5.370538 -5.072895 -0.116682
 C -4.221626 -4.817269 0.645526
 C -3.747705 -1.070302 -0.103942

N	-2.440700	-0.620567	-0.225266
C	-2.401759	0.774929	-0.166600
C	-3.736370	1.216779	-0.014065
C	-4.558477	0.073177	0.026949
C	-1.296139	-1.422972	-0.499876
C	-0.011820	-0.717561	-0.339760
C	0.025626	0.738005	-0.312664
C	-1.161592	1.479673	-0.244801
C	1.318922	1.452854	-0.301774
N	2.451416	0.595399	-0.216053
C	2.407042	-0.796264	-0.160177
C	1.155908	-1.483394	-0.236610
C	3.744435	-1.240366	-0.066255
C	4.577632	-0.091351	-0.069277
C	3.758981	1.034548	-0.161985
O	1.490767	2.665896	-0.347547
C	1.179912	-2.990252	-0.178712
C	-1.210146	2.986878	-0.215516
O	-1.437266	-2.596670	-0.821701
H	3.974598	2.100771	-0.189752
N	-2.512604	-3.328174	1.545915
O	-2.383955	-2.219578	2.072781
O	-1.752999	-4.287979	1.706430
H	-6.841447	-4.223046	-1.473725
H	-5.798547	-1.958930	-1.469953

H	-4.058627	2.252794	0.083066
H	-5.637274	0.045289	0.188332
H	-3.738596	-5.600498	1.234263
H	-5.806177	-6.076742	-0.124616
H	-0.632979	3.382507	0.634870
H	-2.247384	3.341625	-0.145912
H	-0.743994	3.409247	-1.118868
H	4.067260	-2.279840	-0.015591
H	5.666291	-0.075296	-0.009953
H	0.403317	-3.374577	0.499825
H	2.163011	-3.340214	0.167117
H	0.970726	-3.423499	-1.170019

Compound **5**, S₁:

44

C	-3.447110	-3.491812	0.585327
C	-4.173536	-2.386932	0.041438
C	-5.475158	-2.674142	-0.469731
C	-6.013564	-3.960595	-0.469257
C	-5.250492	-5.035270	0.039797
C	-3.981037	-4.795014	0.571154
C	-3.726057	-1.016573	-0.095711
N	-2.439846	-0.563925	-0.294299
C	-2.395496	0.838619	-0.284248
C	-3.760651	1.282993	-0.104640

C	-4.555512	0.158855	0.009033
C	-1.315539	-1.365151	-0.653871
C	-0.029677	-0.697405	-0.427247
C	0.026222	0.726486	-0.404504
C	-1.186894	1.518007	-0.386738
C	1.321683	1.415405	-0.343486
N	2.446917	0.536448	-0.286352
C	2.389507	-0.862798	-0.246078
C	1.154441	-1.521643	-0.322815
C	3.741806	-1.319673	-0.139046
C	4.569652	-0.183967	-0.119533
C	3.751079	0.957690	-0.207832
O	1.521669	2.629662	-0.337350
C	1.093992	-3.016279	-0.201485
C	-1.194158	3.024421	-0.434479
O	-1.479267	-2.492631	-1.116032
H	3.979155	2.022770	-0.216085
N	-2.204065	-3.320041	1.312104
O	-1.918403	-2.178260	1.724785
O	-1.483701	-4.321166	1.491593
H	-7.010524	-4.134350	-0.886922
H	-6.043185	-1.853363	-0.920874
H	-4.076007	2.321993	-0.007138
H	-5.623524	0.133608	0.230767
H	-3.377274	-5.599133	0.997318

H -5.653866 -6.053072 0.036752
H -0.684556 3.452640 0.443044
H -2.226431 3.401381 -0.476038
H -0.644446 3.391043 -1.315080
H 4.053335 -2.363550 -0.096900
H 5.658167 -0.168311 -0.050336
H 0.366359 -3.310801 0.577382
H 2.082059 -3.419169 0.066518
H 0.747633 -3.481793 -1.137463

Compound **5**, CT state:

44

O -4.371040 -1.546471 -2.113290
C -4.013753 -0.991175 -0.856943
C -4.183686 -2.110022 0.152770
C -4.480805 -3.274455 -0.512306
N -4.701371 -2.950777 -1.927761
C -4.786040 0.287049 -0.591706
C -3.956976 1.328570 -0.413362
C -2.544628 0.852927 -0.500101
N -2.623856 -0.488278 -0.869566
C -1.541435 -1.349349 -1.034017
C -0.217819 -0.696828 -0.844938
C -0.140126 0.660137 -0.439030
C -1.371887 1.473587 -0.239911

C	1.154596	1.302922	-0.210809
N	2.269960	0.457794	-0.426759
C	2.207860	-0.878608	-0.842416
C	0.969030	-1.485172	-1.071247
C	3.564370	-1.327504	-0.943646
C	4.394242	-0.250931	-0.585534
C	3.580540	0.850105	-0.268648
C	-4.616150	-4.512701	0.074247
C	-4.420237	-4.537940	1.482775
C	-4.127358	-3.370538	2.199448
C	-3.987599	-2.132192	1.538319
H	3.807205	1.865997	0.048941
C	0.946515	-2.922432	-1.537498
O	1.352361	2.470147	0.143652
C	-1.341693	2.927437	0.175687
O	-1.733481	-2.534003	-1.316264
O	-4.776042	-3.689371	-2.907144
H	-3.993826	-3.421459	3.285110
H	-3.733300	-1.218493	2.088022
H	-4.245298	2.361972	-0.216043
H	-5.878578	0.291722	-0.586567
H	-4.827637	-5.411857	-0.510971
H	-4.510603	-5.491794	2.013362
H	-0.823225	3.058895	1.136768
H	-2.368138	3.314005	0.274962

H -0.800337 3.546928 -0.555048
 H 3.880631 -2.327349 -1.239994
 H 5.484828 -0.251999 -0.553012
 H 0.442977 -3.571646 -0.805184
 H 1.974394 -3.281894 -1.693031
 H 0.384034 -3.027408 -2.477402

Compound 7, S₀:

50

C 3.752127 0.970937 -0.195007
 N 2.438692 0.548849 -0.234329
 C 2.373965 -0.839834 -0.135307
 C 3.705230 -1.299616 -0.028520
 C 4.554787 -0.163199 -0.067244
 C 1.112385 -1.508745 -0.186781
 C -0.045874 -0.731489 -0.315618
 C 0.014165 0.723540 -0.331727
 C 1.318737 1.418710 -0.348623
 C -1.159209 1.487833 -0.295324
 C -2.412905 0.809193 -0.212170
 N -2.476422 -0.585600 -0.219907
 C -1.340980 -1.426519 -0.425822
 C -3.744638 1.281186 -0.144312
 C -4.592178 0.156779 -0.100427
 C -3.801612 -1.004342 -0.144460

C	-4.276319	-2.394094	-0.085990
C	-3.838889	-3.374663	0.875405
C	-4.313624	-4.734367	0.740777
C	-5.296433	-5.048506	-0.243621
C	-5.777019	-4.065296	-1.095698
C	-5.253911	-2.751811	-1.023369
C	-2.911338	-3.145641	1.936665
O	-1.507864	-2.619058	-0.650707
C	-1.181084	2.996059	-0.303512
O	1.509335	2.626571	-0.438103
C	1.108886	-3.010891	-0.063275
H	3.982688	2.032563	-0.256690
H	-6.533575	-4.307756	-1.849303
H	-5.573289	-1.996219	-1.749052
H	-4.048823	2.326556	-0.105932
H	-5.677544	0.151923	0.010214
C	-3.815178	-5.762299	1.595867
H	-5.651888	-6.082060	-0.320717
H	-0.583751	3.401371	0.527897
H	-2.210745	3.370259	-0.224403
H	-0.722850	3.389088	-1.224230
H	4.014184	-2.341266	0.054085
H	5.643645	-0.160834	-0.008764
H	0.360708	-3.328061	0.680055
H	2.101041	-3.370841	0.244457

H 0.826594 -3.488452 -1.014594
 C -2.404864 -4.159244 2.739720
 C -2.859290 -5.488324 2.563063
 N -2.491446 -1.791117 2.320445
 H -1.683883 -3.903050 3.521332
 H -4.199905 -6.780171 1.466818
 H -2.471982 -6.285186 3.205555
 O -1.274152 -1.575891 2.398197
 O -3.386370 -0.980270 2.578727

Compound 7, S₁:

50

C 3.669214 0.847461 0.056343
 N 2.363971 0.447337 -0.065283
 C 2.277026 -0.946162 0.008678
 C 3.617482 -1.429778 0.182103
 C 4.461247 -0.310238 0.206324
 C 1.028855 -1.582716 -0.093760
 C -0.105910 -0.731525 -0.276896
 C -0.015334 0.689548 -0.317023
 C 1.257754 1.354169 -0.195246
 C -1.251095 1.500313 -0.394497
 C -2.462179 0.859893 -0.289111
 N -2.542319 -0.554685 -0.212362
 C -1.420349 -1.385960 -0.497671

C	-3.832465	1.334016	-0.294493
C	-4.667789	0.240754	-0.212309
C	-3.867481	-0.957393	-0.146012
C	-4.356754	-2.303499	0.021517
C	-3.714055	-3.324619	0.820748
C	-4.151529	-4.697255	0.675778
C	-5.287117	-4.996087	-0.128170
C	-5.988264	-3.972988	-0.768994
C	-5.520900	-2.647945	-0.706265
C	-2.686430	-3.098167	1.777004
O	-1.579809	-2.548230	-0.850458
C	-1.206749	2.994780	-0.554811
O	1.504608	2.569900	-0.196632
C	0.951982	-3.080538	0.049850
H	3.914278	1.907968	0.030968
H	-6.874266	-4.205901	-1.369346
H	-6.009800	-1.872022	-1.306204
H	-4.128454	2.383875	-0.300044
H	-5.754821	0.246926	-0.117595
C	-3.452063	-5.742465	1.350164
H	-5.602594	-6.040765	-0.229449
H	-0.723796	3.463387	0.316933
H	-2.218720	3.405563	-0.686241
H	-0.585421	3.268356	-1.421891
H	3.906839	-2.477987	0.257844

H	5.546930	-0.312324	0.317595
H	0.148374	-3.362486	0.750390
H	1.906697	-3.466706	0.439293
H	0.726845	-3.577192	-0.907899
C	-1.998176	-4.125220	2.422588
C	-2.379239	-5.466417	2.189677
N	-2.340147	-1.742429	2.224630
H	-1.212492	-3.867630	3.138651
H	-3.791207	-6.774648	1.205705
H	-1.849325	-6.278254	2.698064
O	-1.133549	-1.462351	2.305287
O	-3.274167	-0.984956	2.508271

Compound **8**, S₀:

56

C	-1.314859	1.415603	0.286691
C	-0.023444	0.716853	0.115692
C	0.023444	-0.716853	-0.115692
C	-1.159001	-1.466465	-0.203933
C	-2.407404	-0.779328	-0.129931
N	-2.464169	0.614268	-0.005938
C	1.159001	1.466465	0.203933
C	2.407404	0.779328	0.129931
N	2.464169	-0.614268	0.005938
C	1.314859	-1.415603	-0.286691

C	3.741466	1.247323	0.158162
C	4.586896	0.126069	0.050592
C	3.793570	-1.031517	-0.048717
C	-3.741466	-1.247323	-0.158162
C	-4.586896	-0.126069	-0.050592
C	-3.793570	1.031517	0.048717
C	4.278096	-2.417003	-0.070212
C	5.372614	-2.738717	-0.905464
C	5.936350	-4.021961	-0.896301
C	5.390950	-4.983955	-0.037310
C	4.311024	-4.699102	0.811066
C	3.759862	-3.413454	0.789818
N	5.974274	-6.342486	-0.021279
O	5.467354	-7.166784	0.743050
O	1.458027	-2.579491	-0.639503
C	1.203038	2.962652	0.390462
C	-4.278096	2.417003	0.070212
C	-3.759862	3.413454	-0.789818
C	-4.311024	4.699102	-0.811066
C	-5.390950	4.983955	0.037310
C	-5.936350	4.021961	0.896301
C	-5.372614	2.738717	0.905464
N	-5.974274	6.342486	0.021279
O	-5.467354	7.166784	-0.743050
C	-1.203038	-2.962652	-0.390462

O	-1.458027	2.579491	0.639503
O	6.927960	-6.557816	-0.772614
O	-6.927960	6.557816	0.772614
H	3.925722	-5.477473	1.472748
H	2.932314	-3.172618	1.462729
H	6.774076	-4.287700	-1.544181
H	5.769654	-1.976547	-1.584167
H	5.677319	0.118509	0.091096
H	4.050562	2.285049	0.277126
H	0.848632	3.241168	1.395707
H	2.225259	3.339547	0.250457
H	0.532232	3.470947	-0.318134
H	-3.925722	5.477473	-1.472748
H	-2.932314	3.172618	-1.462729
H	-6.774076	4.287700	1.544181
H	-5.769654	1.976547	1.584167
H	-5.677319	-0.118509	-0.091096
H	-4.050562	-2.285049	-0.277126
H	-2.225259	-3.339547	-0.250457
H	-0.848632	-3.241168	-1.395707
H	-0.532232	-3.470947	0.318134

Compound **8**, S₁:

56

C	-1.293537	1.373238	0.399337
---	-----------	----------	----------

C	-0.019255	0.698366	0.132977
C	0.019255	-0.698366	-0.132977
C	-1.195513	-1.487213	-0.169802
C	-2.407791	-0.804244	-0.084268
N	-2.452460	0.599000	0.051852
C	1.195513	1.487213	0.169802
C	2.407791	0.804244	0.084268
N	2.452460	-0.599000	-0.051852
C	1.293537	-1.373238	-0.399337
C	3.771959	1.264863	0.072817
C	4.588648	0.152938	-0.068938
C	3.775010	-1.020903	-0.145354
C	-3.771959	-1.264863	-0.072817
C	-4.588648	-0.152938	0.068938
C	-3.775010	1.020903	0.145354
C	4.257869	-2.389006	-0.130878
C	5.477857	-2.685438	-0.796936
C	6.033448	-3.967599	-0.755550
C	5.364409	-4.965943	-0.031232
C	4.165660	-4.708698	0.653377
C	3.614853	-3.426302	0.596959
N	5.940107	-6.322126	0.018190
O	5.318387	-7.179439	0.652146
O	1.428287	-2.508322	-0.856637
C	1.207639	2.990112	0.283758

C	-4.257869	2.389006	0.130878
C	-3.614853	3.426302	-0.596959
C	-4.165660	4.708698	-0.653377
C	-5.364409	4.965943	0.031232
C	-6.033448	3.967599	0.755550
C	-5.477857	2.685438	0.796936
N	-5.940107	6.322126	-0.018190
O	-5.318387	7.179439	-0.652146
C	-1.207639	-2.990112	-0.283758
O	-1.428287	2.508322	0.856637
O	7.005236	-6.507862	-0.577096
O	-7.005236	6.507862	0.577096
H	3.687946	-5.510976	1.219764
H	2.700015	-3.213692	1.154925
H	6.960663	-4.209540	-1.279134
H	5.974120	-1.903162	-1.381066
H	5.679895	0.134608	-0.049319
H	4.088087	2.299017	0.209596
H	0.901530	3.317078	1.290328
H	2.211034	3.383079	0.062714
H	0.490203	3.445522	-0.416819
H	-3.687946	5.510976	-1.219764
H	-2.700015	3.213692	-1.154925
H	-6.960663	4.209540	1.279134
H	-5.974120	1.903162	1.381066

H -5.679895 -0.134608 0.049319
H -4.088087 -2.299017 -0.209596
H -2.211034 -3.383079 -0.062714
H -0.901530 -3.317078 -1.290328
H -0.490203 -3.445522 0.416819

Compound **10**, S₀:

56

C -0.009243 -0.725096 0.014624
C 0.009243 0.725096 -0.014624
C 3.795258 3.497272 0.497853
C 4.200225 2.485585 -0.404252
C 5.190690 2.844939 -1.350317
C 5.753714 4.128758 -1.385536
C 5.317897 5.109460 -0.478942
C 4.329026 4.790878 0.463110
C 3.730213 1.093792 -0.423493
N 2.422065 0.641831 -0.323661
C 2.390606 -0.754561 -0.348820
C 3.728438 -1.194579 -0.483244
C 4.547365 -0.049102 -0.522994
C 1.163385 -1.464973 -0.199244
C 1.249153 1.450320 -0.342204
O 1.336404 2.642885 -0.612215
C 1.211329 -2.971026 -0.269079

N	2.820950	3.223379	1.566735
O	2.807821	2.085695	2.045346
O	2.092418	4.155679	1.918428
H	6.516996	4.366354	-2.133326
H	5.497553	2.091913	-2.083596
H	4.056156	-2.233405	-0.505341
H	5.637353	-0.021735	-0.565878
H	3.960444	5.529108	1.179106
H	5.742053	6.117967	-0.502935
H	1.096831	-3.414596	0.733361
H	2.165298	-3.301300	-0.704521
H	0.382468	-3.363294	-0.877611
C	-3.795258	-3.497272	-0.497853
C	-4.200225	-2.485585	0.404252
C	-5.190690	-2.844939	1.350317
C	-5.753714	-4.128758	1.385536
C	-5.317897	-5.109460	0.478942
C	-4.329026	-4.790878	-0.463110
C	-3.730213	-1.093792	0.423493
N	-2.422065	-0.641831	0.323661
C	-2.390606	0.754561	0.348820
C	-3.728438	1.194579	0.483244
C	-4.547365	0.049102	0.522994
C	-1.163385	1.464973	0.199244
C	-1.249153	-1.450320	0.342204

O -1.336404 -2.642885 0.612215
 C -1.211329 2.971026 0.269079
 N -2.820950 -3.223379 -1.566735
 O -2.807821 -2.085695 -2.045346
 O -2.092418 -4.155679 -1.918428
 H -6.516996 -4.366354 2.133326
 H -5.497553 -2.091913 2.083596
 H -4.056156 2.233405 0.505341
 H -5.637353 0.021735 0.565878
 H -3.960444 -5.529108 -1.179106
 H -5.742053 -6.117967 0.502935
 H -1.096831 3.414596 -0.733361
 H -2.165298 3.301300 0.704521
 H -0.382468 3.363294 0.877611

Compound **10**, S₁:

56

C -0.010471 -0.709612 0.017879
 C 0.010471 0.709612 -0.017879
 C 3.637957 3.497779 0.392651
 C 4.172197 2.442189 -0.399795
 C 5.291990 2.774012 -1.215326
 C 5.839162 4.059253 -1.248374
 C 5.266870 5.083525 -0.468112
 C 4.170003 4.795864 0.352854

C	3.699741	1.070015	-0.481542
N	2.402472	0.611845	-0.375400
C	2.370816	-0.791844	-0.425279
C	3.734048	-1.224210	-0.604241
C	4.530969	-0.090563	-0.631083
C	1.175412	-1.488233	-0.270672
C	1.221387	1.414051	-0.439321
O	1.292299	2.583203	-0.816985
C	1.148660	-2.984451	-0.431667
N	2.584785	3.269975	1.383866
O	2.469354	2.128341	1.850559
O	1.881466	4.237432	1.706689
H	6.694053	4.268881	-1.899282
H	5.702839	1.995164	-1.866370
H	4.062810	-2.263346	-0.634663
H	5.620934	-0.057935	-0.674629
H	3.709960	5.561878	0.981164
H	5.678066	6.097606	-0.491603
H	1.001261	-3.488416	0.536796
H	2.085491	-3.335701	-0.890143
H	0.303553	-3.289204	-1.072130
C	-3.637957	-3.497779	-0.392651
C	-4.172197	-2.442189	0.399795
C	-5.291990	-2.774012	1.215326
C	-5.839162	-4.059253	1.248374

C	-5.266870	-5.083525	0.468112
C	-4.170003	-4.795864	-0.352854
C	-3.699741	-1.070015	0.481542
N	-2.402472	-0.611845	0.375400
C	-2.370816	0.791844	0.425279
C	-3.734048	1.224210	0.604241
C	-4.530969	0.090563	0.631083
C	-1.175412	1.488233	0.270672
C	-1.221387	-1.414051	0.439321
O	-1.292299	-2.583203	0.816985
C	-1.148660	2.984451	0.431667
N	-2.584785	-3.269975	-1.383866
O	-2.469354	-2.128341	-1.850559
O	-1.881466	-4.237432	-1.706689
H	-6.694053	-4.268881	1.899282
H	-5.702839	-1.995164	1.866370
H	-4.062810	2.263346	0.634663
H	-5.620934	0.057935	0.674629
H	-3.709960	-5.561878	-0.981164
H	-5.678066	-6.097606	0.491603
H	-1.001261	3.488416	-0.536796
H	-2.085491	3.335701	0.890143
H	-0.303553	3.289204	1.072130

Compound **13**, S₀:

C	3.857589	-3.484124	0.989321
C	4.208645	-2.504993	0.019840
C	5.083114	-2.813995	-1.044262
C	5.617222	-4.103548	-1.180561
C	5.283678	-5.092855	-0.247522
C	4.407745	-4.765431	0.797651
C	3.763593	-1.103722	0.145609
N	2.445960	-0.653183	0.123343
C	2.409267	0.730872	0.311540
C	3.747532	1.162662	0.458210
C	4.574171	0.023721	0.352580
C	1.301428	-1.443375	-0.198464
C	0.016286	-0.716530	-0.127024
C	-0.016286	0.716530	0.127024
C	1.169097	1.438956	0.326712
C	1.225707	2.926835	0.567377
O	1.448433	-2.623066	-0.494189
H	5.684375	-6.107186	-0.309579
N	4.081192	-5.860979	1.730930
C	2.973060	-3.131042	2.160094
H	6.289556	-4.338532	-2.011518
H	5.324746	-2.032135	-1.771627
H	5.660695	-0.014278	0.445768
H	4.071762	2.187021	0.637636

H	0.726528	3.189621	1.513252
H	2.267155	3.274225	0.598772
H	0.686677	3.475684	-0.219937
H	3.306815	-3.627865	3.083533
H	2.985269	-2.042104	2.323604
H	1.937741	-3.454119	1.970519
O	2.926865	-5.911227	2.166926
O	4.981216	-6.663254	1.993370
C	-3.857589	3.484124	-0.989321
C	-4.208645	2.504993	-0.019840
C	-5.083114	2.813995	1.044262
C	-5.617222	4.103548	1.180561
C	-5.283678	5.092855	0.247522
C	-4.407745	4.765431	-0.797651
C	-3.763593	1.103722	-0.145609
N	-2.445960	0.653183	-0.123343
C	-2.409267	-0.730872	-0.311540
C	-3.747532	-1.162662	-0.458210
C	-4.574171	-0.023721	-0.352580
C	-1.301428	1.443375	0.198464
C	-1.169097	-1.438956	-0.326712
C	-1.225707	-2.926835	-0.567377
O	-1.448433	2.623066	0.494189
H	-5.684375	6.107186	0.309579
N	-4.081192	5.860979	-1.730930

C	-2.973060	3.131042	-2.160094
H	-6.289556	4.338532	2.011518
H	-5.324746	2.032135	1.771627
H	-5.660695	0.014278	-0.445768
H	-4.071762	-2.187021	-0.637636
H	-0.726528	-3.189621	-1.513252
H	-2.267155	-3.274225	-0.598772
H	-0.686677	-3.475684	0.219937
H	-3.306815	3.627865	-3.083533
H	-2.985269	2.042104	-2.323604
H	-1.937741	3.454119	-1.970519
O	-2.926865	5.911227	-2.166926
O	-4.981216	6.663254	-1.993370

Compound **13**, S₁:

62

C	3.724439	-3.462755	0.871622
C	4.214911	-2.448126	-0.004156
C	5.261477	-2.727384	-0.919299
C	5.816780	-4.008785	-1.008960
C	5.341610	-5.030342	-0.174834
C	4.311309	-4.734300	0.728918
C	3.754418	-1.061358	0.053999
N	2.440886	-0.614587	0.071774
C	2.412042	0.786886	0.210759

C	3.781862	1.222683	0.283352
C	4.584347	0.091330	0.180823
C	1.296018	-1.393660	-0.295156
C	0.017685	-0.701727	-0.123135
C	-0.017685	0.701727	0.123135
C	1.202272	1.481679	0.224957
C	1.222643	2.984938	0.319885
O	1.455820	-2.551785	-0.686464
H	5.751846	-6.042359	-0.204843
N	3.857338	-5.857469	1.572651
C	2.706183	-3.158267	1.943117
H	6.612333	-4.216268	-1.731414
H	5.605859	-1.927924	-1.583796
H	5.673320	0.046147	0.246823
H	4.109471	2.250930	0.436474
H	0.797126	3.333911	1.273821
H	2.251604	3.360591	0.218897
H	0.606006	3.438098	-0.473577
H	2.964019	-3.659795	2.889041
H	2.659390	-2.074012	2.126273
H	1.709989	-3.515515	1.642127
O	2.650352	-5.930570	1.822544
O	4.716961	-6.657533	1.952186
C	-3.724439	3.462755	-0.871622
C	-4.214911	2.448126	0.004156

C	-5.261477	2.727384	0.919299
C	-5.816780	4.008785	1.008960
C	-5.341610	5.030342	0.174834
C	-4.311309	4.734300	-0.728918
C	-3.754418	1.061358	-0.053999
N	-2.440886	0.614587	-0.071774
C	-2.412042	-0.786886	-0.210759
C	-3.781862	-1.222683	-0.283352
C	-4.584347	-0.091330	-0.180823
C	-1.296018	1.393660	0.295156
C	-1.202272	-1.481679	-0.224957
C	-1.222643	-2.984938	-0.319885
O	-1.455820	2.551785	0.686464
H	-5.751846	6.042359	0.204843
N	-3.857338	5.857469	-1.572651
C	-2.706183	3.158267	-1.943117
H	-6.612333	4.216268	1.731414
H	-5.605859	1.927924	1.583796
H	-5.673320	-0.046147	-0.246823
H	-4.109471	-2.250930	-0.436474
H	-0.797126	-3.333911	-1.273821
H	-2.251604	-3.360591	-0.218897
H	-0.606006	-3.438098	0.473577
H	-2.964019	3.659795	-2.889041
H	-2.659390	2.074012	-2.126273

H -1.709989 3.515515 -1.642127

O -2.650352 5.930570 -1.822544

O -4.716961 6.657533 -1.952186

5. Electrochemical and spectroelectrochemical studies

General Remarks. Cyclic voltammograms were obtained using CH Instruments Electrochemical Analyzer model 620c and 660. The experimental setup was a single-cell and three-electrode system consisting of a 2 mm² platinum disk (working electrode), a platinum coil (counter electrode), and an Ag|Ag⁺ pseudo-reference electrode calibrated with ferrocene as the internal standard. The monomer concentration was 1.0 mM (in the presence of 0.1 M Bu₄NBF₄) in DCM and ACN. HOMO and LUMO energies were calculated using the following equation: $HOMO \text{ (LUMO)} \text{ (eV)} = - 5.1 - (E_{\text{onset}} - E^{\circ})$, where E_{onset} is the onset potential of the first oxidation or reduction peak for the HOMO and LUMO, respectively, and E° is the half-wave potential of the Fc|Fc⁺ couple.²⁷ UV-vis-NIR spectrometer HP 5453 was used with thin-layer optical cell characterized by the optical path of 0.2 mm length, consisting of a quartz cuvette containing ITO/quartz electrode (20±5 V/sq, Praezisions Glas & Optic GmbH), Teflon separator (0.2 mm), silver wire (pseudo-reference electrode) and platinum mesh (counter electrode).

Description of electrochemical and spectroelectrochemical properties. A principle goal for developing fluorescent nitroaromatics is to meet the demands for electron-deficient (i.e., *n*-type) organic systems with promising optical properties for photonics and optoelectronics. Our spectroscopy studies demonstrate how weakening the electronic coupling of the DPND core with the nitro groups permits large fluorescence quantum yields and long singlet excited state lifetimes. This weakening of the electronic coupling, however, can compromise the electron deficiency of the chromophores, defeating the purpose of these nitroaromatics as photosensitizers and electron acceptors. Therefore, we resort to electrochemical studies, employing cyclic voltammetry (Figure S72 and Table S11) to examining how the nitro groups affect the energy levels of the frontier orbitals of the DPNDs and their electron-accepting ability.

²⁷ S. Trasatti, *Applied Chemistry* **1986**, 58, 955-966.

For the measurements, we select DCM and ACN solutions of 0.1 M $\text{N}(n\text{-C}_4\text{H}_9)_4\text{BF}_4$ as electrolyte media, as our spectroscopic studies reveal large differences in optical properties of the DPND dyes for these two solvents. Furthermore, the electrochemical windows of DCM and ACN electrolyte solutions are wide enough to permit observation of both oxidation and reduction of these compounds under the same conditions.

The cyclic voltammograms (CVs) of DPND dyes reveal one or two oxidation waves between about 1.0 and 1.4 V vs. SCE (Table S11). Except for **7**, the oxidation of all DPNDs show reversibility in both solvents, suggesting some degree of stability of the radical cations of these dyes (Figure S74). The reduction potentials for oxidation, $E_{\text{DPND}^{\bullet}\text{||DPND}}^{(1/2)}$ and $E_{\text{DPND}^{\bullet\bullet}\text{||DPND}^{\bullet\bullet}}^{(1/2)}$, do not vary much among the series of dyes. Therefore, the charges of the oxidized species are most likely localized on the DPND core, and the thirteen dyes appear to be equally good electron donors. These findings are consistent with the localization of the HOMOs of these dyes regardless the aryl substituent (Figure S69). For most dyes, the values of $E_{\text{DPND}^{\bullet}\text{||DPND}}^{(1/2)}$ for DCM are more positive than those for ACN by about 0.1 to 0.3 V, which is consistent with the solvation energy of the charged species.²⁸ The reduction potential for oxidation accounts for the conversion of radical cations to non-charged species, or from dications to singly charged cations. Thus, an increase in solvent polarity stabilizes the species with larger charges and causes negative shifts in the observed reduction potentials.

Negative potential sweeps of the dye samples produce reduction waves in the range of about –0.6 to –1.4 V vs. SCE, indicating that many of these nitroaryl DPND derivatives are excellent electron acceptors. The reduction potentials, $E_{\text{DPND}^{\bullet\bullet}\text{||DPND}^{\bullet}}$, varied widely among the dyes and, with a few exceptions, the CVs show irreversibility. These trends suggest that the nitro groups strongly affect the energy levels of the LUMOs.

²⁸ D. Bao, B. Millare, W. Xia, B. G. Steyer, A. A. Gerasimenko, A. Ferreira, A. Contreras, V. I. Vullev, *J. Phys. Chem. A* **2009**, *113*, 1259–1267.

Except for **7**, **12** and **13** in DCM, the reduction potentials of all nitroaryl derivatives of DPND are more positive than the reduction potentials of **1** and **2** in both solvents. This finding is a clear indication that the nitro groups make these compounds better electron acceptors. The derivative **8**, bearing two nitro groups with the strongest through-bond electronic coupling with the DPND core, shows the most positive reduction potentials, making it the best electron acceptor among the studied dyes. In ACN, $E_{\text{1/2}}^{(\text{1/2})}$ is about -0.6 V vs. SCE, and for comparison, $E_{\text{1/2}}^{(\text{1/2})} \approx -0.95$ V vs. SCE and $E_{\text{1/2}}^{(\text{1/2})} \approx -0.9$ V vs. SCE. That is, the nitro groups induce a 0.3 V improvement on the electron accepting capabilities of **8**. On the other side of the spectrum, **13** has reduction potentials that are quite similar to those of **1**, which is consistent not only with the weak coupling of the *meta* nitro groups with the DPND core, but also with the break in the π -conjugation with the aromatic substituents because of the large dihedral angles induced by the ortho methyl groups (Figure S1 and S2).

These findings have important implications for understanding the electronic properties of these nitroaromatics. The electron-withdrawing nitro groups make not only the nitroaryl substituents, but the whole molecules electron deficient. Breaking the electronic coupling between the DPND core and the aryl substituents considerably compromises the electron-accepting capabilities of these compounds. In fact, the major portions of the LUMOs of the nitroaryl DPND dyes resides on the DPND cores (Figure S69)

Koopmans' theorem relates the reduction potentials of the first oxidation and the first reduction with the energy levels of the HOMOs and LUMOs, respectively. As evaluated for ACN, the values of E_{HOMO} for the different DPND dyes cluster around -5.8 eV vs. vacuum, while the values of E_{LUMO} spread between about -4.1 and -3.7 eV vs. vacuum (Table S11). These findings are consistent with the propensity of the nitro groups in these DPND dyes to affect the LUMOs more strongly than they do the HOMOs.

Overall, the electrochemical studies demonstrate that for most of the compounds, weakening the coupling of the nitro groups with the DPND core, which is important for maintaining the photophysical properties of these dyes, does not wholly compromise the desired electronic properties gained from including such strongly electron-withdrawing substituents.

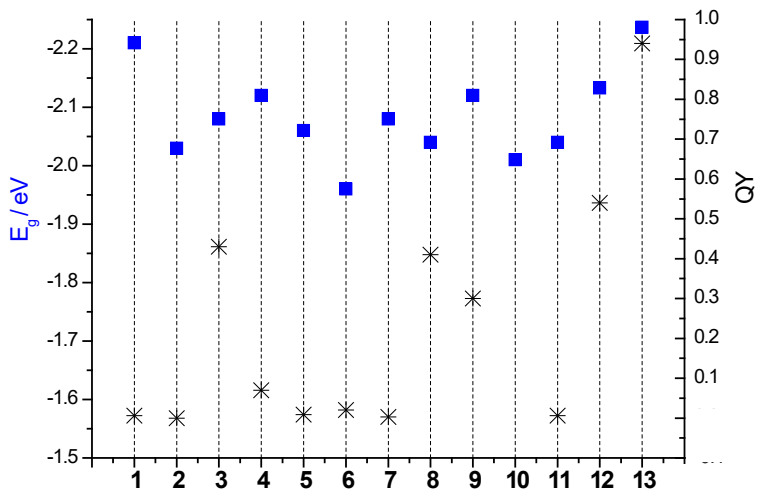
Table S11. Summary of electrochemical parameters of sample in 0.1 M *n*-Bu₄NBF₄ solution in DCM or ACN, potentials vs Fc⁺|Fc. Reversibility (+) or irreversibility (-) of the redox system. Selected effective emitters (red), ineffective emitters (blue).

DCM / <i>n</i> -Bu ₄ NBF ₄									
Cmpd	<i>E</i> ^{red2} /V vs Fc/Fc ⁺	<i>E</i> ^{red1} /V vs. Fc/Fc ⁺	<i>E</i> ^{ox1} /V vs. Fc/Fc ⁺	<i>E</i> ^{ox2} /V vs. Fc/Fc ⁺	<i>E</i> _{onset} ^{red} /V vs. Fc/Fc ⁺	<i>E</i> _{onset} ^{ox} /V vs. Fc/Fc ⁺)	<i>E</i> _{LUMO} /eV	<i>E</i> _{HOMO} /eV	<i>E</i> _g /eV
1	---	-1.614	0.803	---	-1.509	0.705	-3.77	-5.99	2.22
		+	-						
2	---	-1.609	0.692	0.808	-1.480	0.554	-3.80	-5.83	2.03
		+	-						
3	---	-1.484	0.787	---	-1.359	0.717	-3.92	-6.00	2.08
		+	-						
4	-	-1.696	-1.521	0.782	---	-1.411	0.709	-3.87	-5.99
		+	+	-					2.12
5	-	-1.572	-1.391	0.775	1.022	-1.372	0.690	-3.91	-5.97
		+	+	-					2.06
6	-	-1.711	-1.486	0.768	0.972	-1.380	0.584	-3.90	-5.86
		+	+	-					1.96
7	---	-1.585	0.708	---	-1.454	0.628	-3.83	-5.91	2.08
		-	-						
8	---	-1.413	0.865	---	-1.276	0.760	-4.00	-6.04	2.04
		+	-						
9	-	-1.720	-1.458	0.868	0.972	-1.343	0.773	-3.94	-6.05
		+	+	-					2.11
10	-	-1.535	-1.391	0.825	---	-1.287	0.718	-3.99	-6.00
		+	+	-					2.01
		+	+	+					
11	-	-1.629	-1.444	0.781	0.890	-1.326	0.718	-3.95	-6.00
		+	+	-	--				2.044
12	-	-1.741	-1.512	0.869	1.002	-1.371	0.762	-3.91	-6.04
		+	+	+	+				2.133
13	-	-1.903	-1.570	0.834	0.986	-1.469	0.768	-3.81	-6.05
		+	+	+	+				2.237

ACN / <i>n</i> -Bu ₄ NBF ₄									
Cmpd	<i>E</i> ^{red2} /V (vs Fc/Fc ⁺)	<i>E</i> ^{red1} /V (vs Fc/Fc ⁺)	<i>E</i> ^{ox1} /V (vs Fc/Fc ⁺)	<i>E</i> ^{ox2} /V (vs Fc/Fc ⁺)	<i>E</i> _{onset} ^{red} /V (vs Fc/Fc ⁺)	<i>E</i> _{onset} ^{ox} /V (vs Fc/Fc ⁺)	<i>E</i> _{LUMO} /eV	<i>E</i> _{HOMO} /eV	<i>E</i> _g /eV
1	---	-1.614	0.722	---	-1.394	0.641	-3.74	-5.77	2.04

		+	-						
2	---	-1.441	0.715	0.858	-1.339	0.602	-3.79	-5.73	1.94
		+	-	-					
3	-1.395		0.748	1.015	-1.232	0.682	-3.90	-5.81	1.91
	+		-	-					
4	-1.599	-1.402	0.736	0.945	-1.307	0.666	-3.82	-5.80	1.97
	+	+	-	-					
5	-1.602	-1.374	0.735	---	-1.277	0.669	-3.85	-5.80	1.95
	+	+	-						
6	-1.636	-1.382	0.756	---	-1.293	0.689	-3.84	-5.82	1.98
	+	+	-						
7	---	-1.502	0.660	---	-1.396	0.593	-3.73	-5.72	1.99
		-	-						
8	---	-1.277	0.937	---	-1.01	0.763	-4.12	-5.89	1.77
		+	-						
9	-1.656	-1.364	0.778	0.942	-1.265	0.670	-3.87	-5.80	1.94
	+	+	-	-					
10	-1.556	-1.364	0.781	1.047	-1.263	0.680	-3.87	-5.81	1.94
	+	+	+	+					
11	-1.571	-1.344	0.823	0.936	-1.233	0.708	-3.90	-5.84	1.94
	+	+	-	-					
	+	+	-	-					
12	-1.772	-1.506	0.801	0.937	-1.352	0.580	-3.51	-5.71	2.20
	+	+	-	-					
13	-1.895		0.759	0.959	-1.363	0.650	-3.77	-5.78	2.01
	+	+	-	-					

a)



b)

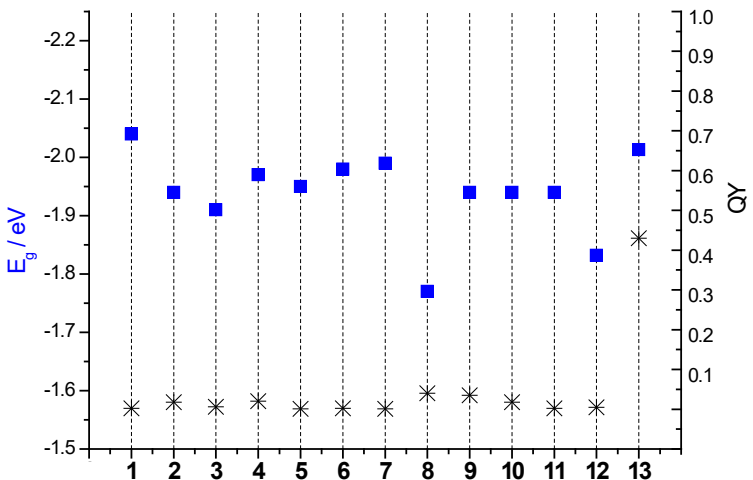


Figure S72. Electrochemical band gap energy (E_g) of **1-13** series in electrolyte solutions and quantum yield of fluorescence (QY) in dichloromethane (a) and acetonitrile (b).

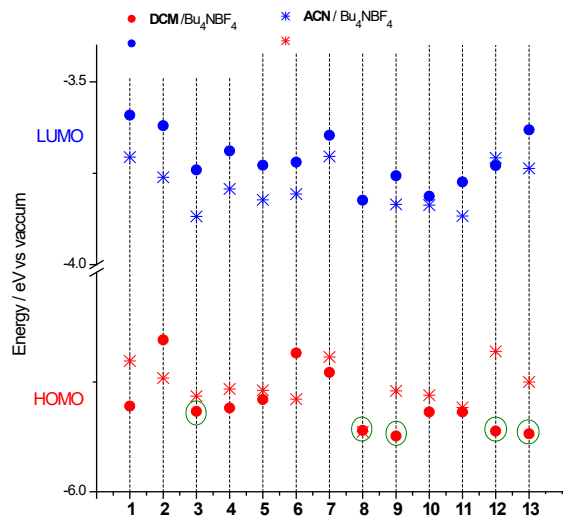


Figure S73. Energy diagram of the frontier orbitals of compounds **1-13**, determined on the basis of electrochemical measurements in various electrolyte solutions with oxidation potentials marked with a green circle for the most efficient emitters in DCM.

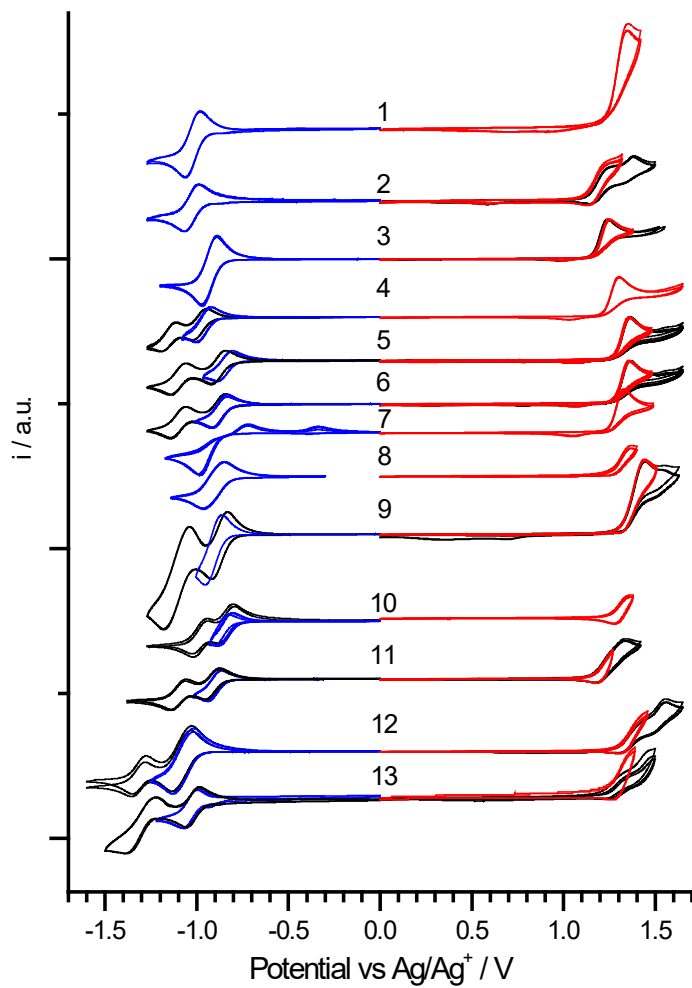


Figure S74. Cyclic voltammograms of sample (1 mM with 0.1 M *n*-Bu₄NBF₄ in DCM with the potential range limited to the generation of the radical cation, diradical dication/dication (red, black traces) and radical anion, diradical dianion (red, black traces).

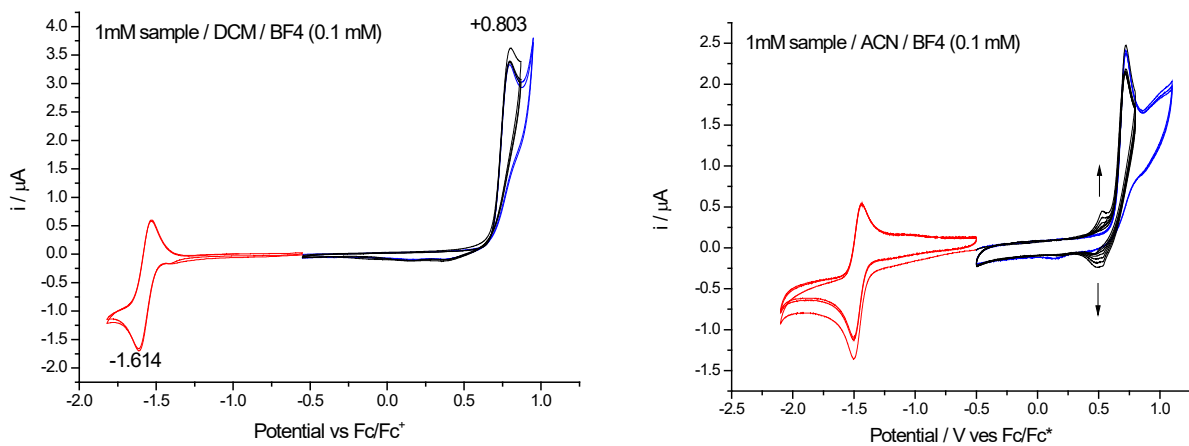


Figure S75. Cyclic voltammograms of **1** (1 mM with 0.1 M *n*-Bu₄NBF₄ in DCM with the potential range limited to the 1st oxidation (black curve) and 1st reduction peak (black curve).

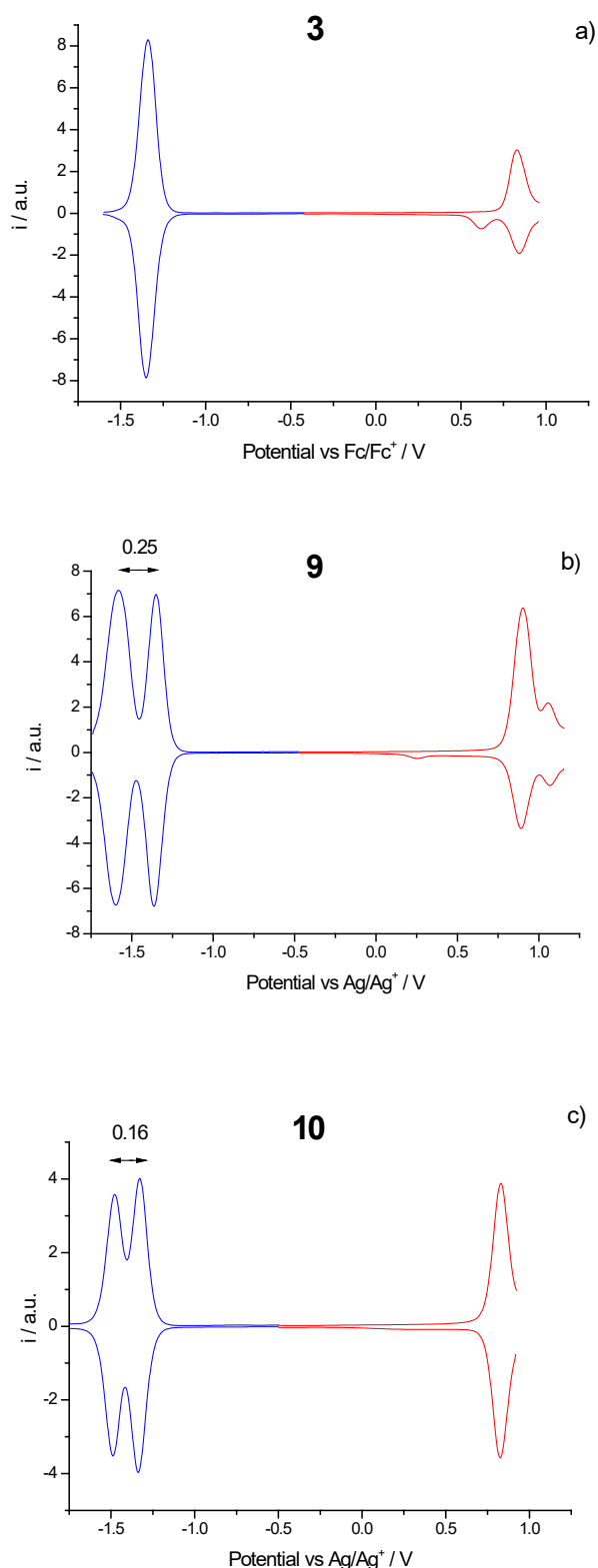


Figure S76. Square-wave voltammograms of sample substituted by NO_2 in various position: *para*- (a), *meta*- (b); *ortho*- (c), 1 mM with 0.1 M $n\text{-Bu}_4\text{NBF}_4$ in DCM with the potential range limited to the generation of the diradical dication/dication (red) and diradical dianion (blue).

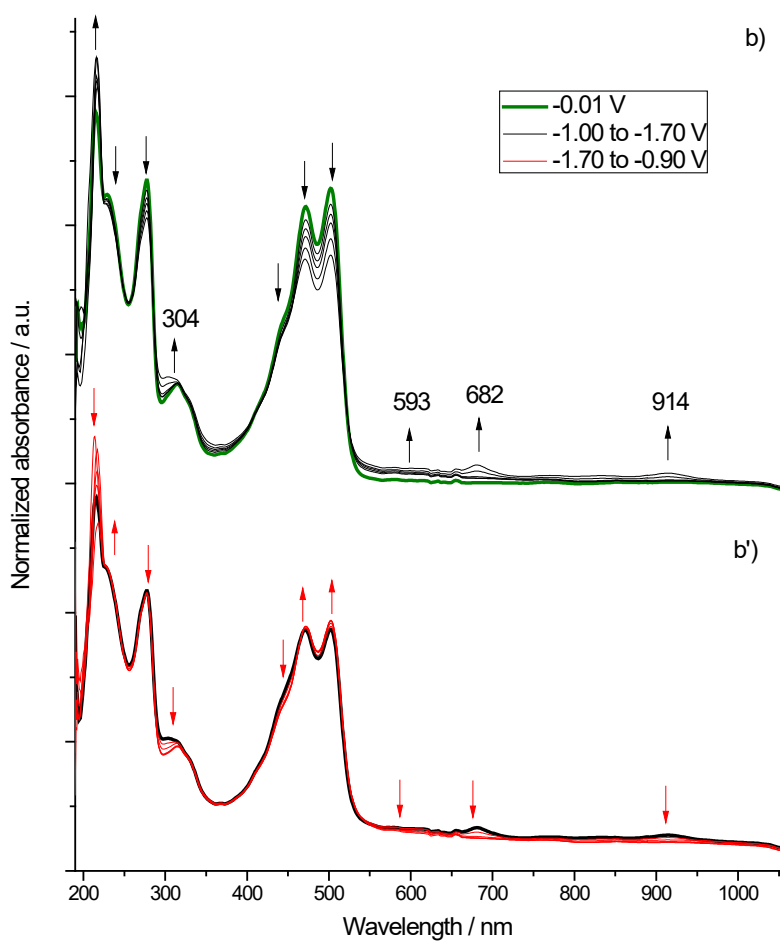


Figure S77. UV-vis-NIR spectra of **1** during stepwise polarization in the range of 1st oxidation (a) and 1st reduction peak (b) and after reverse suitable polarization (a', b') in 0.1 M *n*-Bu₄NBF₄/DCM.

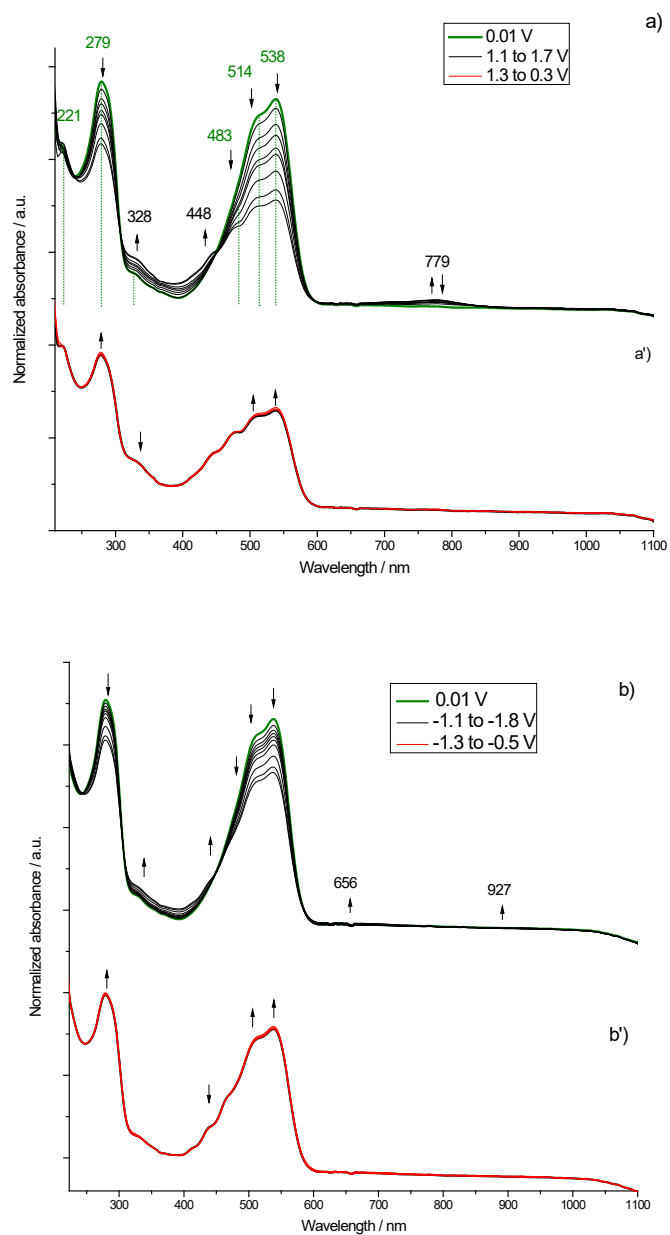


Figure S78. UV-vis-NIR spectra of **2** during stepwise polarization in the range of 1st oxidation (a) and 1st reduction peak (b) and after reverse suitable polarization (a', b') in 0.1 M *n*-Bu₄NBF₄/DCM.

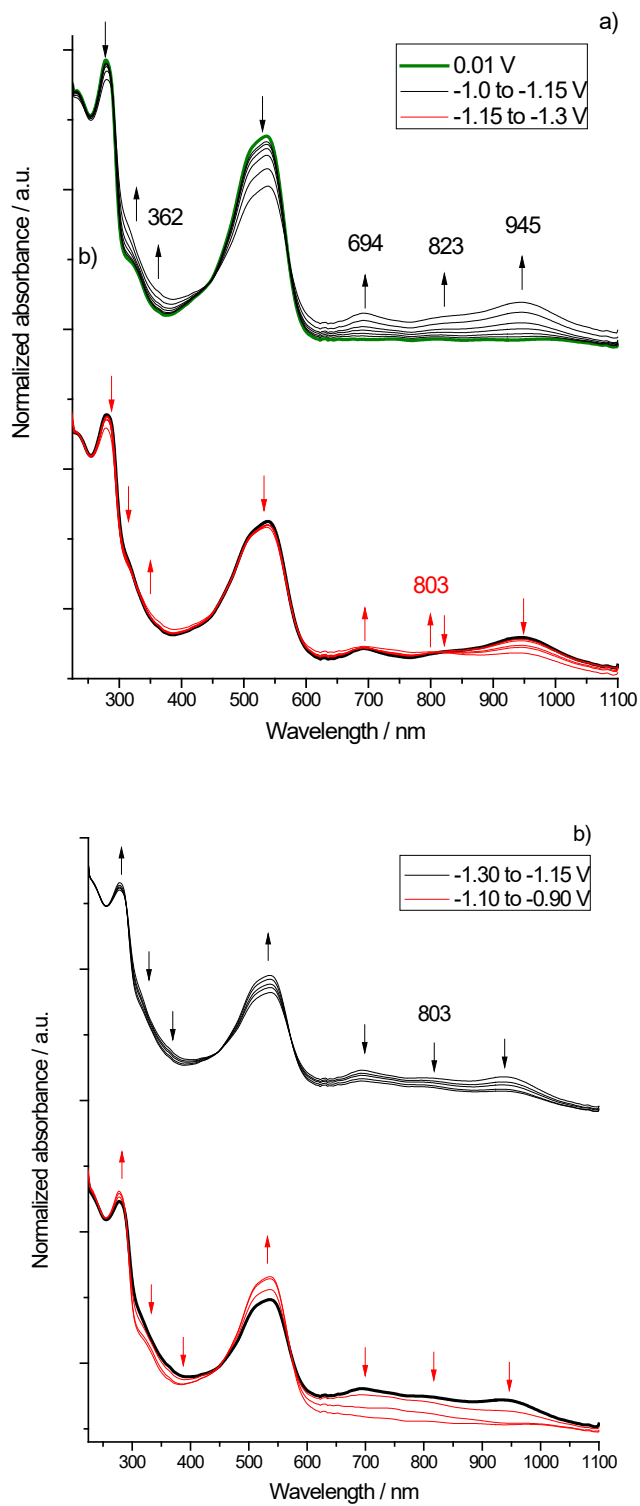


Figure S79. UV-vis-NIR spectra of **10** during stepwise polarization in the range of 1st (black) and 2nd reduction peak (red) (a) and after reverse polarization (b) in 0.1 M *n*-Bu₄NBF₄/DCM.

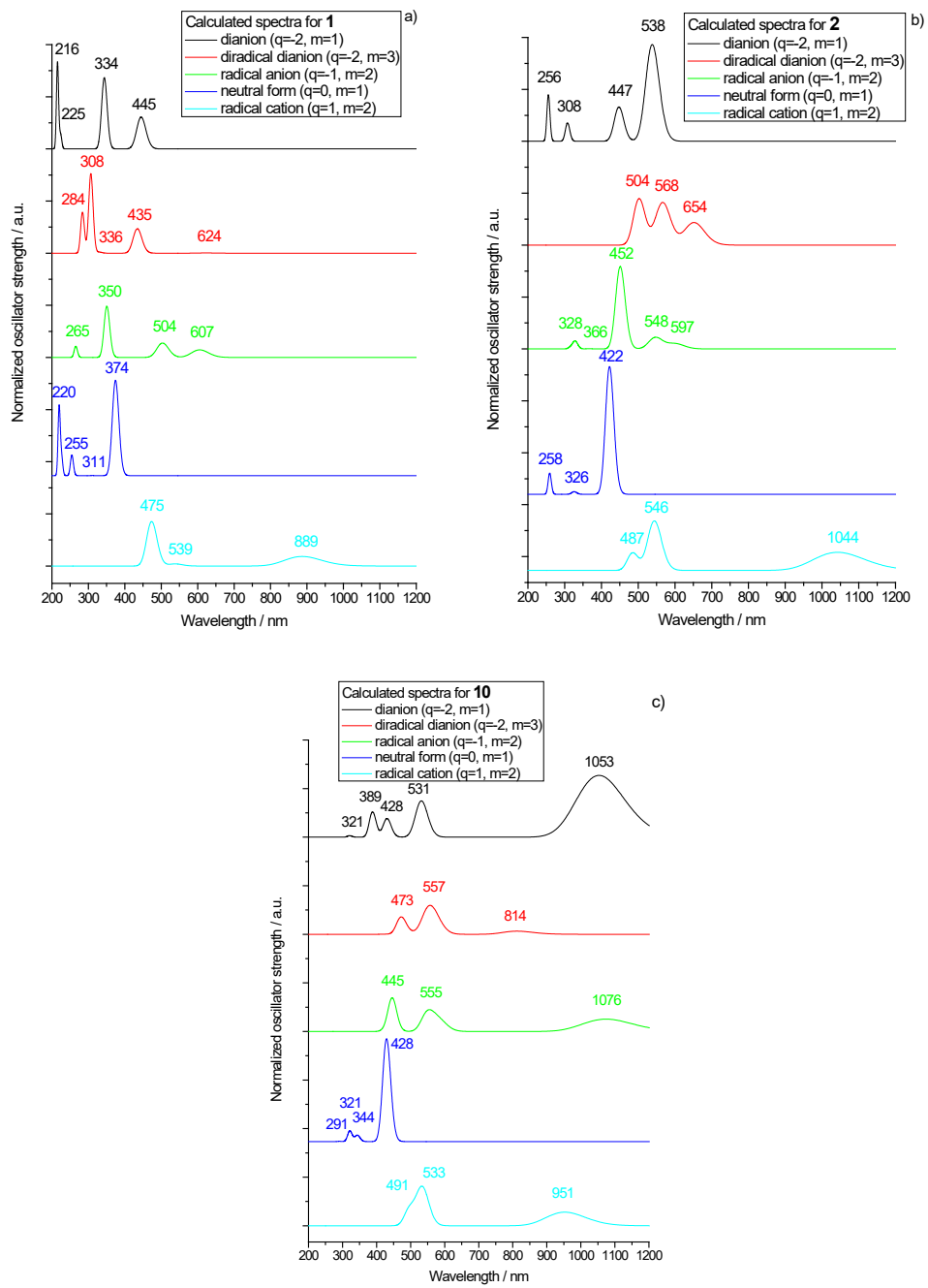


Figure S80. Simulated UV-Vis-NIR spectra of **1** (a), **2** (b), **10** (c) states calculated at TDDFT/CAM-uB3LYP/6-31G(d)/CPCM(DCM).

6. Phosphorescence studies.

General Remarks. Low temperature emission spectra were measured with a synchronous-chopper spectrophosphorimeter.²⁹ The sample, precooled in liquid nitrogen (77 K), was inserted into a cold liquid helium cryostat. It was excited by a 405 nm diode laser and the emission photos were observed at right angle. The spectra, dispersed by a McPherson207 spectrograph/monochromator were collected using an Andor DU424A-BR-DD camera or a Hamamatsu H10721-20 photomultiplier working in the photon counting mode.

Another possible dissipation excitation energy channel for the investigated molecules is intersystem crossing (ISC). According to theoretical investigations (ADC(2)/cc-pVDZ), for an exemplary dye **8** the calculated T₂ state (2.61 eV) energetically lies closely to the S₁ state (2.50 eV). Thus, we should take into account the possibility of the ISC from the S₁ to the T₂ state followed by population of the T₁ state (1.53 eV, 810 nm). The presence of ISC can be explored by searching for phosphorescence. Experiments performed for all the investigated dyes in dichloromethane at a low temperature (5 K) revealed no phosphorescence up to 1000 nm, even employing a sensitive, red CCD camera. Experiments were also performed for **8** in iodoethane (at 5 K), which due to the heavy atom effect, constitutes an efficient photosensitizer. The negative result of our search for phosphorescence leads us to the conclusion that ISC should be eventually ruled out as an efficient energy dissipation channel in dichloromethane.

The fluorescence spectrum of **1** in DCM is significantly shifted towards the blue region in respect to the fluorescence spectra of other compounds, both at room temperature and at 5 K (Figure S81). This spectrum has two maxima, at 520 nm and at 562 nm. The spectrum of compound **4** has maxima located at 548 and 618 nm. It is easily to see that the red band is more intense at 5 K, if compared with room temperature. The first bands of **6**, **7** and **11** spectra overlap with the second

²⁹ B. Kozankiewicz, J. Prochorow, *Mol. Cryst. Liq. Cryst.* **1987**, *148*, 93-109.

band of **1**, but the red bands of these compounds are much more intense and located at 607 nm, 615 nm and 622 nm, respectively. For compounds **3** and **9** the situation is opposite, the blue bands are more intense than the red ones. The largest red shift was observed for compound **10**.

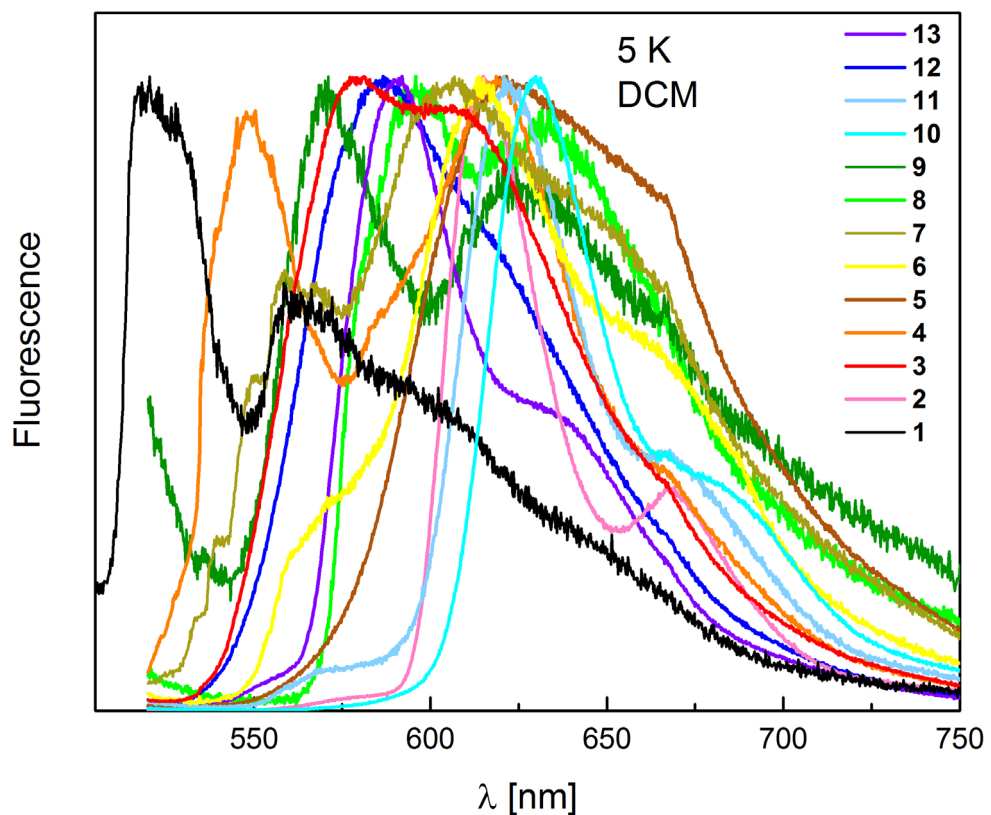


Figure S81. Fluorescence spectra of the DPND compounds for DCM rigid solution at 5 K.

7. ^1H and ^{13}C NMR spectra of new compounds.

Note: despite the fact that the samples were dried overnight under high vacuum at 70 °C there are traces of solvents that disturb an alkyl region of NMR spectra.

